Heat Transfer and Pressure Drop Investigation for Prescribed Heat Fluxes on both the Inner and Outer Wall of the Annular Duct

By Muteba Kandindi

11278405

Submitted in partial fulfilment of the requirements for the degree of Master of Sciences / Applied Sciences (Mechanics)

in the

FACULTY OF ENGINEERING, BUILT ENVIRONMENT AND INFORMATION TECHNOLOGY

at the

UNIVERSITY OF PRETORIA

Study Leaders

Prof Jaco Dirker

Prof JP Meyer

Date of submission

December 2016

Abstract

Heat exchangers are used in industrial processes to recover heat between two processes fluids and are widely used. Although the equations for heat transfer and pressure drop characteristics in a double-pipe heat exchangers are available, there is still need to completely understand how these characteristics interact which geometrical factors like annular diameter ratio or some thermal boundaries conditions which have not yet drawn more attention from the research community.

The purpose of this study was to experimentally measure the heat transfer and pressure drop characteristics of a concentric annular duct of ratio 0.593 for different heat fluxes simultaneously on the inner and outer tube in the turbulent flow regime and to describe or discuss the impact or interaction of heat flux ratios on the flow and heat transfer behaviour.

An experimental set-up was designed to achieve this goal. It consisted of an overall facility and a removable test section. The test section allowed for the measurement of the temperature along the length of the test section, the pressure drop, the heat flux inputs and the flow rate. These quantities were used to determine the heat transfer coefficients and friction factors of the system.

The concentric duct was an annulus formed of a single (15.88-mm-outer diameter and 14.46-mm-inner diameter) copper tube inserted inside a 0.91mm- thick- copper tube of 26.76 mm of inner diameter. The overall length of the annular duct was 4.84 m. To transfer heat, a heating element made of constantan wire was wrapped around each heat transfer area.

Heat transfer and pressure drop data were obtained on heating the inner and the outer wall separately with four different heat flux densities and eight heat flux ratio were used for the case of simultaneously heating both walls. Reynolds numbers for

unilateral heating range from 5 800 to 12 000 while bilateral heating were focus around two Reynolds numbers, 6 500 and 9 500.

Satisfactory results were found between the measurements of this experiment and currently available literature for the case of unilateral heating. An estimate of the accuracy of the experimental setup showed the maximum relative error was about 5 % in the determination of the Nusselt number and 1.8 % for the friction factor.

Diabatic friction factors have been presented using adiabatic friction factors with a correction term which considered the effect of temperature difference between the fluid and walls. Heat flux density ratio showed to have an impact on the heat transfer characteristics. The Nusselt number on the inner wall could be enhanced by 19% with increasing the heat flux ratio up to 2.3 times.

Acknowledgements

I would like to acknowledge the following people who made invaluable contribution to this study by their help and support:

- My supervisor, Prof J. Dirker, whose continuous guidance, assistance, enthusiasm, relentless contribution through this challenging journey were crucial to the completion of this study. With all my heart, I say "Thank you". You are a true gift.

- Prof J.P Meyer for his ongoing support throughout this study.

- Mr D. Gouws whose input and help were vital in all my experimental work.

- Mr K. Ntombeni for his inspirational personality, unceasing assistance and knowledge in processes of manufacturing heat exchangers.

- My family and friends for their words of encouragement and support during this period.

- All my colleagues and companions in the Laboratory: Warren Van Zyl, Louw Cotzee, Nicolas Kotze, Dr. Kunle Adelaja, D.R.E Ewim, Madder Steyn, Francois Prinsloo, Japie Westhuizen, Dickson Ndenguma, Wesley Reid, Junior Yekoladio. Your inputs were valuable for this project. Special thanks to my officemate, Tshimanga Ntumba for always being there when I need him.

- The technical and support staff: Tersia Evans, Chris Govinder, Neels Smith, Mc Donald Ketsee, Edwin Mohale.

Content

List of figures

List of tables

Nomenclature

a	annular diameter ratio (D_o/D_i)	-
a^*	geometry function	-
A_c	cross sectional area of annulus	m^2
$A_{s,i}$	surface area outside inner tube	m^2
$A_{s,o}$	surface area inside outer tube	m^2
Cp	specific heat	kJ/(kg.K)
C	Sieder-Tate type equation annulus tube coefficient	-
CV	control volume	
D_h	hydraulic diameter	m
D_i , D_{oi}	diameter of outside of inner tube	m
$D_{ins,i}$	inside diameter of the insulation	m
$D_{ins,o}$	outside diameter of the insulation	m
D_{ii}	diameter of inside of inner tube	m
D_o, D_{io}	diameter of inside of outer tube	m
$\frac{dp}{dx}$	pressure drop slope	N/m
E	modulus of elasticity	GPa
EB	energy balance	
F	view factor	
f	friction factor of the annulus	-
f_a	adiabatic friction factor of the annulus	
f_{ann}	friction factor in Gnielinski correlations	
F_{ann}	geometric factor for Gnielinski correlations	
f_o	friction factor based on the shear stress on the outer wall	
$I.D$	circular tube inner diameter	
g	gravitational acceleration	m/s^2
$\bar{h}$	average heat transfer coefficient	$W/(m^2.K)$

h	log mean temperature difference heat transfer coefficient	W/(m^2.K)
I	current	A
I_x	second moment of area	m^4
j	Colburn j-factor	
k	thermal conductivity	W/(m.K)
K	factor which takes into account the temperature dependence of fluid properties	-
L	tube length	m
$L_{h,i}$	heat transfer length on the inner tube	m
$L_{h,o}$	heat transfer length on the outer tube	m
L_s	standard length between thermocouples stations or between spacers	m
L_{pd}	pressure drop length	m
l	unsupported axial length of tube	m
M	mass per meter	kg/m
$\dot{m}$	mass flow rate	kg/s
$O.D$	circular tube outer diameter	
N	summation counter	-
n	Prandtl number exponent	-
Nu	Nusselt number	-
ΔP	pressure drop	Pa
p	number of variables in a function	
P	Dittus-Boelter type equation exponent	-
Pr	Prandtl number	-
$\dot{Q}$	heat transfer rate	W
$\dot{Q}_{input}$	heat generated by heating element	W
$\dot{Q}_{output}$	heat received by the fluid	W
$\dot{Q}_{rad}$	heat loss by radiation	
$\dot{q}_w$	heat flux	W/m^2

$\dot{q}_{w,i}$	heat flux density on the inner tube	W/m^2
$\dot{q}_{w,o}$	heat flux density on the outer tube	W/m^2
q^*	heat flux ratio	
Re	Reynolds number	-
Re^*	modified Reynolds number	-
R	electric resistance at temperature T	Ω
R_{TO}	electric resistance at temperature T_o	Ω
R_i	electric resistance of the inner heater	Ω
R_o	electric resistance of the outer heater	Ω
T	temperature	°C
T_b	bulk fluid temperature	°C
T_{in}	inlet temperature	°C
T_{ih}	temperature of the inner heater	°C
T_{heater}	temperature of the heating element	°C
T_{LMTD}	log mean temperature difference	°C
T_{out}	outlet temperature	°C
T_{oh}	temperature of the outer heater	°C
T_{wi}	temperature of the inner wall of the annulus	°C
T_{wo}	temperature of the outer heater	°C
V	velocity	m/s
U	voltage	V
$\bar{u}$	mean velocity of fluid in tube or channel	m/s
x	horizontal direction parallel to the annular duct length	m
y	vertical direction perpendicular to the annular duct length	m
y_δ	vertical displacement	m
w	distributed load	N/m
ε/d	relative roughness	

Greek Symbols

α	temperature coefficient of resistance	/ °C
δ	differential variation	m
ε	emissivity	
σ	Stefan – Boltzmann constant	W/(m^2.K^4)
τ_o, τ_i	shear stress on the outer wall or inner wall	N/m
μ	viscosity	kg/(m.s)
ρ	density	kg/m^3
Δ	variation	
$\emptyset_w$	factor binding friction and *j*-factor	

Subscripts

amb	ambient
bulk	property of fluid at bulk temperature
CV	referring to a control volume
i	inner
in	referring to the inlet
ins	referring to the insulation

j	numerical index
heater	referring to heating element
o	outer
out	referring to the outlet
st	standard
w	wall

Chapter 1: Introduction

1.1 Introduction

The process of heat transfer is familiar to us all. On a cold day, we put on more clothing to reduce heat loss from our warm bodies to the cool surroundings while on warmer days we may want to increase heat loss. Fundamental studies of heat, its measurement and transmission have long captivated the scientific community. Specifically, the engineering discipline of heat transfer is concerned with methods of calculating rates of heat. These methods are used by engineers to design components and systems in which heat transfer occurs.

Heat transfer considerations are in almost all areas of technology. However, the discipline that has been most concerned with heat transfer is chemical and mechanical engineering because of the importance of heat transfer in numerous energy conversion systems used in mechanical and chemical processes, from coal-fired or nuclear power plants to solar water heaters. A common thermal design problem is the transfer of heat from one fluid to another. Devices used for this purpose are called heat exchangers.

Heat exchangers are widely used in domestic or industrial applications. The needs for transferring internal thermal energy of a substance between two or more fluids available at different temperatures are common in engineer practice. A familiar example is the automobile radiator, in which heat is transferred from the hot engine coolant to cold air blowing through the radiator core. The common vapour cycle refrigeration of air-conditioning system has an evaporator where heat is absorbed at low temperature and a condenser where heat is rejected at a higher temperature. The domestic refrigerator is made with a condenser usually in the form of a tube coil with cooling fins to assist transfer of heat to the surroundings (Mills, 1992).

These applications of heat exchangers can range from simple devices to very complex engineering systems. A power plant, whether the fuel be fossil or nuclear, has a boiler in which water is evaporated to produce steam to drive the turbines, and a condenser in which the steam is condensed to provide a low back pressure on the turbines and for water recovery. An oil refinery has a great variety of heat transfer equipment, including rectification columns and thermal crackers. Many heat exchangers are used to transfer heat from one process stream to another, to reduce the total energy consumption by the refinery.

More recently the development of faster computers is guided by the ability of controlling the temperature of very small electronic components, which dissipate large amounts of heat. Transistors and diodes are some illustrations, they must not overheat.

To achieve multiple uses which they are intended for, according of the geometry of the flow configuration, the type of heat transfer surface or the materials of construction, heat exchangers have been manufactured under numerous types: double-pipe heat exchangers, compact heat exchangers, shell-and-tube heat exchanger, plate and frame heat exchangers, regenerative heat exchangers, etc.

The design of heat transfer equipment involves a trade-off between two conflicting goals of low capital cost (high overall heat-transfer coefficient, small heat transfer area) and low operating cost (low-pressure drop). Because of their simplicity and their relative low cost, the double-pipe heat exchangers that consist of two concentric pipes benefit from intensive technological and engineering applications such as cooling of turbine rotors, cooling of high speed gas bearings, condensers for sea water distillation, and in the chemical vapour deposition processes for the fabrication of semiconductor devices, food processes, thermal insulation, thermal storage systems, cooling channels of nuclear reactors, underground electrical transmission cable using pressurized gas, etc.

As consequence, many investigations have been devoted to this kind of geometry. However, this geometry is still not completely understood (Ouild-Rouiss *et al.*, 2009): while we understand physical laws describing the convection phenomenon, we do not have exact coefficient correlation yet. Having this in mind, one may wonder why experimental investigation keeps being performed on the annulus at research levels, or in a better sense, in which directions are conducted current investigations on this particular geometry. To answer the question, let us analyse how the progress in basic research and scientific foundations of the science of heat transfer achieved at research institutions and universities is merged with the engineering advances made in the industries throughout the world in the design, operation, rating and performance of heat exchangers.

The subject of heat transfer research is the design, performance and development of all kinds of heat exchanging equipment. Deviating from the classical meaning of science, heat transfer research has no value in itself but only in connection with actual engineering problems. The goal of heat transfer research is to predict design and performance data for heat exchanging equipment.

The method applied in heat transfer research is to investigate the engineering problems under well-defined conditions thus enabling us to find out the ruling phenomena and laws. The means for predicting design and performance data is the theory. The theory usually combines mathematically a set of variables and invariables. The latter ones usually are to be determined by experiments. The variables permit predictions beyond the range already known by experience.

Two approaches of theory in engineering science are applicable to heat transfer. There are engineering problems whose actual conditions cannot be quantified completely. In this case, we can expect at the best to achieve a physically based qualitative analysis. On the other hand, there are engineering problems for which the ruling physical laws

are unknown. In this case we can expect at the best to achieve an empirically based quantitative correlation. To solve engineering problems, both qualitative and quantitative analyses are needed. In a few cases, both kinds of analyses can be presented by one unique theory. In the majority of engineering problems, we have to be content with either one or the other kind of analyses. Studies on heat transfer and flows in turbulent concentric annuli fall on these kinds of analyses. Therefore, as far as possible both kinds should be tried, even if there will remain at the moment seemingly unbridgeable gaps between them encouraging future research (Afgan *et al.*, 1974).

Having said this, it is possible to solve practical problems to establish theories without knowing the fundamental physical laws ruling the involved phenomena, by introduction of certain summarizing variables covering a variety of other fundamental physical constants without knowing their more or complex interactions. It is revealed that a conveniently derived quantity used by heat exchanger design engineer for thermal analysis and performance is the heat transfer coefficient.

Let us consider a single forced convection problem. The heat flux $\dot{q}_w$ is found to be approximately proportional to the difference of temperature ΔT, when the flow parameters are kept constant. This is the so-called "Newton's Law of cooling". In these circumstances, for the purposes of calculation, it is convenient to use the ratio $\frac{\dot{q}_w}{\Delta T}$, i.e the heat transfer coefficient.

For concentric annuli, it is expected that many parameters influence the heat transfer coefficient: the annular diameter ratio, the relative direction of heat flow, the set of physical properties such as thermal conductivity, density, viscosity, etc. Although intense investigations have been carried out to determine the influence of annular ratio on the heat transfer coefficients, there is still a lack of publications and correlations on the influence of the ratio of heat rates over both walls of an annular duct on the heat

transfer coefficients. Therefore, this is one of the two main topics to be addressed in this experimental work. The other topic is related to the pressure drop.

Three different thermal boundary conditions will be considered in this study: (1) uniform heating of the outer surface only, while the inner surface is adiabatic, (2) uniform heating of the inner surface, the outer surface is adiabatic and (3) heating on both surfaces. Since experimental data from heating on the outer surface or on the both surfaces are scarcer than those for heating only on the inner surface, this work will be a substantial contribution for further development of theories and correlations related to annulus.

An annular diameter ratio of 0.593 has been retained in this investigation.

Since laminar forced convection for fully developed velocity and developing temperature for water flow in concentric annulus where heat fluxes on the two surfaces are specified has almost been completely solved (Kays and Crawford, 1980), our investigation will cover the turbulent flow and heat transfer with Reynolds number ranging from 4 000 to 15 000.

1.2 Objectives

The purpose of this study was:

- To design and build an experimental system allowing the capture of the required information in order to compute parameters of interest.
- To collect experimental data on heat transfer and pressure drop characteristics for prescribed wall heat fluxes on both the inner and outer walls of a concentric annular duct of specified size.
- To investigate the effect of the heat flux ratio on the heat transfer and pressure drop characteristics.

Experimental data collected in this study is to contribute to a data-base of experimental results for a possible development of heat transfer and pressure drop correlations.

1.3 Organization of the document

This dissertation consists of seven chapters. Each chapter starts with an overview of what will be developed in its core.

Chapter 2 gives an oversight of relevant literature on heat transfer and pressure drops on concentric annular ducts. Parameters that affect performance will be emphasized. Analogy between heat transfer and pressure drop will also be introduced.

Chapter 3 will discuss the experimental setup, the experimental procedure and will end with a validation of adiabatic friction factors.

Chapter 4 will start with the description of equations used to compute the heat transfer and pressure drop characteristics and quantities of interest for the study. It will then present a summary on the uncertainty analyses of measured variables.

Chapter 5 will focus on the analysis of results obtained for the case of unilateral heating conditions.

Chapter 6 will deal with data captured for the case of heating both walls.

The last chapter (Chapter 7) will contain the conclusion of the dissertation. The dissertation ends with appendices, which contain the full uncertainty analysis of the system.

Chapter 2: Literature study

2.1 Introduction

As stressed in the introductory chapter, investigating pressure drop and heat transfer in fluid flow in an annular passage is among the most important heat transfer studies, owing to its presence in several applications. There are numerous published investigations comprising experimental and numerical explorations that deal with different types of fluid and boundary conditions as well as the geometry of annular passages.

Fluid flows are categorized as laminar, transitional and turbulent. For decades laminar and turbulent types of flows were the ones drawing much attention. But recently transitional flows are getting more attention from research community than what was dedicated in the past. Many reasons may justified the sudden interest of this type of flow. One of them is related to the efficiency needs of the future. More surface area is added to exchangers, with the implications that flow rates per tube drops. The efficiency requirements also imply reduced compressor and pumping power, with the overall trend being that many heat exchangers will start to operate in the transition region of flow (Olivier and Meyer, 2009). Therefore the need to understand this type of flow has become vital.

Laminar flow theory in annular ducts is well developed, and analytical solutions can be readily derived for laminar flows. Useful developments can be found in the excellent book of Shah and London (1978). However, it is still very difficult to analyse the small-scale random fluctuations of turbulent flow. Experimental studies on turbulent regimes were widely conducted to understand the flow behaviour to design applications.

Throughout the present review, we will focus on work done on the turbulent region of circular concentric configuration.

2.2 Historical review

The review will first address the pressure drop problem and secondly its heat transfer counterpart. It will end with a brief introduction on analogy between heat transfer and pressure drop characteristics.

2.2.1 Pressure drop

Pressure drop literature will be broken down in two subsections, the first deals with adiabatic cases and the last with diabatic cases.

a) Adiabatic case

Pressure drop in concentric annular ducts were intensively investigated in the past. Much frictional pressure loss data on concentric annular ducts were already available at the beginning of the last century. However, the correlations derived by different authors showed large discrepancies when compared among each other (Jones and Leung, 1981). These may be due to different levels of accuracy in experimental data and the scope underlying each experiment. Herein a review is done on some works which were based on the need of a functional dependency of the turbulent flow with the radius ratio.

Early in the 20th century, steady fully developed flow in concentric annuli was studied in an attempt to parallel the well-known work of Nikuradse (1933), Stanton and Pannel (1914) and others in the plain tube and parallel plate. Two parameters, relative roughness ε/d and Reynolds number Re, were considered sufficient to correlate friction factors in circular ducts, and with suitable empirical modification in non-circular tubes. However, unfortunately results for annuli were not as successful as the prior cases. The thumb rule in design was to use a friction factor which is 1.1 times higher than that for plain tubes.

Davis (1943), in analysing some of these early results concluded that the friction factor, f, for smooth concentric annuli was a function of the radius ratio, a , and had a higher

value than that for a plain tube at the same Reynolds number. He suggested the following equation (after being rewritten):

$$f = 0.055Re^{-0.2}(1-a)^{0.1} \qquad 2\text{-}1$$

Here $a = {}^{D_i}/_{D_o}$ is the ratio of the inner radius,D_i, to the outer radius, D_o, and f is defined as:

$$f = -\frac{dp}{dx}\frac{(D_o - D_i)}{2\rho\bar{u}^2} \qquad 2\text{-}2$$

In this expression, f corresponds to the definition of the fanning friction factor, The Reynolds number was based on the hydraulic diameter, $D_o - D_i$, and $\frac{dp}{dx}$ is the slope of the pressure drop, ρ is the density and $\bar{u}$ is the mean velocity of the fluid. The above-mentioned correlation was deducted by Davis after correlating results from thirty radius ratios with a ranging from 0.364 to 0.99, Reynolds numbers between 3000 and 40 000 with air and water as media. Since the approach which was followed, was to consider the parallel plate as a limiting case of the annular duct, this expression has the drawback that it does not reduce to the value for the parallel plate channel as a becomes unity.

Following another approach, Rothfus *et al.* in (Quarmby, 1967) proposed that two friction factors should be used based either on the shear stress on the outer wall, τ_o, or on that at the inner wall, τ_i. For the outer wall they suggested:

$$\frac{1}{\sqrt{f_o}} = 4.0\log\left(Re\sqrt{f_o}\right) - 0.40 \qquad 2\text{-}3$$

This is similar to the well-known result of Nikuradse (White, 2009). In this correlation the Reynolds number is based on $\frac{\left(r_o^2 - r_i^2\right)}{2\,r_m}$ where r_m is the radius of maximum velocity. A similar expression was proposed for the inner friction factor. The Reynolds number range was 10 000 to 45 000 with a = 0.336 and 0.592 using water as the working fluid. Their experimental results showed a significant dependence of the friction factor with

the radius ratio. In a similar way, Lee and Barrow (1964) correlated friction factors and found that the friction factor increased with the radius ratio and was significantly higher than Davis's results. They used air with radius ratios 0.258, 0.387 and 0.613 and with Reynolds numbers between 10 000 and 50 000.

Later, Brighton and Jones (1964), after an intensive investigation on seven annuli with radius ratios from 0.063 to 0.562 and 4 000 < Re < 300 000, concluded that the friction factor was independent of Reynolds number within the limits of their experimental accuracy. This was a contradiction on previous work. They use water and air as working fluids.

Jonsson and Sparrow (1966) also presented results for concentric annuli. Their result confirmed that the friction factor was radius-ratio-dependent, but with its value decreasing while the radius ratio increases. This was contrary to all previous results in which a radius ratio dependence has been found.

Based on the findings of the afore-mentioned investigations, it is clear that there was little agreement between publications of different authors considered. From this it is inconclusive, whether the friction factor is indeed dependent on the radius ratio, and how it is appropriately related to an appropriate Reynolds number.

While the idea of dependence of friction loss on the radius ratio was gaining more support among investigators in subsequent researches, the formulation used to describe this dependence continued to be a matter of discussion.

In a paper published in the last century, Jones and Leung (1981) combined two ideas:

- the similarity which can be shown mathematically between concentric annuli and circular tubes in laminar flow , and
- the idea described by Frederickson and Bird (1958) to use a laminar based length dimension to predict the turbulent friction factors of power-law fluids in fluids in smooth concentric annuli.

They rewrote the Colebrook equation in terms of a modified Reynolds number Re^* to predict friction factors for concentric annuli. This rewritten equation can be read as:

$$\frac{1}{\sqrt{f}} = 2\log_{10} Re^*\sqrt{f} - 0.8 \qquad 2\text{-}4$$

With

$$Re^* = \frac{\rho V D_h}{\mu} \cdot \frac{(1+a^2)\ln a + (1-a^2)}{(1-a)^2 \ln a} \qquad 2\text{-}5$$

More recently Gnielinski (2009) correlated a large data set of experimental result collected from various authors through five decades and proposed the following equation:

$$\frac{1}{\sqrt{f}} = 1.8\log_{10} Re^* - 1.5 \qquad 2\text{-}6$$

With Re^* defined as in Jones and Leung correlation, equation 2-5.

Kaneda *et al*. (2003) by integrating numerically the equations of conservation using a theoretically based correlating equation for the turbulent shear stress for fully developed turbulent flow in annuli derived a new equation. Their equation, designated as predictive rather than correlative because it was formulated without recourse to the experimental data it is proposed to represent, reads:

$$\frac{f}{8} = \left[1.61 + \frac{1}{0.436}\ln\left(\frac{Re_{Dh}}{\sqrt{8/f}}\right) - \frac{550}{Re_{Dh}\sqrt{f/8}}\right]^{-2} \qquad 2\text{-}7$$

b) Diabatic case

All correlations presented so far were derived from data obtained for adiabatic conditions. Under single-phase conditions, a strong effect due to applied heat on pressure drop has been observed when the difference between the fluid bulk and the wall temperature is high. The effect of property variation is to alter the velocity profile, which results in different friction coefficients than would be obtained if properties were constant

This effect is principally the result of a temperature gradient in the fluid close to the heated wall, which tends to lower the near-wall viscosity and hence decreases the wall-shear stress. Leung *et al*. (2005) reviewed attempts made to address this problem. It is reported in their paper that in order to account for heating effects, Sieder and Tate (1936) introduced a correction term to the friction-factor equation for unheated channels The correction term is expressed as a function of the viscosity ratio determined at the bulk and near-wall temperatures, as follows:

$$\frac{f}{f_a} = \left(\frac{\mu_b}{\mu_w}\right)^{-m} \qquad 2\text{-}8$$

The exponent was optimized using available experimental data. For turbulent single-phase flows, Sieder and Tate (1936) suggested to use m = 0.14. Rohsenow and Clark (1951) indicated that the aforementioned value was valid mainly for a combined pressure drop due to friction and acceleration. A value of m = 0.60, on the other hand, was considered to be more appropriate for calculating only the frictional pressure loss. Other studies, however, recommended values between 0.14 and 0.60. Maurer and LeTourneau (1963) indicated that a value of m = 0.25 was able to correctly fit their data. Furthermore, they noted that the value of the exponent was sensitive to variations in both the flow rate and density of the fluid. Dormer and Bergles (1969) suggests that a value of m = 0.35 fit well their results.

W. R. Van Zyl *et al*. (2012) investigated four annular channels with diameter ratios 0.483, 0.579, 0.593 and 0.712 with two different heat flux directions across the inner tube, namely a heated and a cooled annulus. They found that friction factors for heated annulus were on average 9 % lower than for a cooled annulus. This was due to the reversed nature of the viscosity ratio value for the heated and cooled cases.

2.2.2 Heat transfer

This section will focus on the available correlations for heat transfer coefficients with regard of the different thermal boundary conditions. The condition of inner wall and

outer wall heating will be presented first and an overview to solve the bilateral thermal condition will briefly be given.

a) Heating from the inner wall

In the absence of exact solutions of the conservation equations for heat transfer in annuli, scientists tackled this particular geometry by using the relative information obtained on the subject of heat transfer to fluids flowing in turbulent motion inside circular tubes and extended these studies to annular ducts. First attempts were made using two equations generally used to correlate data for tubes

The first one is the Dittus and Boelter (1930) equation and it reads as:

$$Nu = 0.0225\, Re^{0.8} Pr^{n} \qquad 2\text{-}9$$

where n is 0.4 for heating and 0.3 for cooling, and the fluid properties are taken at the bulk fluid temperatures. The second equation is that proposed by Colburn (1933) and is of the form

$$\left(\frac{h}{\rho C_p \bar{u}}\right) Pr^{2/3} = 0.023\, Re^{-0.2} \qquad 2\text{-}10$$

In this latter case fluid properties are taken at film conditions.

These two equations were used with the substitution of an equivalent diameter equal to $D_o - D_i$, based on the wetted perimeter (the hydraulic diameter), or an equivalent diameter based on the heated perimeter and equal to $\left(\frac{D_o^2 - D_i^2}{D_i^2}\right)$.

It can be seen that these equations do not explicitly take into account the dependence of heat transfer coefficients on the ratio of the diameters which is almost admitted when considering the shape of velocity profile. In the case of flow in annular duct, the maximum velocity is shifted to the inner wall of the duct as the diameter ratio decreases.

Many attempts were made to improve these correlations to fit experimental data from various authors, these include additional terms designed to take into account the effect of diameters ratio of an annular duct as well as the variation of fluid properties with temperature.

Dirker and Meyer (2004) reviewed many correlations on heat transfer characteristics in annular ducts based on these models. Their review revealed that although various correlations are available in the literature, they are not in a good agreement. From their experimental investigation on nine different annular diameter ratios in concentric ducts, they proposed a new correlation. In Table 2-1, some correlations found in Dirker and Meyer (2004) are reproduced.

Table 2-1: Heat transfer characteristics as recapitulated from Dirker and Meyer (2004)

Authors	Correlation	Equation number	Diameter ratio range	Reynolds Number range	Medium
Foust and Christian (1940)	$Nu = \frac{0.04}{a\left(\frac{1}{a}+1\right)^{0.2}} Re^{0.8} Pr^{0.4}$	2-11	0.543, 0.833	3 000 - -60 000	water
Davis (1943)	$Nu = 0.038 a^{-0.15}\left(\frac{1}{a}-1\right)^{0.2} Re^{0.8} Pr^{1/3}\left(\frac{\mu_o}{\mu_w}\right)^{0.14}$	2-12	0.000147, 0.847	Not specified	All media
Monrad and Pelton (1942)	$Nu = 0.023\left[\frac{2\ln\frac{1}{a}-\frac{1}{a^2}+1}{\frac{1}{a}-a-\frac{2}{a}ln\frac{1}{a}}\right] Re^{0.8} Pr^{n}$ with n= 0.4 for heating and 0.3 for cooling	2-13	0.0588, 0.408, 0.606	12 000 – 220 000	Water , air
Wiegand *et al.*(1945)	$Nu = 0.023\, a^{-0.45} Re^{0.8} Pr^{n}\left(\frac{\mu_o}{\mu_w}\right)^{0.14}$ with n= 0.4 for heating and 0.3 for cooling	2-14	0.1 - 1	Not specified	Fluids with $\mu \leq 2\mu_{water}$
Mc Adams (1943)	$Nu = 0.023\, Re^{0.8} Pr^{1/3}\left(\frac{\mu_o}{\mu_w}\right)^{0.14}$	2-15	Not specified	Not specified	Not specified
Mc Adams (1954)	$Nu = 0.03105\, a^{-0.15}\left(\frac{1}{a}-1\right)^{0.2} Re^{0.8} Pr^{\frac{1}{3}}\left(\frac{\mu}{\mu_w}\right)^{0.14}$	2-16	0.000147, 0.847	Not specified	All media
Stein and Begell (1958)	$Nu = 0.02\, a^{-0.5}\, Re_{D_h}^{0.8}\, Pr^{1/3}$	2-17	0.812, 0.864, 0.59	30 000 – 390 000	Water
Pethukov and Roizen (1964)	$Nu = \frac{0.06759\, a^{-0.16}}{\left(\frac{1}{a}+1\right)^{0.2}}\zeta Re^{0.8}$ where $\zeta = 1 + 1.75\left[\frac{\frac{1}{a}-5}{\left(\frac{1}{a}-1\right)Re}\right]^{0.6}$ for $a \geq 0.2$ or $\zeta = 1$ for $a \leq 0.2$	2-18	0.07 - 1	10 000 – 300 000	Air

Authors	Correlation	Equation number	Diameter ratio range	Reynolds Number range	Medium
Crookston (1968)	$Nu = 0.023a^{-0.25}\,Re^{\,3/4}\,Pr^{1/3}$	2-19	0.0625, 0.0323, 0.1	17 000 – 100 000	Air
Dirker and Meyer (2004)	$Nu = C_o Re^P Pr^{\frac{1}{3}}\left(\frac{\mu}{\mu_w}\right)^{0.14}$ where $P = 1.013e^{-\frac{0.067}{a}}$ and $C_o = \frac{0.003a^{1.86}}{\frac{0.063}{a^3} - \frac{0.674}{a^2} + \frac{2.225}{a} - 1.157}$	2-20	0.198, 0.313, 0.367, 0.45, 0.57, 0.595	4 000 – 30 000	Water

The Reynolds and the Nusselt numbers are based on the hydraulic diameter, $D_h = D_o - D_i$

Due to the fact that correlations are still showing discrepancies, new correlations or modifications of old ones keep emerging. Swamee *et al*. (2008) rewrote Sieder and Tate equations for heat transfer in annulus heated from the inner tube as:

$$Nu = \frac{0.027}{\left(1+\frac{1}{a}\right)^{0.2}} Re^{0.8} Pr^{\frac{1}{3}} \left(\frac{\mu}{\mu_w}\right)^{0.14} \qquad 2\text{-}21$$

Gnielinski (2009), using a large number of sets of experimental results comparing from various authors, improved a correlation available in Gnielinski (1987) on heat transfer coefficients on annular ducts. The older correlation by Gnielinski, based on the equation of Prandtl for fully developed turbulent flow in circular tube was believed to be more representative or globalizing since it takes into account numerous factors affecting heat transfer coefficients: diameter ratio, thermal entry length, change of physical properties, thermal boundaries. In its original form the correlation reads:

$$Nu = \frac{\left(\frac{f_{ann}}{8}\right)(Re-1000)\,Pr}{k_1 + 12.7\sqrt{f_{ann}/8}\,(Pr^{2/3}-1)}\left[1+\left(\frac{D_h}{L}\right)^{2/3}\right] F_{ann} K \qquad 2\text{-}22$$

Where $k_1 = 1$ and

$$f_{ann} = (1.82\ \log Re - 1.64)^{-2} \qquad 2\text{-}23$$

$$F_{ann} = 0.86\ a^{-0.16} \qquad 2\text{-}24$$

The factor $\left[1+\left(\frac{D_h}{L}\right)^{2/3}\right]$ in equation 2-22 is intended to take into account the thermal entry length, F_{ann} is the correction factor which bears the effect of the thermal boundary condition and K counts for the variation of fluid properties with temperature, $K = \left(\frac{Pr_b}{Pr_w}\right)^{0.11}$ for liquids and $K = \left(\frac{T_b}{T_w}\right)^{n}$ for gas. The exponent n is $n = 0$ in case of cooling a gas while heating a gas leads to different values for each gas. The validity of this equation is for all Reynolds numbers greater than 2300. This correlation by Gnielinski was derived prior to data by Dirker and Meyer (2004).

Adding results from Dirker and Meyer (2004), the newer correlation by Gnielinski derived for Reynolds number higher than 10 000 suggests new values f_{ann} and F_{ann} and replaces (Re -1000) by Re.

$$f_{ann} = (1.8 \log Re^* - 1.5)^{-2} \quad 2\text{-}25$$

$$Re^* = Re \frac{(1+a^2)\ln a + (1-a^2)}{(1-a)^2 \ln a} \quad 2\text{-}26$$

$$F_{ann} = 0.75\, a^{-0.17} \quad 2\text{-}27$$

In Table 2-2, a summary of data gathered by Gnielinski to derive a new correlation is given.

Table 2-2 : Dataset used in the new Gnielinski correlation for heating from the inner wall of the annulus

Authors (Year)	Diameter ratio	Heated Length	Medium
Monrad and Pelton (1942)	0.4082	1.72 m	Water
	0.6061	1.72 m	
McMillen & Larson (1944)	0.625	3.34 m	Water
	0.77	3.34 m	
Carpenter *et al.* (1946)	0.75	2.44 m	Water
Knudsen and Katz (1950)	0.789	2.74 m	Water
Miller *et al.(1955)*	0.745	0.125 m	Water
Krischer (1961)	0.842	3.55 m	Water
Kays and Leung (1962)	0.192	1.22 m	Air
	0.255	1.22 m	
	0.375	1.22 m	
	0.5	1.22 m	

Authors (Year)	Diameter ratio	Heated Length	Medium
Pethukov and Roizen (1963)	0.0718	3.2 m	Air
	0.143	3.2 m	
	0.244	3.2 m	
	0.546	3.2 m	
	0.696	3.2 m	
Lee and Barrow (1964)	0.258	3.71 m	Air
	0.387	3.71 m	
	0.613	3.71 m	
Quarmby (1967)	0.347	2.9 m	Air
	0.178	2.9 m	
	0.107	2.9 m	
Dirker and Meyer (2004)	0.198	6 m	Water
	0.313	6 m	
	0.367	6 m	
	0.45	6 m	
	0.57	6 m	
	0.595	6 m	

In the Figure 2-1, all correlations gathered so far and which are valid for the Reynolds range and medium applicable in this study and for annular ratio equal or superior to 0.593 are compared for water at a Prandtl number of 6 (bulk temperature of 25.65°C) and Reynolds number ranging from 5 000 to 16 000 for a = 0.593.

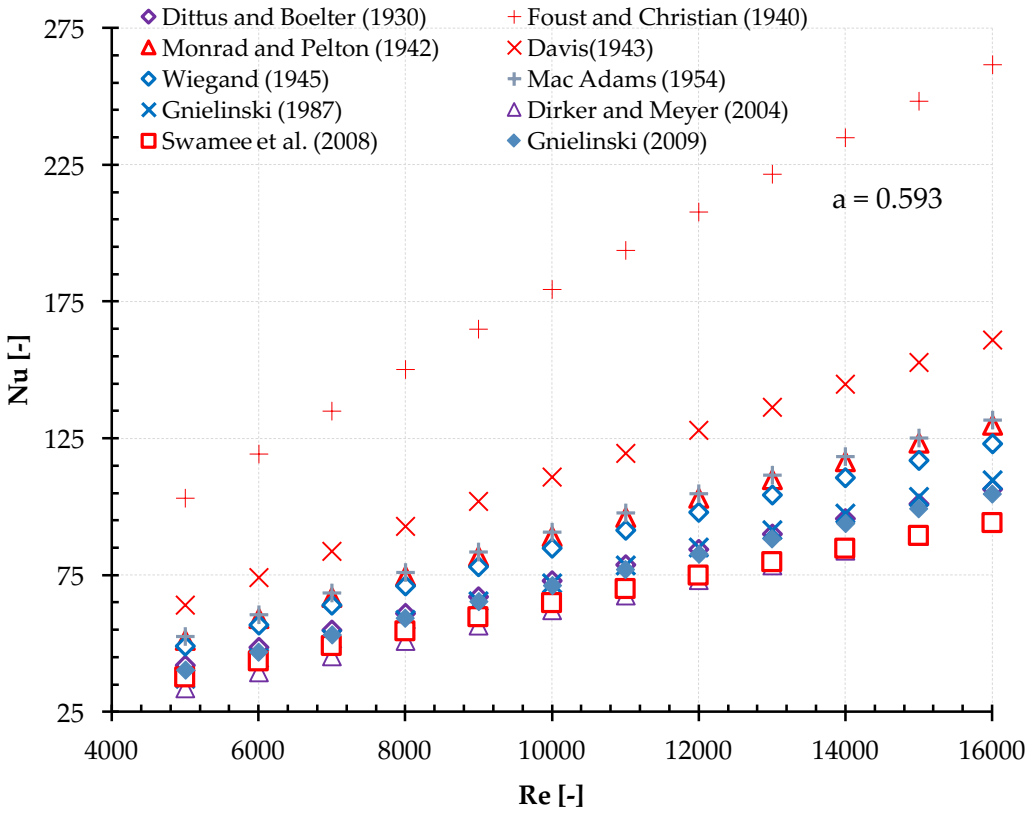

Figure 2-1: Different predictions of Nusselt numbers for Pr = 6 with Reynolds numbers ranging from 4 000 to 16 000 (Heat flux 18 000 W/m²) at annular ratio of 0.593.

Knowing the Reynolds number, the heat flux and the bulk temperature, each curve is obtained by solving iteratively the Nusselt number correlation until convergence is reached for the wall temperature. All correlations are predicting an increase of Nusselt number as Reynolds number increases. In the considered Reynolds number range, correlations predicted an approximate linear increase of Nusselt number with Reynolds numbers.

The correlation by Foust and Christian and the correlation by Davis seem to over predict the Nusselt number in a very drastic manner while the correlation of Dirker and Meyer provides the lower boundary. Correlations of McAdams and Monrad and Pelton give similar predictions, while deviations from each other increase as the Reynolds number increases. For Reynolds numbers greater than 10 000, the newer correlation by Gnielinski gives predictions which are slightly lower than its older version.

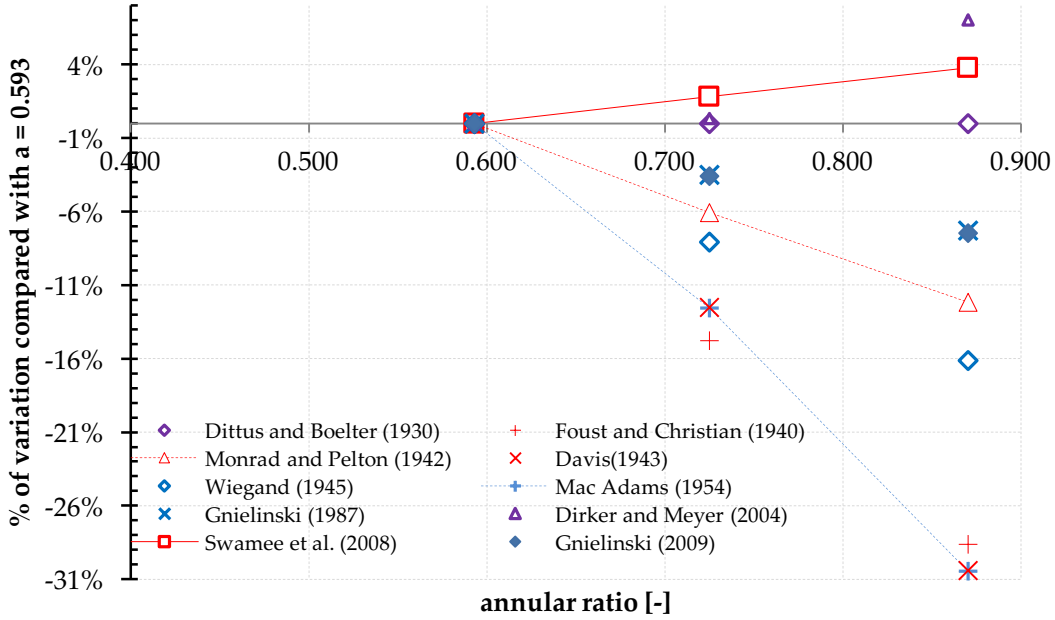

Figure 2-2: Change in the Nu as function of the annular ratio a.

W. R. Van Zyl *et al*. (2012) conducted a series of investigations on four annular diameter ratios 0.483, 0.579, 0.593 and 0.712 with two different heat flux directions across the inner tube, namely a heated and a cooled annulus. They used three different methods (a log-mean temperature difference calculation, a linear and a non-linear regression scheme) to compute the Nusselt numbers. Their experimental lied on average 8 % higher than the correlation of Gnielinski (2009) for the case of heating the annulus. They also examined the local Nusselt numbers along the axial length of their test sections, they found out that local Nusselt numbers towards the annulus inlet were larger and they decreased toward the annulus outlet for all diameter ratios. They attributed the fact to the development of the thermal boundary over the heat exchanger. This suggests an in-depth investigation on the dependency of the average Nusselt number of different authors with the length of heat exchanger. No new correlation has been proposed by these authors.

b) Heating from the outer wall

Heating annulus from the inner wall of the annular duct is the thermal boundary which is the most important case from a practical point of view. This fact justifies that

many correlations are found on this thermal boundary and little attempts have been made to solve the case of heating the outer wall of the annular duct; therefore, correlations are scarce for this thermal boundary condition.

Monrad and Pelton (1942) correlated experimental data obtained for a diameter ratio of 0.541 and found that their data fitted best with the original equation by Dittus and Boelter (equation 2-9).

Pethukov and Roizen (1963) recommended that the Nusselt in this case can be determined from a suitable turbulent flow relation in circular tube multiplied by a correction factor to allow for the effect of diameter ratio. This correction is of the form:

$$F_{ann} = 1 - 0.14\left(\frac{D_i}{D_o}\right)^{0.6} \qquad 2\text{-}28$$

This factor has been used with a correlation proposed for circular tubes and it reads in Gnielinski (1987) as:

$$Nu = \frac{\left(\frac{f_{ann}}{8}\right)(Re - 1000)\,Pr}{1 + 12.7\sqrt{f_{ann}/8}(Pr^{2/3} - 1)}\left[1 + \left(\frac{D_h}{L}\right)^{2/3}\right]F_{ann}\left(\frac{\mu}{\mu_w}\right)^{0.14} \qquad 2\text{-}29$$

where $f_{ann} = (1.82\log Re^* - 1.64)^{-2}$, L is the length of the heat exchanger, μ , μ_w are respectivity dynamic viscosities at bulk and outer-wall temperatures.

Gnielinski (2009) proposed a new correlation similar to the equation 2-22 suggested for the case of heating from the inner tube by changing

$$F_{ann} = 0.9 - 0.15\,a^{0.6} \qquad 2\text{-}30$$

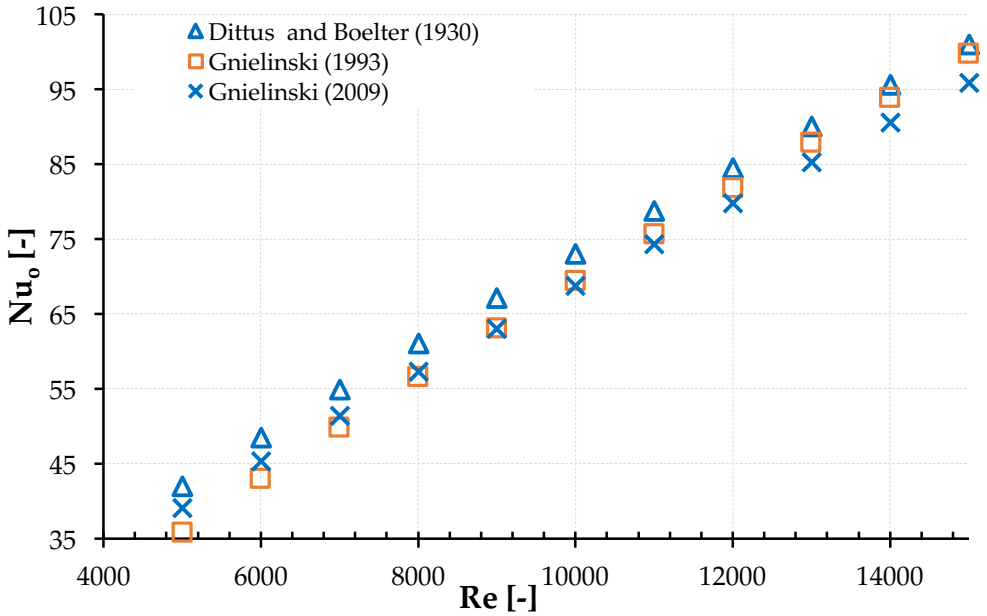

Figure 2-3: Different predictions of the Nusselt numbers in the case of heated outer wall for Pr = 6 and Reynolds numbers ranging from 5000 to 15 000. (18 000 W/m²) at annular ratio of 0.593.

The three correlations reported so far as in Figure 2-3 show an almost linear increase of the Nusselt number with the Reynolds number. As for the case of the inner tube, the new correlation by Gnielinski (2009) for the outer wall heating case predicts, for Reynolds number greater than 10 000, values which are lower than the first version. This is due to the fact that changes were made on the friction factor and the geometric factor. As Reynolds number increases, the constant change on the geometric factor outweighs the variation of the friction factor.

c) Bilateral heating

Previous literature that is directly relevant to the present study is rather limited. Heat transfer experiments in concentric annular channels with both wall heated are scarce. The very few experiments reported in subsequent paragraphs showed that heat flux ratio impacts the heat transfer characteristics of the turbulent flow in bilaterally heated annular channels.

Kays and Leung (1963) conducted experimental investigation with both walls of the annulus being uniformly heated and for radius ratio 0.192, 0.255, 0.374 and 0.5. The

Reynolds numbers range was from 10 000 up to 160 000 with air as working fluid and the annular duct disposed vertically. Their tests runs were used as a check to validate their numerical analysis which is in light of new development of models of turbulence misleading. It was noted that the heat flux ratio can have a large influence on Nusselt number, and that the outer tube Nusselt number can be either above or below the inner tube Nusselt number depending upon the heat flux ratio. Their results also showed that the average Nusselt numbers for cases with both walls heated could be higher than that for cases with only one wall being heated. As they tested with several radius ratios, they have also noticed that , when only one wall was heated, the Nusselt number decreased with increasing the radius ratio, but when both walls were heated, this trend reversed.

Pethukov and Roizen (1963) also reported a few data measurement for the case of bilateral heating both walls with isoflux boundary conditions with annular ratio 0.244. Their results also clearly pointed out that the heat transfer characteristics for the case of bilateral heating differ from those in the case of unilateral heating. As cited in (Zeng *et al.*, 2007), Sun *et al.* performed series experimental investigation on forced flow and heat transfer with water flowing in bilaterally heated narrow annular ducts with gap sizes of 1.0 mm and 0.9 mm. Comparing to unilaterally heating conditions, they found that bilaterally heating condition enhanced the heat transfer on the inner surface of an annulus when Reynolds number is higher and reduced the heat transfer on the inner surface of an annulus when Reynolds number is small.

Peng *et al.* (2003) also had conducted experimental investigation on the flow and heat transfer with distilled water as circulating fluid in narrow annular ducts with gap sizes of 1.0, 1.5 and 2.0 mm. Their experimental results showed that different to that of unilaterally heating conditions, the heating flux at the inner wall of an annulus had great impact upon the heat transfer between the outer wall and the circulating water, and vice versa. Compared with unilaterally heating conditions, the heat transfer at the

inner wall of an annulus will be enhanced while the heat transfer at the outer wall will be reduced slightly under the case of bilaterally heating conditions.

It is also worth noting that many theoretical investigations were devoted to bilaterally heated annuli. While it is acknowledged that many earlier numerical investigations were subject to considerable errors (Quarmby and Anand, 1969, Kays and Leung, 1963), mainly because of the inaccuracy of theoretical structure of turbulent models and the assumption of coincidence between zero shear and the maximum velocity, more accurate predictions for flow and convection in concentric annuli for all thermal boundaries may now be found in recent literature (Kaneda *et al.*, 2003, Yu *et al.*, 2005a, Yu *et al.*, 2005b, Yu *et al.*, 2005c).

Zeng *et al.* (2007) performed numerical predictions for the characteristics of convective heat transfer on the conditions of turbulent flow in bilaterally heat narrow annuli with gap size 1.0, 1.5 and 2.0 mm. They have found that heat transfer characteristics in bilaterally heated annuli are influenced both by heat flux ratio and Reynolds number. With the decrease of the ratio of heating flux at the outer wall to that at the inner wall, the Nusselt number at the inner surface of an annulus will decrease and leads enhancement to the Nusselt number at the outer wall. In addition, when the heat flux ratio is high, the Nusselt numbers at the inner wall were greater than that of the outer wall. However, when the heat flux ratio become lower than a certain value, which depends on the gap size of an annulus and the Reynolds number, the heat transfer coefficient between the outer wall of the annulus and the fluid will surpass the heat transfer between the inner wall of the annulus and the fluid. The decrease of the gap size will yields heat transfer deterioration on the inner wall of an annulus, but leads to heat transfer enhancement on the outer wall.

2.2.3 Analogy between heat transfer and pressure drop

It is always desirable to have a relation between pressure drop and heat transfer so that we can calculate one when the other is available. Since in the case of flow of fluids

through tubes there is a reasonable good correlation between heat transfer and friction factor (Monrad and Pelton, 1942), it might be expected that a similar correlation would be possible in other geometries as well. It will be useful for the sake of clarity on computing the *j*-factor to recapitulate some old analogies between momentum and heat transfer.

One of the first of analogy was postulated by Reynolds in 1874 (Churchill, 1999). His result in modern notation can be written:

$$\frac{f}{8} = \frac{Nu}{Re.Pr} \qquad 2\text{-}31$$

This was an important analogy since it allows determining the heat transfer coefficient for fluids with Pr ≈ 1 knowing the friction factor which is easier to measure. Because of limitation of Reynolds analogy, the desire of having an analogy that is applicable over a wide range of Prandtl number has led Prandtl to derive the following analogy that shifts the dependence of Nu from proportionality to $Re.\left(\frac{f}{8}\right)$ to proportionality to $Re.\left(\frac{f}{8}\right)^{1/2}$ and it reads:

$$Nu = \frac{Re\left(\frac{f}{8}\right)Pr}{1 + \delta^{+}(\mathrm{Pr}-1)\left(\frac{f}{8}\right)^{1/2}} \qquad 2\text{-}32$$

Where $\delta^{+}$is an experimental quantity depending on the momentum and energy boundary layer. The reasons of failure of the Prandtl analogy and many more developed later are beyond the scope of this investigation.

Solutions for convection equations over a flat plate for laminar flow led to the modified Reynolds analogy or Chilton-Colburn analogy described as

$$\frac{f}{8} = \frac{Nu}{Re.Pr^{1/3}} = j \qquad 2\text{-}33$$

This quantity j is called Colburn j-factor and will be used later in this study. Experimental studies show that is also applicable approximately for turbulent flow over a surface (Colburn, 1933). It is noted in Olivier and Meyer (2009) that $j = \frac{f}{8}\emptyset_w$, where $\emptyset_w$is a function of the duct geometry, the flow type, the boundary condition and the Prandtl number.

2.3 Chapter conclusion

This chapter has dealt with the archival literature for three different thermal boundary conditions: (1) heating from the inner wall of the annulus only, (2) heating from the outer wall of the annulus only and (3) heating from both walls of the annulus.

Many correlations are found in the archival literature regarding the first thermal boundary condition enumerated above, which in the practical point of view represents the most important case. Very few investigations were performed regarding the two other thermal boundary conditions.

In order to understand the thermal interferences between inner and outer walls and their impact upon pressure drop and convective heat transfer, more accurate experimental results are needed. Experimental results collected in this study will then be compared with some of the results from earlier investigations summarized in this chapter.

Experimental results obtained in this study will then be compared with some of the correlations described in here.

Chapter 3: Experimental set-up

3.1 Introduction

This chapter describes the experimental set-up and the experimental procedure followed in this study. It starts off with an overview of the components of the set-up, the experimental test section and the instruments used. Then it describes the data acquisition system used as well as the experimental procedure followed to collect data including the calibration of thermocouples and pressure transducers. Lastly, adiabatic friction factors results are presented for validation of the pressure drop experimental procedure.

3.2 Experimental facility

This section will be broken in three subsections:

a. Layout of the experimental facility
b. Test section
c. A quick description of instruments used

3.2.1 Layout of the experimental facility

Consider Figure 3-1 that gives a schematic representation of the test facility. Flowing from the storage reservoir (item 2), the test fluid was pumped through the flow loop by two electronically-controlled positive displacement pumps (items 3, 3'). The two pumps installed in parallel, were helical rotor pumps and were designed to handle mass flow rates up to 1.8 and 0.63 kg/s with respectively achievable pumping depths up to 70 and 35 m. They were controlled by vector drives coupled to the pump motors and were not intended to work simultaneously. Only one pump was used at a time, the second one was kept for back-up reasons. This lead to a configuration with two flow lines, 3-4-5-6 and 3'-4'-5'-6'.

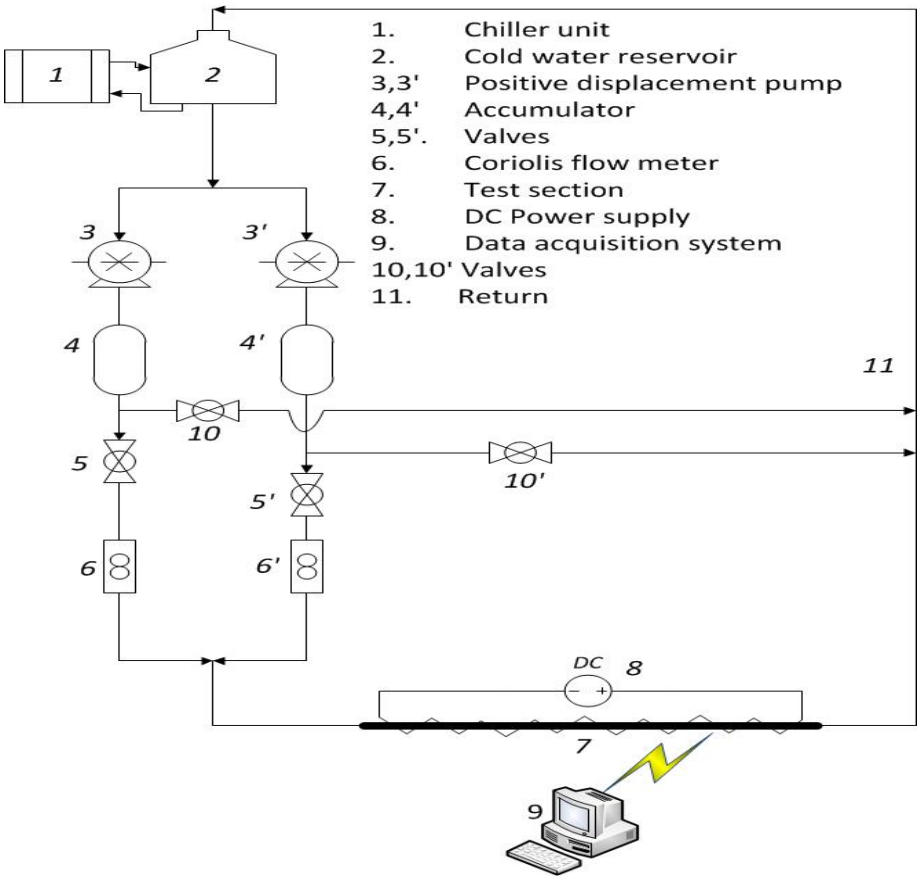

Figure 3-1: Schematic layout of the experimental facility.

On each flow line, the pump was followed by an accumulator (item 4 or 4'). It served to overcome the pulsations introduced in the system by the use of positive-displacement pumps and to ensure the stability of the flow at low flow rates. An excellent way to deal with the stability problem was also to run the pump at high flow rate and then to use a by-pass line between the pump and the return (lines 10-11 and 10-11'); flow through these by-pass lines were regulated by the appropriate ball valve (items 10 or 10'). From the accumulator, before entering the test section, the water flowed through a Coriolis flow meter (items 6 or 6') which measured mass flow rates. The two Coriolis flow meters could respectively read maximum mass flow rates of 0.61 kg/s and 1.88 kg/s and were also able to measure the fluid density or the temperature of the fluid.

Heated water from the test section (item 7) was then returned to the 2 500 litre-storage reservoir to be recycled. The storage reservoir was connected to a chiller unit which maintained the temperature in the storage tank at constant temperature of approximately 20 °C. The water that was used to fill the tank was not distilled and came from the municipal supply. Other researchers who performed previous experiments in the same laboratory did not observe any fouling problems by using this supply (Hallquist, 2012). Heat sources of the test section were fed by DC power supplies (item 8).

3.2.2 Test section

The test section, shown schematically in Figure 3-2, consisted of a horizontal annular duct manufactured from hard-drawn copper tubes. The test section had a wetted surface length of 4.795 m, an inner wall diameter of D_i = 15.88 mm (±10 μm) and an outer wall diameter of D_o = 26.76 mm (±10 μm). This resulted in an annular diameter ratio of a = 0.593 and a hydraulic diameter D_h of 10.88 mm.

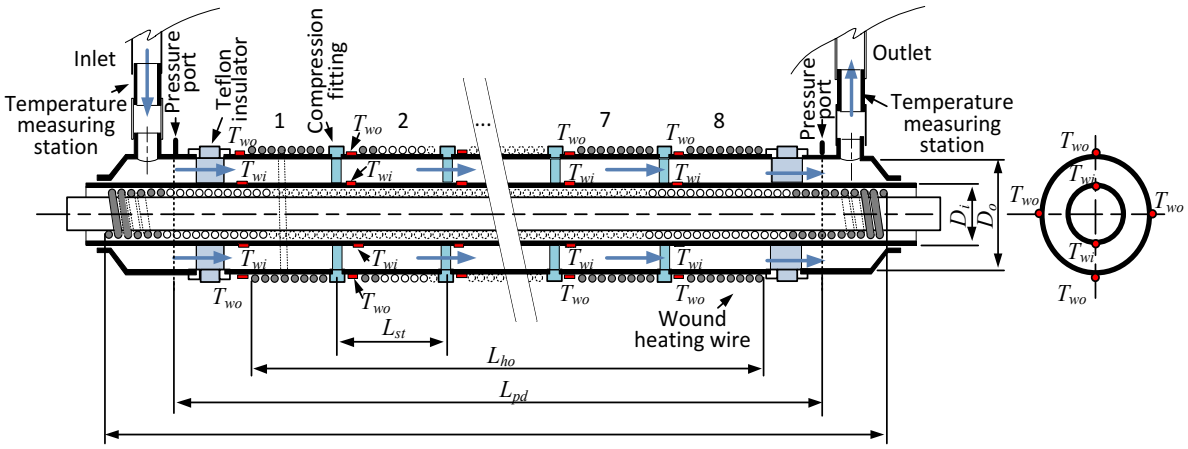

Figure 3-2 : Schematic layout of the test section

a) Inner tube construction

The inner tube of the annulus had a wall thickness of 0.71 mm and a length of 4.795 m. This also represented the overall length of the heat exchanger, of which a limited portion with a length of L_{hi} = 4.675 m (see Figure 3-2) was internally heated. The tube

had eight temperature measuring stations, each equipped with two thermocouples (one at the top and one at the bottom), which were equally spaced at L_{st} = 580 mm in the axial direction (except for the last two stations which were spaced at 640 mm). These thermocouples are labeled T_{wi} in Figure 3-2. The thermocouple tips (0.8 mm in diameter) were embedded and soldered into small grooves machined in the axial direction into the tube wall so that they were mounted as close as possible to the wetted surface. The grooves were 0.5 mm deep, 30 mm long, and 1.5 mm wide and, after the insertion of the thermocouples, were carefully refilled with tin solder (where needed) to produce a smooth tube surface. The thermocouples wires leading to the data acquisition system passed across the gap size in the annulus and were channelled through the annulus before exiting the annulus. The thermocouple leads occupied 5% of the annular flow passage cross sectional area at a typical measuring station.

b) Outer tube construction

The outer wall of the annulus was made of eight modular portions and were assembled via compression fittings. The assembled outer tube had a total length of 4.690 m and was fitting to the inner tube using coupling reducers on either end. Water-resistant flexible sealant glue was used to fill the gap between the reducer and the inner tube, as well as between the reducer and the outer tube. The outer tube also had eight temperature measuring stations, each equipped with four thermocouples (one at the top, one at the bottom, and one on either side) and were equally spaced along the length of the outer wall. These thermocouples are labeled T_{wo} in Figure 3-2. The thermocouples were attached on the walls by a soldering process in a groove previously machined. To prevent sagging of the inner tube, and to ensure that the annulus was concentric, spacers were needed at regular intervals. Therefore, each of the compression fittings were specifically manufactured to receive three 1.27 mm diameter radially aligned pins spaced at 120° as is shown in Figure 3-3. At the support positions the pins occupied 5.7% of the cross sectional area of the annular flow passage. The inner diameter of the compression fittings was also carefully machined to match

the inner diameter of the outer tube of the annulus. The pins were kept in position and sealed by using external clamps.

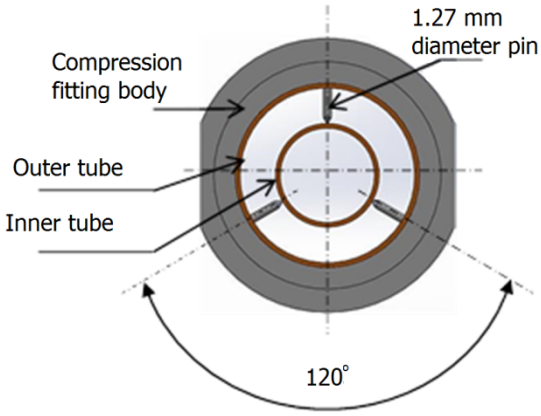

Figure 3-3: Profile of the compression fitting with pins.

A standard length of 580 mm for each modular section was retained, except for the first and last portions whose lengths were accommodated to fit the constructional needs of the inlet and outlet section of the annulus. This standard length was determined by applying a safety factor of 2 to a bending analysis performed on the inner tube. The aim of the analysis was to get the allowable length between spacers which prevent the vertical displacement (y_δ) of the inner tube from exceeding 0.55 mm or a maximal eccentricity of less than 0.1, eccentricity being defined as:

$$e = \frac{y_\delta}{D_o - D_i}$$

According to Shigley *et al.* (2006), the vertical displacement of a circular cross section is:

$$y_\delta = \frac{wx}{24EI_x}(2lx^2 - x^3 - l^3) \qquad 3\text{-}1$$

Where x is the distance along the tube length and l is the total unsupported tube length. The second moment of area is given by $I_x = \frac{\pi}{64}(D_o^4 - D_i^4)$.

The modulus of elasticity E for copper is $E = 119x10^9$ Pa. The distributed load, w, is the weight of the inner tube given as:

$$w = Mg \qquad 3\text{-}2$$

Where M is the mass of the inner tube per meter and g the gravitational acceleration.

Concentricity was important because as eccentricity increases at a given Re, the asymmetry of the flow pattern becomes more pronounced. Carlson and Irvine (1961) in their measurement of friction factors in triangular ducts in turbulent flow showed that as the asymmetry of the flow increases the smaller the friction factor. This is also valid for eccentric annulus. The same behavior affects the heat transfer rate; strong eccentricity severely reduces the heat transfer rate in the annular channel. However, many experiments (Lee and Barrow, 1964), (Maudou et al., 2011, Kline and Tavoularis, 2016) did not show any significant change on heat transfer rate or pressure for eccentricity lower than 0.1. Therefore, designing the annular channel with a maximal eccentricity of 0.1 makes disregarding the influence of eccentricity in this study a good assumption.

c) Inlet and outlet of the annulus

The inlet and the outlet ports to the annulus were perpendicular to the flow passage in the horizontal plane and were constructed from conventional industrial circular tube fittings. These ports were spaced 4.680 m apart in the axial direction and resulted in a length-to-hydraulic-diameter ratio of 430. They were equipped with temperature measuring stations to obtain the bulk fluid temperature of the entering and leaving water. Each measuring station (one directly before the inlet and one directly after the outlet) consisted of four T-type thermocouples equally spaced around the periphery of a short copper tube that was well insulated from the laboratory and the test section itself. Due to the turbulent nature of the flow, the copper tube segments adopted the relevant bulk fluid temperature. Rubber hosing was used to connect the measuring

stations to the test section and the flow loop tubing in order to reduce thermal heat conduction.

Since the outer wall was in direct contact with the heating wires, it was thermally isolated from the inlet and the outlet regions with Teflon connectors (see Figure 3-4), to reduce axial conduction from the test section which may influence water temperature measurements and affect the thermal boundary condition on the outer wall. The thermal conductivity of Teflon was 0.23 W/(m.K). The Teflon isolator with female thread was tightened in an aluminium compression seat which was coupled to the outer tube of the annular duct through a brass ferrule and compression nut.

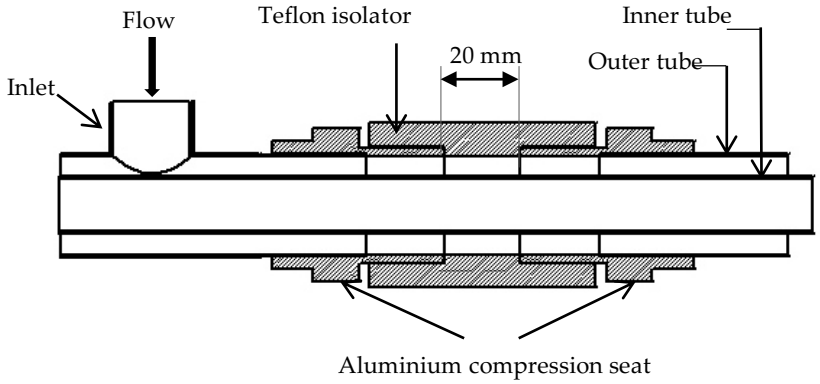

Figure 3-4 : Section view of the isolator

Additional thermocouples were used to read the temperatures of the surrounding lab, the insulation, the inner and the outer heaters. Each of these measurements was obtained by using the average of two thermocouples placed at the same location. All thermocouples were calibrated using a PT 100 with an accuracy of 0.1°C.

d) Pressure ports

Two pressure ports having an outer diameter of 3 mm were positioned in the vertical plane at an axial distance of L_{pd} = 4.640 m from each other (See Figure 3-2). They were connected with the annulus through a 0.8 mm-diameter drilled hole. The diameter of this hole was designed according to Rayle (1959), whose publication suggests that the diameter of the hole should be smaller than 10% of the outer tube's inner-diameter.

This ensured that the taps did not cause significant flow obstruction within the tube, which could lead to a localised eddy forming within the tap resulting in an error in pressure readings. 3-mm inner-diameter-nylon tubing was used to connect the pressure port to the differential pressure transducer. Once incorporated into the test section, water was pumped through the system and the nylon tube was bled of air.

e) Thermal boundary achievement

The thermal conditions in the heat transfer segment of interest in this work were constant surface heat fluxes on the inner wall and the outer wall of the annulus. This could have been realized coiling an electrical resistance wire around the tube or by direct Joule heating of the tube by sending current through it if the tube is manufactured from high electrically uniform material. The last option appears to be relatively expensive and resulted in a significant risk of electrocution. Therefore, the first option, making use of wound resistance wire was adopted for the design of the thermal boundary condition.

The achievement of some levels of heat fluxes aimed in this study could have led to significantly high temperatures of the heating elements and could have resulted into significant changes of the electrical resistance of heating wires if common material for resistance wire was used (such as Nichrome which is widely used as heating wire). The temperature dependency of the electric resistance of a conducting material to temperature is generally given by:

$$R = R_{T0}(1 + \alpha\,(T - T_0)) \qquad 3.1$$

Here R_{T0} and R are respectively the resistances at temperatures T_0 and T. α is the temperature coefficient and differs from material to material. It may be positive or negative and could also be temperature dependent. For most materials, electrical resistivity decreases with an increase in temperature. In this study the designed heating wire was made of constantan. It has the following benefit applications: its

electrical resistance varies slightly with the temperature and α is not significantly temperature dependent. For constantan, literature gives α to be equal to -3×10^{-5}/°C in the temperature range of 0 to 100 °C for a straight wire. In the particular case of the heating wire used in this study in its actual geometrical configuration, this value was experimentally determined to be -15×10^{-5} /°C by testing of samples.

Inner heating element

The inner wall of the annulus was heated by inserting a heating rod inside the inner tube. The heating rod was constructed using Gauge 30 heating wire (height : 0.6 mm; width : 1mm) coiled around a 12.7 mm-diameter tube. Six heating wires of 341 ohms each were spiralled in parallel with no gap. Multiple wire were used to limit the current in each wire. From initial tests, it was found that each of these wires could carry a DC current of up to 2 A. A maximum allowable current of 1.8 A per wire was, however, adopted in order to not exceed a DC voltage drop of 620 V across each heating element wire for safety reasons. Therefore, a combined total power rate of 6700 W could be supplied to the 6 heating elements. Power cables which were not in contact with the heat transfer area were made of copper and insulated. To keep the heating wires aligned, a heat-resistant (clothed) tape was wrapped over the wires and the remaining gap (0.5 mm) between the inner heater and the inner wall was filled with heat sink compound which had a thermal conductivity of 0.5 W/ (m^{2}K). The length of the inner heater $L_{h,i}$ was 4.675 m (see Figure 3-2)

Outer heating element

To obtain constant heat flux on the outer tube of the annulus, a gauge 24 (height : 1.3 mm; width : 1.9 mm) heating wire was wound around the outer tube. Four wires of 64 ohms each were connected in parallel and were spiralled with a gap of 5 mm. One wire was able to carry electric current of up to 5.5 A. This led to a maximal power rate of 7600 W which could be supplied from the outer surface of the annulus. Special care was taken when wrapping the heating element to ensure that they were not positioned too closely to the thermocouples attached to outer tube which could result on

inaccurate outer wall temperatures. The heating elements were able to provide a maximum heating flux of 21 000 W/m^2 on the inner tube and 18 000 W/m^2.

f) Insulation and heat losses

Outer heater

The entire test section was insulated with 63 mm of armaflex insulation whose thermal conductivity was 0.036 W/(m^{2}K) according to the specification sheet of the manufacturer. A one-dimensional heat loss calculations were conducted with an approximation of what may be the temperature of the heating element for different heat fluxes at a Reynolds number of 8000, as it will be in the range to be tested. A summary of the expected heat loss rates are given in Table 3-1, along with the anticipated percentage of the total heat input that would have been lost to the surrounding via the insulation layer. It can be seen that for all that heat fluxes, the heat losses were estimated to be less than 1% of the total heat input.

Table 3-1: Estimate of the outer heater temperatures and heat losses for different heat fluxes at Re = 8000

Heat Flux [W/m^2]	**3500**	**7000**	**10 500**	**14 000**	**17 500**	**21 000**
Heater Temperature [^{o}C]	37.9	57.7	77.5	97.3	117.1	136.8
Heat loss to surroundings	0.88%	0.93%	0.94%	0.95%	0.95%	0.96%

These values were expected to slightly increase as the Reynolds number decreases toward 4 000, and visa-versa for increasing Reynolds numbers.

Inner heating element

The inner gap of the tube used in the inner heating rod was filled with air which is a better insulation material than armaflex used for the outer tube, however, this technique is subjected to radiation. If it were to be assumed that the wall of the inner

heater had the same temperature as the heating element, heat loss by radiation is given by:

$$\dot{Q}_{rad} = A_s F \varepsilon \sigma (T_{wall}^4 - T_{amb}^4) \qquad 3.2$$

With A_s the wall area, F the view factor, ε the emissivity of the polished copper ≈ 0.052 T_{amb} the absolute ambient temperature. By taking the maximum wall temperature value of T_{wall} to be equal to 120°C and the surrounding temperature, T_{amb} to be 20°C, it was found that $\dot{Q}_{rad} = 7.5\ W$. (This conservative value was computed with a view factor close to 1 while it is expected to be close to zero). Therefore the heat loss on the inner wall was less than 1% the value of heat rate to be supplied through the inner wall and this value was expected to become even lower for high heat rates.

Correction on wall temperature measurements

The temperatures of the outer surface of the inner tube and the inner surface of the outer tube of the annulus were needed to determine the heat transfer coefficients. Thus, the thermocouple measurement on the inner and outer tube walls had to be used and adjusted to take into account the temperature drop due to conduction across the wall thickness from the radial position where the thermocouple tips were placed to the radial position of the wetted surface.

The temperature drop was calculated from the following equation:

$$\Delta T_{drop} = \frac{\dot{Q}_w}{\left(\frac{2\pi L k}{\ln\left({}^{r_2}/_{r_1}\right)}\right)} \qquad 3\text{-}3$$

Where $\dot{Q}_w$ is the power supplied through the heated wall, $L = L_{h,i}$ or $L_{h,o}$ is the length of the heated wall, k is the thermal conductivity of the material between the tip of the thermocouple and the fluid. (Copper for the inner surface of the outer wall of the annulus and tin-lead soft solder for the outer surface of the inner wall of the annulus). The thermal conductivity of the copper was obtained from Abu-Eishah (2001) and that

of the tin-lead soft solder was found from the manufacturer datasheet and it was estimated at 50 W/(m.K). Table 3-2 gives an estimate of typical values of temperature drop. In general the temperature drop was less than 0.1°C. For heating of outer wall, these corrections could be ignored in the calculation without any loss of accuracy because of the small impact it had on the average wetted wall temperature calculations.

Table 3-2: Typical values for temperature drop for wall measurements.

	Inner wall heated				Outer wall heated			
$\dot{Q}_w$.(W)	1490	2235	3370	4560	1300	2600	3930	5410
ΔT_{drop}.(°C)	0.032	0.048	0.072	0.097	0.003	0.005	0.008	0.011

g) Additional instruments

DC power supplies

Elektro-automatik controlled-laboratory-power supplies were used to provide DC current for heating elements. These devices are microprocessor-controlled and can thus deliver fast and accurate measurement and indication of actual values of 0.2 % of the nominal voltage, current and power level. They are equipped with a flexible auto ranging output stage which provides a higher output voltage at lower output current, or a higher output current at lower output voltage, always limited to some specified maximum nominal output power. A single unit can deliver output voltages of between 16 V and 360 V, output currents between 4 A and 30 A and output power ranges of between 320 W and 3 000 W. Connecting more than one unit in series, an output voltage of 660 V can be achieved. This was the configuration used in this study when a high voltage was required.

Pressure transducers

A DP 15 typical variable reluctance pressure transducer was used to measure pressure differences. It consisted of a diaphragm of magnetically permeable stainless steel

clamped between two blocks of stainless steel. This pressure transducer was used in combination with a CD 208 Modular multi-channel unit for excitation and signal conditioning. This four-channel CD 280 contains a plug-in power supply and four plug-in carrier demodulators. Each channel converts full scale AC carrier signal as low as 17 mV/V to an output of +-10 V (DC) with individual zero and span adjustments.

Two diaphragms (rated 8.6 kPa and 22 kPa) were used, depending on the anticipated pressure drop in the test section. The diaphragms were calibrated using a 3 m water column in conjunction with a relatively high accurate T140 pressure calibrator (0.025 % accuracy in terms of its full scale value of 200 kPa).

3.2.3 Data acquisition system

The measurement process involved several steps between the measured quantity and the data output that is proportional to it. Most of the transducers used in modern measurement practice operate with electrical/electronic signal conditioning. Since the experimental setup used several measuring instruments (thermocouple, pressure transducer, flow meter) to monitor and acquire various process variables, a multi-channel digital data logger attached to a computer was required. A National Instrument data logger supplied with general purpose software (Labview 2010) was used for creating virtual instruments based on add-on cards that reside in the slots available in a PC.

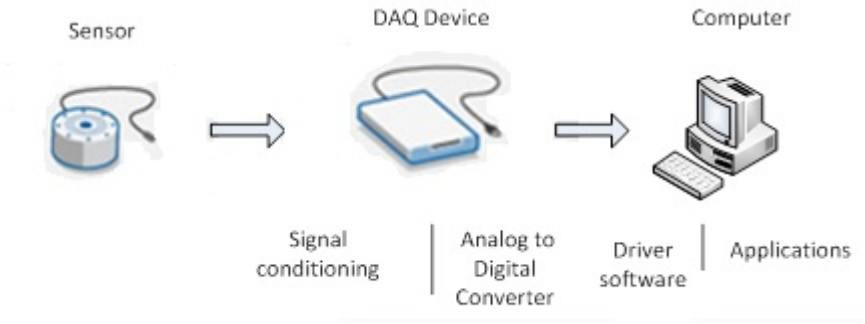

Figure 3-5: Flow diagram of the DAQ system.

3.3 Experimental procedure

This section describes the procedure followed to collect the experimental data. Before any experimental work was conducted all measuring components and devices were calibrated

3.3.1 Calibration of thermocouples

Thermocouples were calibrated with a PT100 temperature probe with an accuracy of 0.1 °C. At least seventeen data points were taken between 15 °C and 55 °C upward and downward, with any single data point being represented as an average of 120 readings. Each thermocouple channel output was plotted against the PT100 output and a fitting polynomial curve was determined for each thermocouple as shown in Figure 3-6.

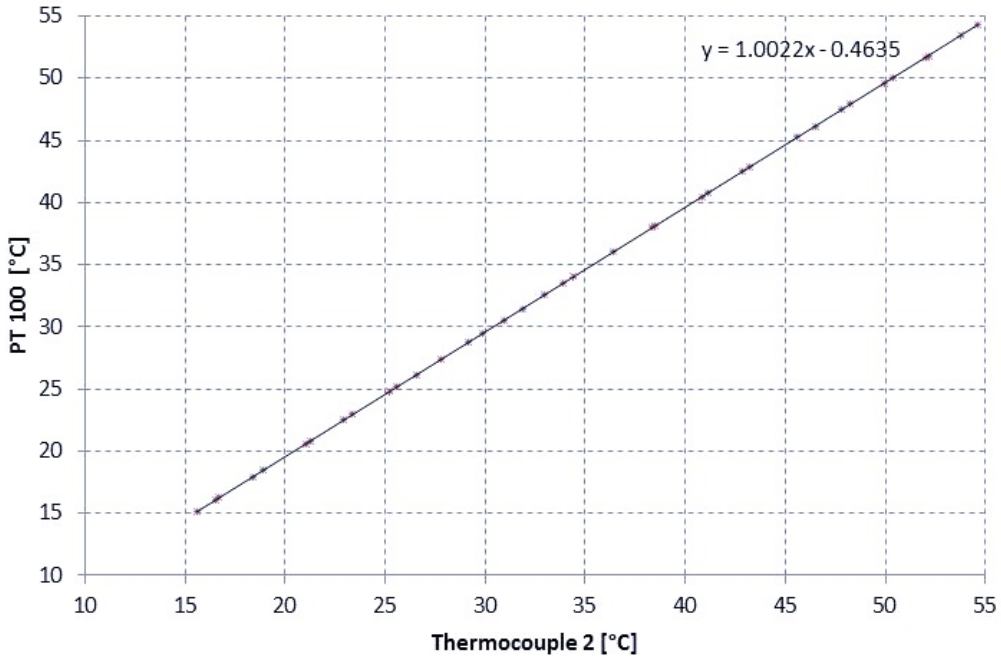

Figure 3-6: Calibration curve for thermocouple 2 on the inner tube.

3.3.2 Calibration of pressure transducers

The diaphragms were calibrated using a 3 m water column in conjunction with a relatively high accurate T140 pressure calibrator (0.025 % accuracy in terms of its full

scale value of 200 kPa). Its two-port differential design allows to connect in parallel the pressure transducer and to measure the exact static pressure. A calibration curve of the 22 kPa-diaphragm is given below (Figure 3-7).

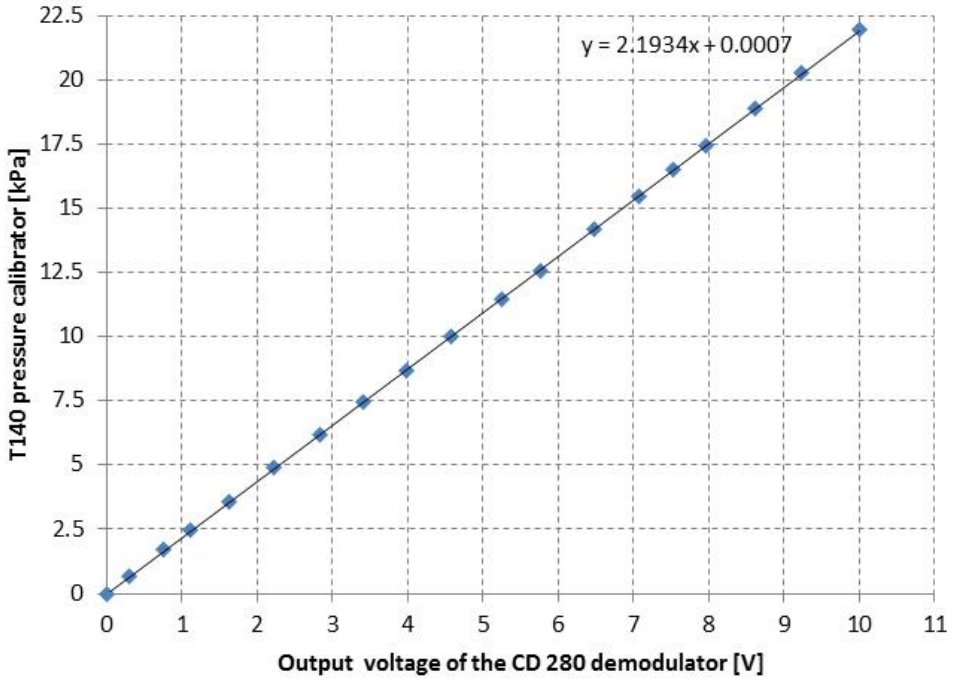

Figure 3-7: Calibration curve of the pressure transducer

3.3.3 Capturing of results

After the test facility system was switched on, it was important to eliminate the thermal inertia of the water loop system to efficiently achieve steady-state conditions. This was done by operating the facility without changes at high flow rates. Pressure transducers were also primed to assure that there were no air bubbles in the system which could lead to inaccurate pressure readings.

Once the thermal state of the facility was stabilised, the mass flow rate was set approximately to the desired value for conditions during which data were to be captured. There-after the heating elements were switched on and were brought gradually to the desired value in order to achieve the specified heat flux. Since, when adding heat it changes the fluid properties, small changes were made to the flow rate

until steady-state conditions were achieved. Standard deviations of each measurement were used to define steady-state conditions.

The threshold for the standard deviation on each measurement in best case should not exceed the half value of the expected uncertainty or accuracy. For instance, thermocouple reading was considered to be at steady state once its standard deviation for the last minute of measurement was less than 0.05°C; mass flow rates were considered steady when the standard deviation was less than 0.07 %, while that of the pressure drop less than 0.6°% for the small diaphragm and 0.8°% for the big diaphragm.

After the heating elements were switched on and changes were made to the mass flow rate, it took approximately twenty minutes to an hour for steady state conditions to be achieved. Data were only captured once these conditions were met and an energy balance error of less than 1.5% was achieved. Here the energy balance error was defined as the ratio of the heat loss to the average of the input and output heat rates. This energy balance criterion could not be achieved in some low heat fluxes cases for heating from the outer tube. In these circumstances data were captured in any case once steady state conditions were achieved.

The Labview data logger program allowed for monitoring whether steady state-conditions were reached, by displaying inlet and outlet temperatures, heaters temperatures, energy balances, Reynolds numbers and heat fluxes. The program was implemented to allow the data to be automatically captured with regard of parameters of interest, namely the Reynolds numbers and the applied heat fluxes.

With regard to the capturing of data, one file for each mass flow rate (or Reynolds number) was used. Each file consisted of 120 data points with each point being captured at a rate of 3 Hz. These 120 data points were averaged to obtain a single value which was used in the calculations that followed during data analysis phase. The files

contained thermocouple, pressure drop and mass-flow readings. Currents and voltage were recorded manually.

Three series of experiments were conducted. In the first series, the inner wall was heated and the outer wall was insulated. Four different heat flux densities were applied on the inner wall. Each flux was tested with twelve different Reynolds numbers unequally distributed between 5 800 and 12 000. In the second set of tests, the outer wall was heated and the inner wall insulated. Similarly, four different heat fluxes were tested with twelve different Reynolds numbers unequally distributed in the same range values as for the inner wall-heated condition. The last series were obtained for the case of simultaneous heating of both walls with eight combinations of heat flux densities (four levels for the outer tube and two levels for the inner tube). Results were presented for two Reynolds numbers.

In total 116 cases of heat transfer and pressure drops will be presented in this work

3.4 Validation of adiabatic friction factor results

The validation friction factor data consisted of a total of 40 data sets with 120 data points per set. The data sets consisted of both increasing and decreasing increments of the Reynolds numbers which spanned for Re = 4 000 to 18 000. These friction factor measurements were taken for adiabatic flow, without any heat transfer to eliminate any varying density and viscosity effects to ensure that results could be compared with correlations developed for adiabatic cases.

In Figure 3-8, the experimental results are compared with the correlations of Jones and Leung (1981), Kaneda *et al.* (2003) and Gnielinski (2009) presented in the literature study.

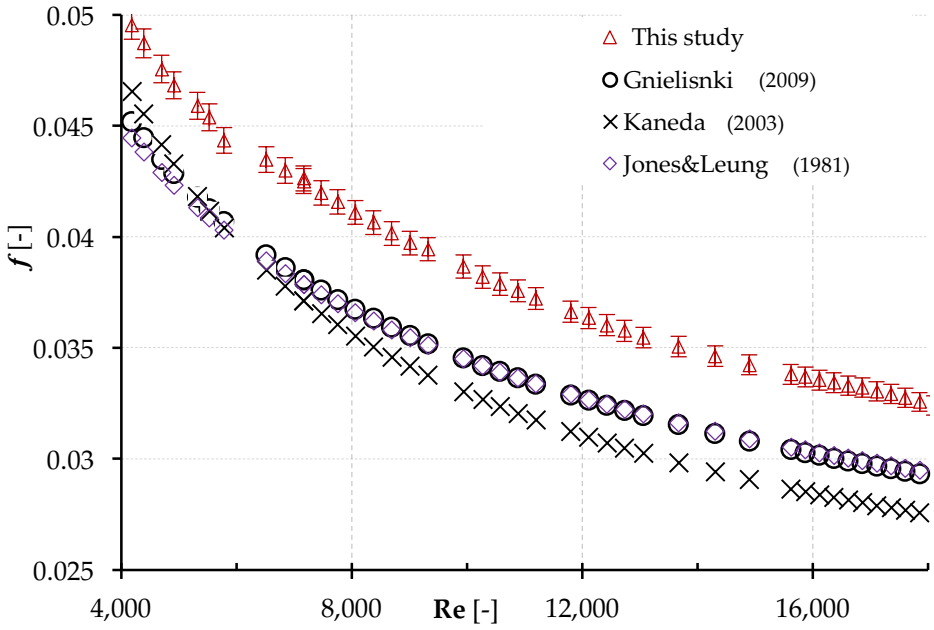

Figure 3-8 : adiabatic friction factor for Reynolds numbers between 4 000 and 18 000

The correlations of Gnielinski and, Jones and Leung under-predict the experimental result on average by 11 % while the correlation of Kaneda *et al.* under-predicts the experimental result by 16 % with lower values (6 %) for the lower Reynolds numbers.

These larger values of friction factors may be attributed to additional disturbances introduced in the flows: spacers to ensure concentricity, thermocouples to take reading from the inner wall of the annulus, coupling used in the construction of the outer tube. worked on a similar outer tube construction and reported larger friction factors.

3.5 Chapter conclusion

In this chapter, an overview of the experimental facility and set-up was supplied, along with the experimental procedure used to collect steady state data for unilateral and bilateral annular wall heating conditions. A validation of adiabatic friction factors results was also described. The next chapter will focus on data reduction methods and uncertainty analysis.

Chapter 4: Data reduction and uncertainties

The objective of the experiment was to obtain the necessary data to determine the heat transfer coefficients and friction factors for a given annular diameter ratio over the turbulent flow region by applying different thermal boundary conditions. This chapter has two main sections. In section 4.1 the data reduction method is discussed. All equations used to define parameters of interest are developed. Section 4.2 presents a summary of expected uncertainties for all measurements. A short conclusion will close the chapter.

4.1 Data reduction

Depending on the heat exchanger flow configuration, many approaches can be used to determine heat transfer coefficients. Widely used methods include the temperature averaged and LMTD (Logarithmic Mean Temperature Difference) heat transfer coefficients methods. This study will only deal with the LMTD heat transfer coefficients. Equations for the energy balance, *j*-factors and friction factors are also developed.

4.1.1 Wall temperature measurement

Throughout calculations made in this study, wall temperature measurements were obtained by extrapolation from the polynomial fit of the thermocouples placed along the length of the heat exchanger. For all the Reynolds numbers tested, a fitting curve was used to predict the temperature of the heated wall.

The goodness of a fitting curve to experimental data was determined by computing the coefficient of determination of the fitted curve. This coefficient usually noted as R^2, compares the estimated value and the actual value of the dependent variable (in this case the temperature as a function of the independent variable, the axial length of the annulus) and ranges in value from 0 to 1. A value of $R^2 = 1$ means that there is a perfect correlation between the estimated value and the actual value. At the other extreme,

R^2 = 0, the regression equation is not helpful in predicting the dependent variable (Gujarati and Porter, 2008).

4.1.2 Average LMTD heat transfer coefficients

For a concentric annulus, two average heat transfer coefficients can be defined depending on whether the inner wall or the outer wall is considered (replace x with i for inner and o for outer wall):

$$h_x = \frac{\dot{Q}_{w,x}}{A_{s,x}\Delta T_{LMTD}} \quad 4\text{-}1$$

Here $\dot{Q}_{w,x}$ is the heat transfer rate to the fluid, $A_{s,x}$ is the heat transfer area and ΔT_{LMTD} is the logarithmic mean temperature difference defined in terms of the relevant wall temperature.

The heat rate supplied by the inner heating element to the fluid, $\dot{Q}_{w,i}$, is

$$\dot{Q}_{w,i} = R_i I_i^2 - \dot{Q}_r \quad 4\text{-}2$$

Here $R_i I_i^2$ is the electric power dissipated by the inner heater, R_i being the electric resistance of the inner heating element and I_i the electric current flowing through the electric resistance. The resistance R_i is

$$R_i = \frac{U}{I_i} \quad 4\text{-}3$$

With U being the voltage across the inner heating element. U and I_i are read of the digital display across the inner heating element. $\dot{Q}_r$is the heat loss due to the radiation of the inside of the inner heating element to the surrounding.

$$\dot{Q}_r = A_{s,i} F \varepsilon \sigma (T_{heater}^4 - T_{amb}^4) \quad 4\text{-}4$$

Here

- $A_{s,i}$is the inside area of the inner heating element;

- F is the view factor;
- ε is the emissivity of the polished copper that made the inside area of the inner heating element;
- σ is the Stefan-Boltzmann constant;
- T_{heater} is the temperature of the inner surface of the inner heating element that was obtained by taking the arithmetic average reading of the two thermocouples placed on the inner surface;
- T_{amb} is the temperature of the surrounding lab that was obtained by taking the arithmetic average reading of the two thermocouples used to monitor the laboratory temperature.

$\dot{Q}_r$ could not exceed 1% of the power supplied by the inner heating element.

The heat rate supplied by the outer heating element to the fluid, , $\dot{Q}_{w,o}$, is

$$\dot{Q}_{w,o} = R_o I_o^2 - \dot{Q}_l - \dot{Q}_r \qquad 4\text{-}5$$

Here $R_o I_o^2$ is the electric power dissipated by the outer heater,

$$R_o = \frac{U}{I_o}$$

being the electric resistance of the outer heating element and I_o the electric current flowing through the electric resistance. $\dot{Q}_r$ is the heat loss due to radiation of the outer layer of the insulation to the surrounding and is very negligible as the temperature difference between the outer insulation and the surrounding was low (<5°C). $\dot{Q}_r$will be dismissed in calculation. $\dot{Q}_l$ is the heat loss due to conduction through the insulation and could be expressed as:

$$\dot{Q}_l = \frac{2\pi L_{h,o} k\,(T_{heater} - T_{amb})}{\ln\left(\frac{D_{ins,o}}{D_{ins,i}}\right)} \qquad 4\text{-}6$$

Here

- $L_{h,o}$is the length of the outer segment being heated;
- k is the thermal conductivity of the insulation material as supplied by the manufacturer datasheet;

- T_{heater} is the temperature on the outer surface of the outer heating element and is obtained by the average temperature of two thermocouples placed on the outer heating element;
- $D_{ins,o}$ and $D_{ins,i}$ are respectively the outer and inner diameter of the insulation.

In equation 4-1, ΔT_{LMTD} is the logarithmic average temperature difference between the inlet and the exit end of the annular duct, is defined as:

$$\Delta T_{LMTD} = \frac{(T_{wx,in} - T_{in}) - (T_{wx,out} - T_{out})}{ln[(T_{wx,in} - T_{in})/(T_{wx,out} - T_{out})]} \quad 4\text{-}7$$

Here $T_{wx,in}$ and $T_{wx,out}$ are the temperatures of the wall at the start and the exit of the heated surface respectively. They were obtained by extrapolation from the polynomial fit of temperatures from the thermocouples placed along the length of the heat exchanger. T_{in} and T_{out} are the bulk fluid temperatures at the inlet and the exit respectively of the annular duct. They were obtained by taking the arithmetic average reading of the four thermocouples used for inlet temperature and outlet temperature measurement.

The heat transfer coefficient was computed at different Reynolds numbers defined as:

$$Re = \frac{\dot{m} D_h}{\mu A_c} \quad 4\text{-}8$$

Here μ, as well as other thermophysical properties such as C_p, Pr, ρ or k were calculated using the fluid property correlations for saturated liquid water by using the method suggested by Popiel and Wojtkowiak [43]. $\dot{m}$, the mass flow rate across the annulus, was obtained by reading of the coriolis flow meter. A_c, the annulus cross sectional area, is computed as:

$$A_c = \frac{\pi}{4}(D_o^2 - D_i^2) \quad 4\text{-}9$$

The corresponding Nusselt number Nu_x is defined as:

$$Nu_x = \frac{h_x D_h}{k} \qquad 4\text{-}10$$

Where k is computed at the average bulk fluid temperature, determined as the arithmetic average between the inlet and the outlet fluid temperatures as measured at the inlet and outlet annular measuring stations.

4.1.3 Local LMTD heat transfer coefficients

The annular flow passage was also subdivided into eight control volumes to allow the computation of the local Nusselt number over the axial length of the annular duct. Figure 4-1 shows how the control volumes were defined. Dashed lines in gray indicate delimitations on control volumes in the case of heating the annular duct form the inner wall only, while dashed lines in red indicate the boundaries of control volumes for the case of heating the annular duct from the outer wall or in the case of bilateral heating.

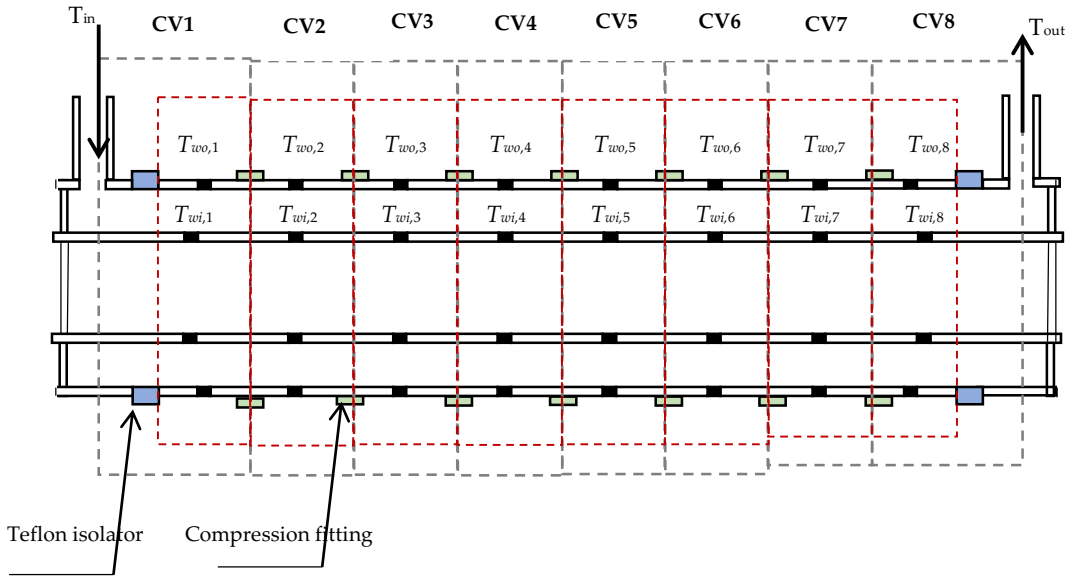

Figure 4-1: Annular duct subdivided into eight control volumes for local Nusselt number.

For each control volume (CV), the logarithmic mean temperature difference is given by:

$$\Delta T_{LMTD} = \frac{(T_{wx,in,cv} - T_{in,cv}) - (T_{wx,out,cv} - T_{out,cv})}{ln[(T_{wx,in,cv} - T_{in,cv})/(T_{wx,out,cv} - T_{out,cv})]} \quad 4\text{-}11$$

Where $T_{wx,in,cv}$, $T_{wx,out,,cv}$ are the temperatures of the wall at the start and the exit of each control volume respectively, and $T_{in,cv}$, $T_{out,cv}$ are the inlet and outlet bulk fluid temperatures for each of the control volume respectively and are obtained from the energy balance equation. $T_{wx,in,cv}$, $T_{wx,out,,cv}$ are obtained by extrapolation from the polynomial fit of the thermocouples placed along the length of the heated portion of the annular duct.

For a control volume i (i = 1, …, 8),

$$T_{in,cv,i} = T_{out,cv,i-1} \quad 4\text{-}12$$

$$T_{out,cv,i} = \frac{\dot{Q}_{w,x,cv}}{\dot{m}C_p} + T_{in,cv,i} \quad 4\text{-}13$$

with the exception of the CV located at the annulus inlet and outlet where

$$T_{in,cv,1} = T_{in} \quad 4\text{-}14$$

$$T_{out,cv,8} = T_{out} \quad 4\text{-}15$$

For the case of bilateral heating, $T_{in,cv,1}$and $T_{out,cv,8}$ are to be corrected using energy balance equation to take into account the fact that the fluid is slightly heated by the heat flux on the inner wall as the inner heating element is slightly longer than the outer heating element.

In equation 4-13, $\dot{Q}_{w,x,cv}$ is heat rate supplied by the heating element over the control volume to the fluid. The heat transfer coefficient and the Nusselt for each control volume are defined as in equations 4-1 and 4-10 with thermal physical properties at the bulk fluid temperature of the control volume ($T_{bulk,CV} = (T_{in,CV} + T_{out,CV})/2$).). The local bulk fluid temperature at the outlet of each control volume was obtained by

applying the energy balance principle based on the input heat flux values. Because the heat flux input was constant, the bulk fluid temperature along the length of the heat exchanger was linear as will be seen at a later stage of this chapter.

4.1.4 Energy Balance

To measure the proficiency of the thermal system under study, energy balanced was calculated by comparing the heat transfer generated by the source (the heating elements), $\dot{Q}_{input}$, to the heat transfer gained by the receiver(Fluid), $\dot{Q}_{output}$. It reads:

$$eb = \frac{\dot{Q}_{input} - \dot{Q}_{output}}{(\dot{Q}_{input} + \dot{Q}_{output})/2} \qquad 4\text{-}16$$

Where $\dot{Q}_{input} = \dot{Q}_{w,i}$ or $\dot{Q}_{w,o}$for the case of unilateral heating (only one wall heated) or $\dot{Q}_{input} = \dot{Q}_{w,i} + \dot{Q}_{w,o}$ for the case of bilateral heating (both walls heated) and

$$\dot{Q}_{output} = \dot{m}C_p(T_{out} - T_{in}), \qquad 4\text{-}17$$

4.1.5 Friction factor

The friction factor can be obtained via the Darcy Weisbach equation:

$$f = \frac{2\,.D_h\,.\Delta P}{\rho\,.V^2\,.L_{pd}} \qquad 4\text{-}18$$

This can be rewritten as:

$$f = \frac{2\,\rho D_h A_c^2 \Delta P}{L_{pd}\dot{m}^2} \qquad 4\text{-}19$$

Here the density of the fluid ρ was evaluated at the average bulk fluid temperature and ΔP was the measured pressure drop (obtained from the calibrated pressure transducer) over the pressure drop length L_{pd}.

4.1.6 Calculation of m

It was earlier reported that by using equation 2-8, $\frac{f}{f_a} = \left(\frac{\mu_b}{\mu_w}\right)^{-m}$, there is a means of correlating the diabatic friction factor to the adiabatic friction factor. From the experimental results, the exponent of the temperature-dependent term, m, can be computed by rewriting the aforementioned equation:

$$m = \frac{\ln \frac{f_a}{f}}{\ln \frac{\mu_b}{\mu_w}} \qquad 4\text{-}20$$

Here f_a is obtained from equation 4-19 for adiabatic test conditions where there was not heat transfer, f is obtained from the same equation where there is heat transfer, μ_b the viscosity at the average bulk fluid temperature and μ_w viscosity ratio at the near-wall temperature

4.1.7 j Factor

The j-factor was defined as:

$$j = \frac{Nu_{LMTD}}{Pr^{2/3}Re} \qquad 4\text{-}21$$

Where Pr and Re were calculated based on the average bulk fluid temperature.

4.2 Uncertainties

The uncertainties of measuring variables are described in this section. A full description on how to compute the uncertainty values are given in Appendix A. These uncertainties were calculated according to the method of Kline and McClintok (1953). Each variable is specified as the measured value plus its uncertainty. The uncertainty is calculated as the Euclidean norm of the bias or fixed errors B_i and the precision or random errors P_i

$$\delta x_i = \sqrt{B_i^2 + P_i^2} \qquad 4\text{-}22$$

4.2.1 Instruments

a) Thermocouples

An average standard deviation of 0.02 °C of the temperature reading combined with a 95% confidence interval leads to a total uncertainty of 0.11 °C.

b) Coriolis flow meters

The manufacturer specified a mass flow rate measurement error of 0.1 % of the measured value. The precision for the Coriolis flow meters with the specified amplifiers was approximately 0.09%. An overall uncertainty of 0.14% was expected for mass flow rate measurement

c) Pressure transducers

Each diaphragm has accuracy or bias of 0.25% of the full-scale value. The precision is determined by the standard deviation of 120 readings. The results are given in Table 4-1

Table 4-1 : Expected measurement uncertainties for pressure transducer (FS: Full scale).

Range	Bias	Precision	Average uncertainty
0 -8.6 kPa	0.25% (FS)	0.9%	1.32%
0 – 22 kPa	0.25% (FS)	1.1%	1.38%

d) Power supplies

As it will be discussed in the next chapter, it was needed to know the resistance of the heating wire as well as the current in order to determine the heat rate. The laboratory power supply model has an allowed maximum deviation of 720 mV when reading the voltage and a 0.06 A when reading current. The resistance of the cable leads were

determined using the Agilent 34970A, Data Acquisition/Swicth Unit. A summary of uncertainty of electrical quantities is given in Table 4-2.

Table 4-2: Uncertainties on electrical quantities.

	Lowest value	Highest value
Voltage	0.14 %	0.51 %
Current	0.32 %	1.17 %
Resistance	0.41 %	1.19 %

4.2.2 Fluid properties

Popiel and Wotjtkowiak (1998) presented simple formulas of thermophysical properties of liquid water for heat transfer calculations from 0 °C to 150 °C. With the exception of viscosity and the Prandtl number, the maximum errors in terms of steam table entries are less than 1 %. Table 4-3 summarizes appropriate uncertainties for properties of interest.

Table 4-3: Uncertainties on thermal physical properties

Fluid Property	Uncertainty
Density	0.004%
Dynamic Viscosity	1%
Specific Heat	0.04%
Prandtl number	2.3%
Thermal conductivity	1%

4.2.3 Calculated parameters

The uncertainty of parameters of interest, Nusselt numbers and friction factors, were determined taking into account uncertainties of variables influencing these parameters. An indication of the expected relative uncertainty on the Nusselt number for Reynolds numbers ranging from 4 000 to 16 000 with different inner wall heat fluxes is given in Figure 4-2. More information on the method used to calculate the Nusselt number and other parameters are supplied in the next chapter. It can be seen that for

heat fluxes above 7000 W/m² the Nusselt number uncertainty was below 6%. Similar uncertainty values were obtained for outer wall heating. (More detailed information is described in Appendix A).

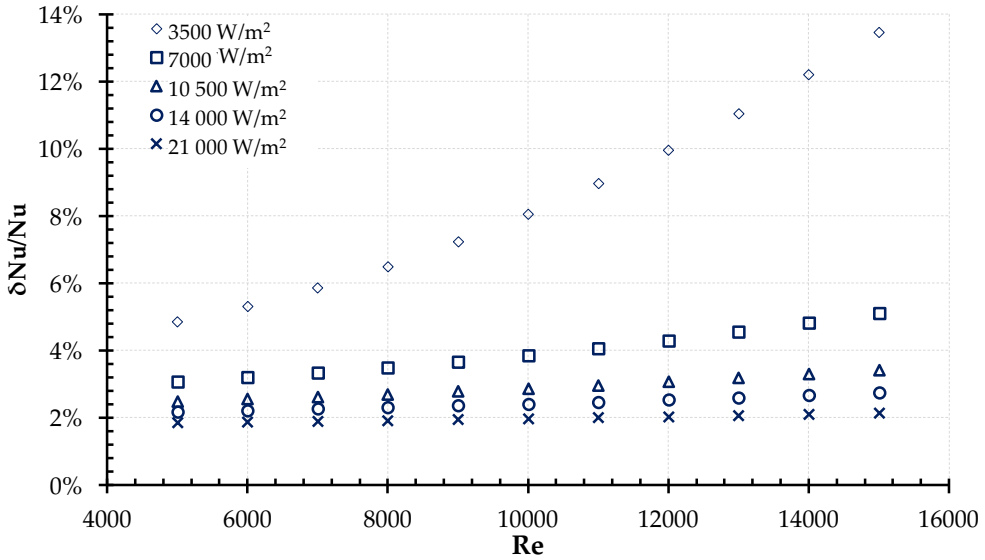

Figure 4-2: Estimates of uncertainties for Nusselt number in the case of inner heating of annulus for different fluxes and Reynold number.

It can also be seen from Figure 4-2 that the relative uncertainty of the Nusselt number at a given Reynolds number increases when the heat flux decreases and it increases with increasing Reynolds number for the same heat flux.

This behaviour can be readily understood when examining the elements that constitute the relative uncertainty of the Nusselt number. By referring to Appendix A, a better understanding can be obtained of the method proposed by Moffat (1988). The following equation is used to compute the uncertainty of a function R of n independent variables $x_1, x_2, \ldots, x_n$

$$\delta R = \left\{ \left(\frac{\partial R}{\partial x_1} \delta x_1 \right)^2 + \left(\frac{\partial R}{\partial x_2} \delta x_2 \right)^2 + \cdots + \left(\frac{\partial R}{\partial x_3} \delta x_n \right)^2 \right\}^{\frac{1}{2}} \qquad 4\text{-}23$$

where δx_i is the uncertainty of the variable x_i and $\frac{\partial R}{\partial x_i}$ the partial derivative of R with respect to x_i.

The method has the effect of suppressing terms which are smaller than a third of the largest term. Then when the temperature difference is small, the terms related to temperature difference weighs more than the other terms in the definition of the Nusselt number. It is obvious that the temperature difference is small when heat fluxes are relatively small for a particular Reynolds number or when the Reynolds numbers are getting higher for a particular heat flux.

4.3 Chapter conclusion

In this chapter, means of computing various quantities and parameters of interest in this study were explored. These quantities and parameters were defined in order to minimise eventual sources of errors. An uncertainty analysis was performed. Predictions made at this stage showed that for the majority of test cases, errors in computing Nusselt Numbers should be lower than 6%.

Chapter 5: Results for unilateral heating conditions

The validation of the methodologies of determining the heat transfer coefficients and friction factors was done by taking measurements for turbulent flow regimes in the annulus and comparing it with established heat transfer and friction factor correlations. This chapter presents results only for the case of unilaterally heating conditions of the annulus.

5.1 Heating the inner wall of the annulus

The case of heating from the inner wall of the annulus is examined in here. It was found a good indication on the proficiency of the thermal system and experimental accuracy. It was noticed an average energy balance of 0.78% with a peak of 1.4% for the worst scenario. (low *Re* combined with low heat flux). The energy balance decreases with increasing the heat flux. Results for the case of unilaterally heating the outer wall will be presented in the next section.

5.1.1 Wall temperature measurements

In this section, temperature profiles for the heat transfer wall, the bulk temperature and the adiabatic wall are presented for Reynolds number about 9540. In each case, four heat flux levels were tested: 6 400 W/m^2, 9 600 W/m^2, 14 500 W/m^2 and 19 200 W/m^2. The annulus inlet was located at x = 0 m and the annulus outlet was at $x = L_{h,i}$ (length of inner heater). The legends on the graphs are as follows: $T_{w,i}$ is the temperature of the inner wall (heat transfer wall) and is given by blue markers, T_{bulk} is the average temperature of the bulk fluid and is given by the red markers, and $T_{w,o}$ is the temperature of the outer wall (adiabatic wall), and is given by the black markers.

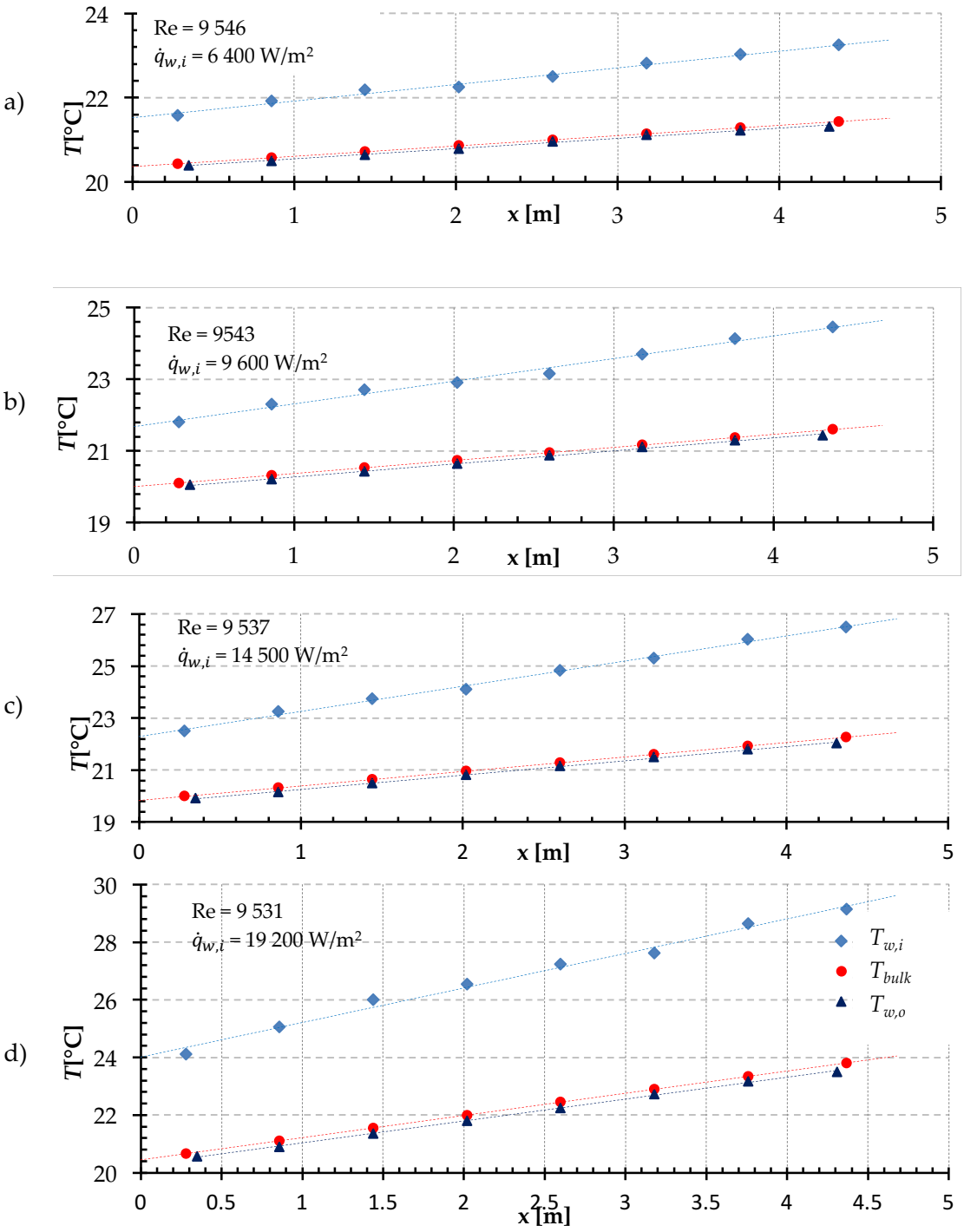

Figure 5-1: Temperature profiles for the case of heating of inner wall at Re ≈ 9 540 with heat fluxes of: a) 6 400 W/m², b) 9 600 W/m², c) 14 500 W/m²and d) 19 600 W/m².

In Figure 5-1, temperatures of the heated wall, the fluid bulk and the adiabatic wall are presented as a function of the axial length of the annulus for various heat fluxes at a Reynold number of about 9 540. The inner tube wall temperatures and the outer wall

temperatures had uncertainties of 0.028 °C and 0.023 °C respectively while the uncertainty of the fluid bulk temperature is 0.039 °C.

It can be seen from the figure that the gradient line of wall temperatures for the heated wall is higher than the bulk temperature gradient. Heat is transferred from the inner wall. As the flow develops, the temperature difference between the wall and the fluid is getting larger.

The experimental data obtained for this case was best fit by a first order equation. The coefficient of determination for experimental data for inner wall temperatures obtained for the case of heating the inner wall ranges from 0.965 to 0.98 which means that 96.5% up to 98% percent of data were predicted satisfactorily from the fit curve within 0.028 °C.

5.1.2 Average LMTD heat transfer coefficients

In this section, the average Nusselt numbers determined for a single control volume spanning the entire length of the heat exchanger test section are presented as a function of the Reynolds numbers. The Nusselt numbers were calculated according to equation 4-10.

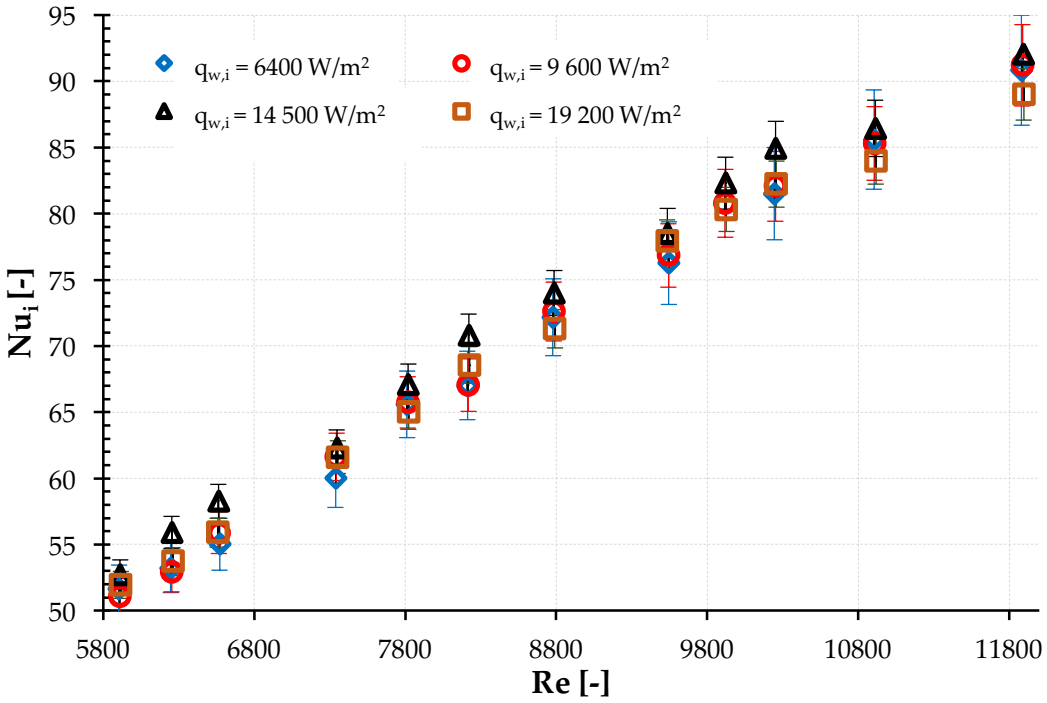

Figure 5-2: Nusselt numbers for heating from the inner wall with different heat fluxes: 6 400, 9 600, 14 500 and 19 600 W/m².

In the Figure 5-2, the Nusselt numbers for the case of heating from the inner wall of the annulus are plotted against the Reynolds numbers ranging from 5 800 to 12 000 for four different heat fluxes: 6 400, 9 600, 14 500 and 19 200 W/m². The graph shows that the Nusselt numbers increase as the Reynolds numbers increase. The uncertainties in computing the Nusselt number with heat flux of 6 400 W/m²vary from 3.5% at low Reynolds number (≈ 5900) and increase steadily to 4.7% at high Reynolds numbers (≈ 12 000). As the heat flux increases, the uncertainty decreases. For the highest heat flux of 19 200 W/m², uncertainty is lowered to 2% for the lowest Reynolds number (≈ 5900) while it is 2.2% at Reynolds number = 11 896. The uncertainty on the Reynolds number was 1.08% while uncertainties decreased from 2.64% on heat flux of 9 600 W/m² to 1.5% on heat flux of 19 200W/m².

Comparing the Nusselt numbers of different heat fluxes at approximately the same Reynolds numbers, there seemed to be no dependency of the Nusselt number with the heat flux rate. Deviations from each other Nusselt number at the same Reynolds numbers were within the accuracy of the measuring system. The highest range of

Nusselt numbers for a specified Reynolds number was less than 3% and the confidence intervals around each value were overlapping closely.

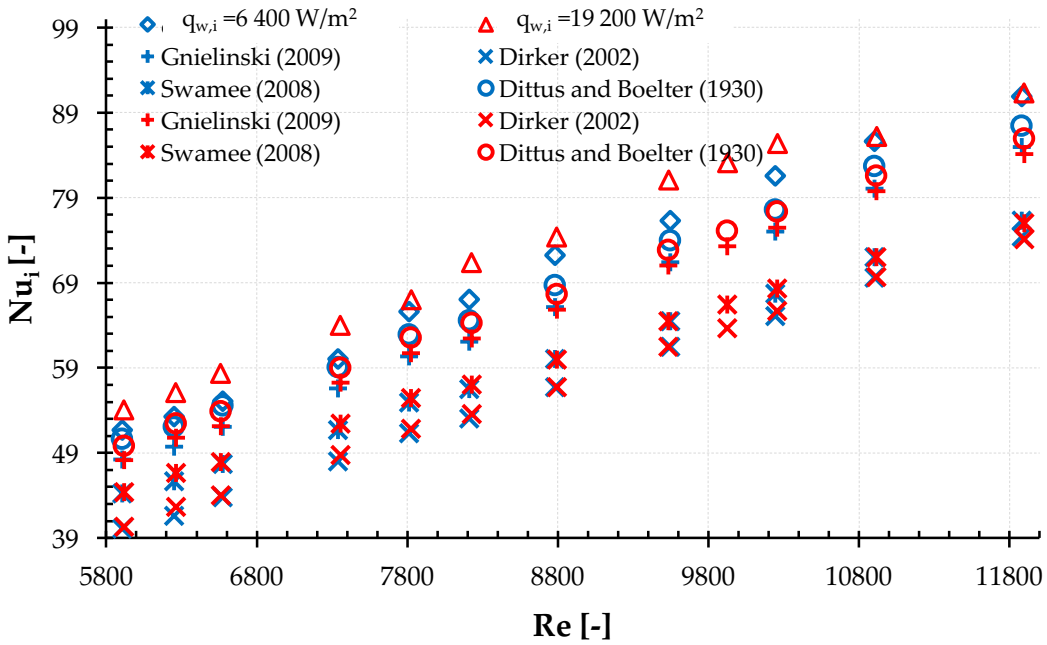

Figure 5-3: Nusselt numbers for heating from the inner wall associated with predictions for heat fluxes 6 400 and 19 600 W/m².

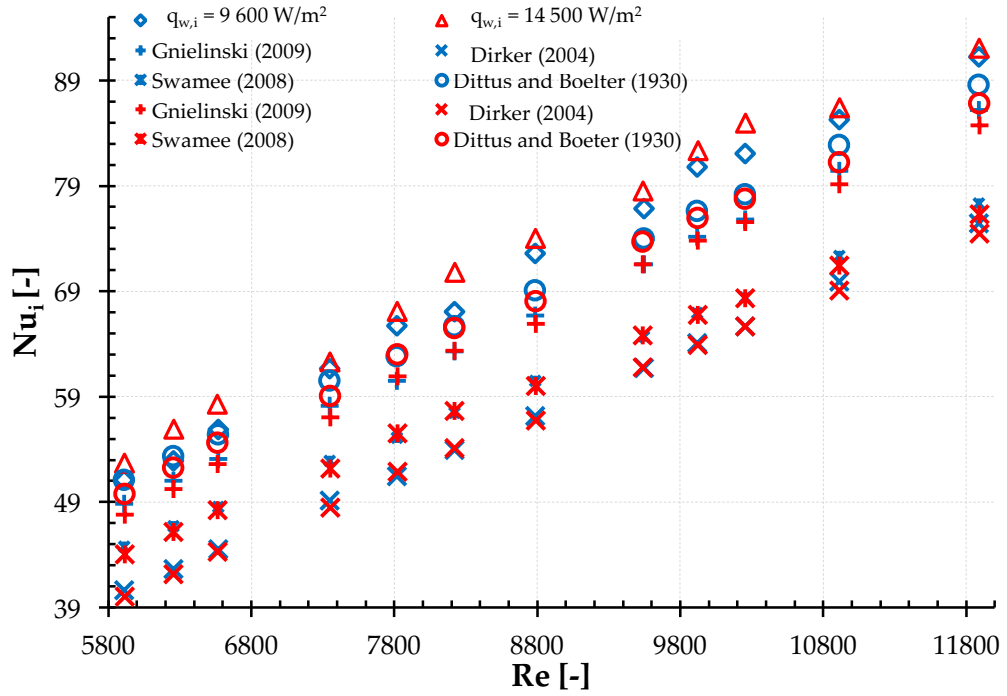

Figure 5-4: Nusselt numbers for heating from the inner wall associated with predictions for heat fluxes 9 600 and 14 500 W/m².

Figure 5-3 and Figure 5-4 show the comparison of the experimental data with predictions derived from correlations of Dittus and Boelter (1930), Dirker and Meyer (2004), Swamee *et al.* (2008) and Gnielinski (2009). In Figure 5-3, the blue colour is used to present experimental data and predictions made out the heat flux $\dot{q}_{w,i}$= 6 400 W/m^2 and the red marks are used for $\dot{q}_{w,i}$= 19 600 W/m^2. The same colour specification is used in Figure 5-4 with the blue colour used for $\dot{q}_{w,i}$= 9 600 W/m^2 and the red colour for $\dot{q}_{w,i}$= 14 500 W/m^2. All correlations seemed to under-predict the Nusselt numbers. Experimental results showed a close agreement with the correlation of Dittus and Boelter from which they deviate on average by 3 %. Average deviations are much higher comparing to other correlations: 6.5 % from the correlation of Gnielinski (2009), 16 % from the correlation of Swamee *et al.* (2008) and 22 % from the correlation of Dirker and Meyer (2004).

5.1.3 Local Nusselt numbers

The local Nusselt numbers were determined using equation 4-11. The calculation of the local Nusselt number is very sensible on the variation of the wall temperature. Control volumes are as defined in Figure 4-1.

Figure 5-5 to Figure 5-8 present the local Nusselt numbers for each control volume as a function of Reynolds number for all heat flux densities. It is observed that for all heat fluxes considered, the more the control volume is located nearest to the annulus inlet, the more its local number is higher. The mean Nusselt numbers given in the Figures were determined by treating the entire heat exchanger as a single control volume as per the results in section 5.1.2

Figure 5-9 gives an overview of the Nusselt numbers of all control volumes versus mean Nusselt numbers and correlations of Gnielisnki (2009) and Dirker and Meyer (2004) for heat flux of 9 600 W/m^2. It has been observed that each control volume, except in few cases (less than 15%), approximately deviates from correlations by a constant percentage with CV 1 showing the highest deviation, on average 27 % from

the correlation of Gnielinski (2009) and 48 % form the correlation of Dirker and Meyer (2004). This deviation steadily decreases as the control volume moved to the exit of the annulus. CV 8 exhibits a negative deviation of 16 % from the correlation of Gnielinski (2009) while its deviation from the correlation of Dirker and Meyer (2004) is nearly 0 %. The local Nusselt number for CV 8 is well predicted by the correlation of Dirker and Meyer (2004).

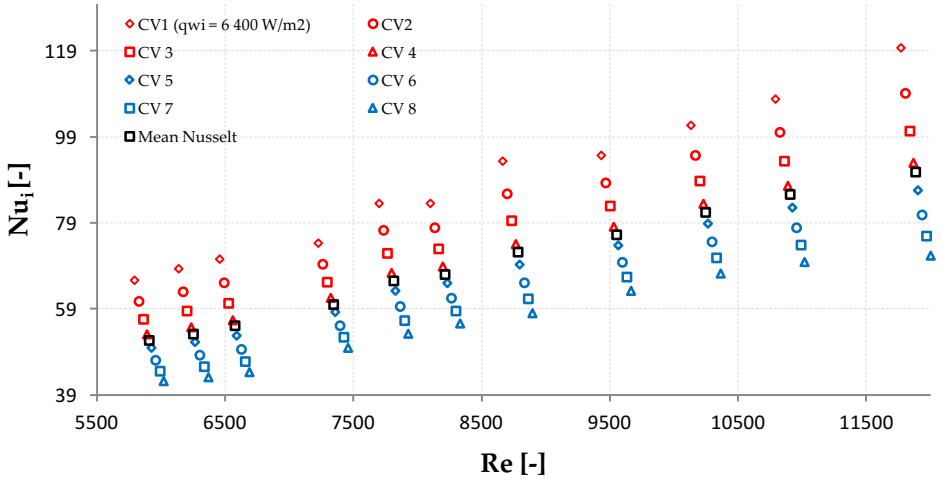

Figure 5-5: Local Nusselt numbers for CV 1 to CV 8 with heat flux of 6 400 W/m².

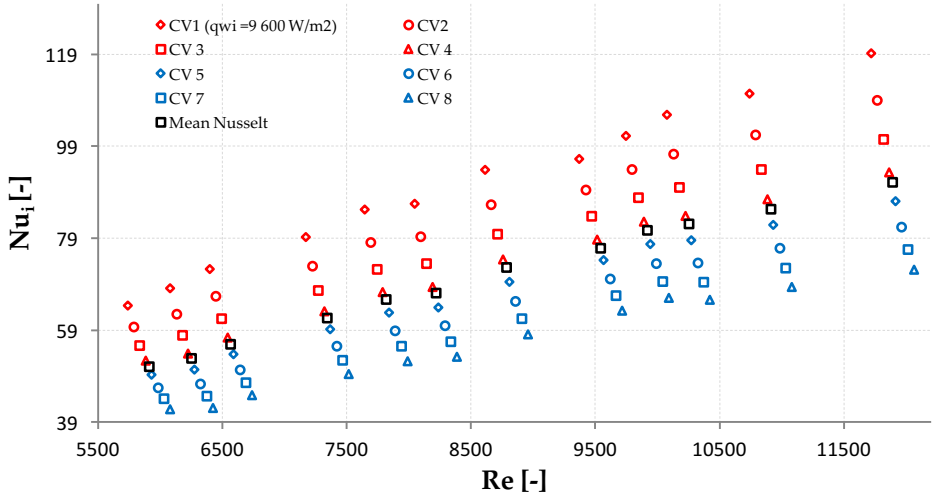

Figure 5-6: Local Nusselt numbers for CV 1 to CV 8 with heat flux of 9 600 W/m².

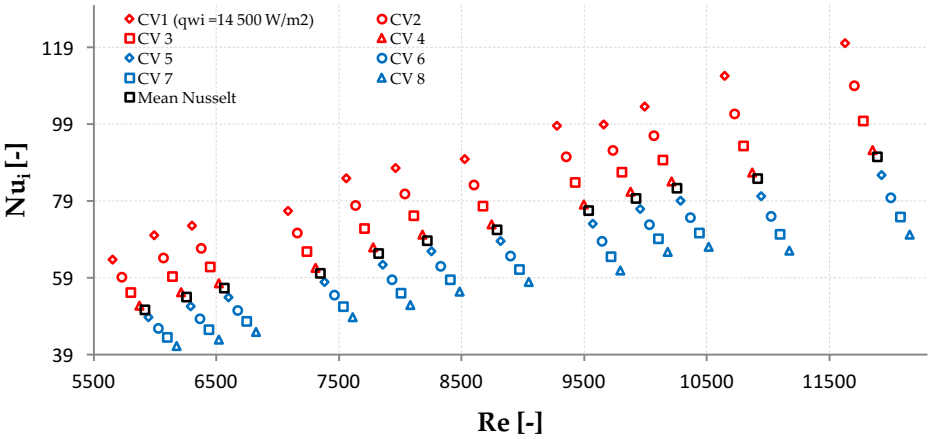

Figure 5-7: Local Nusselt numbers for CV 1 to CV 8 with heat flux of 14 500 W/m².

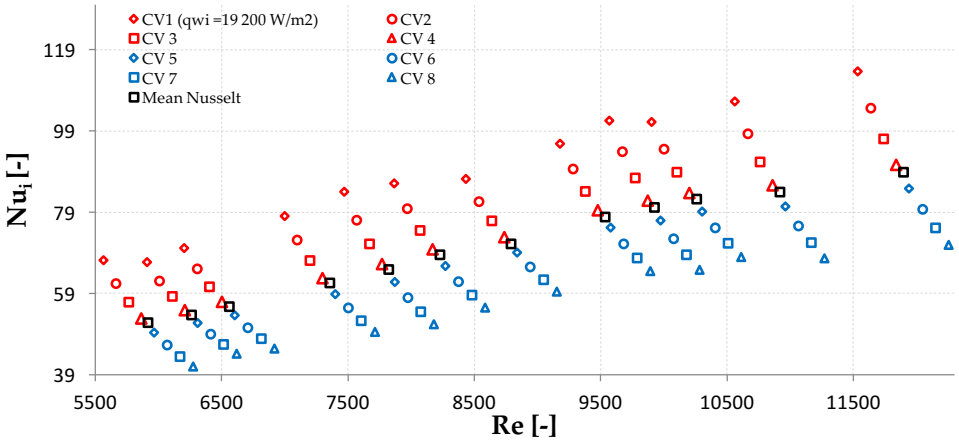

Figure 5-8: Local Nusselt numbers for CV 1 to CV 8 with heat flux of 19 200 W/m².

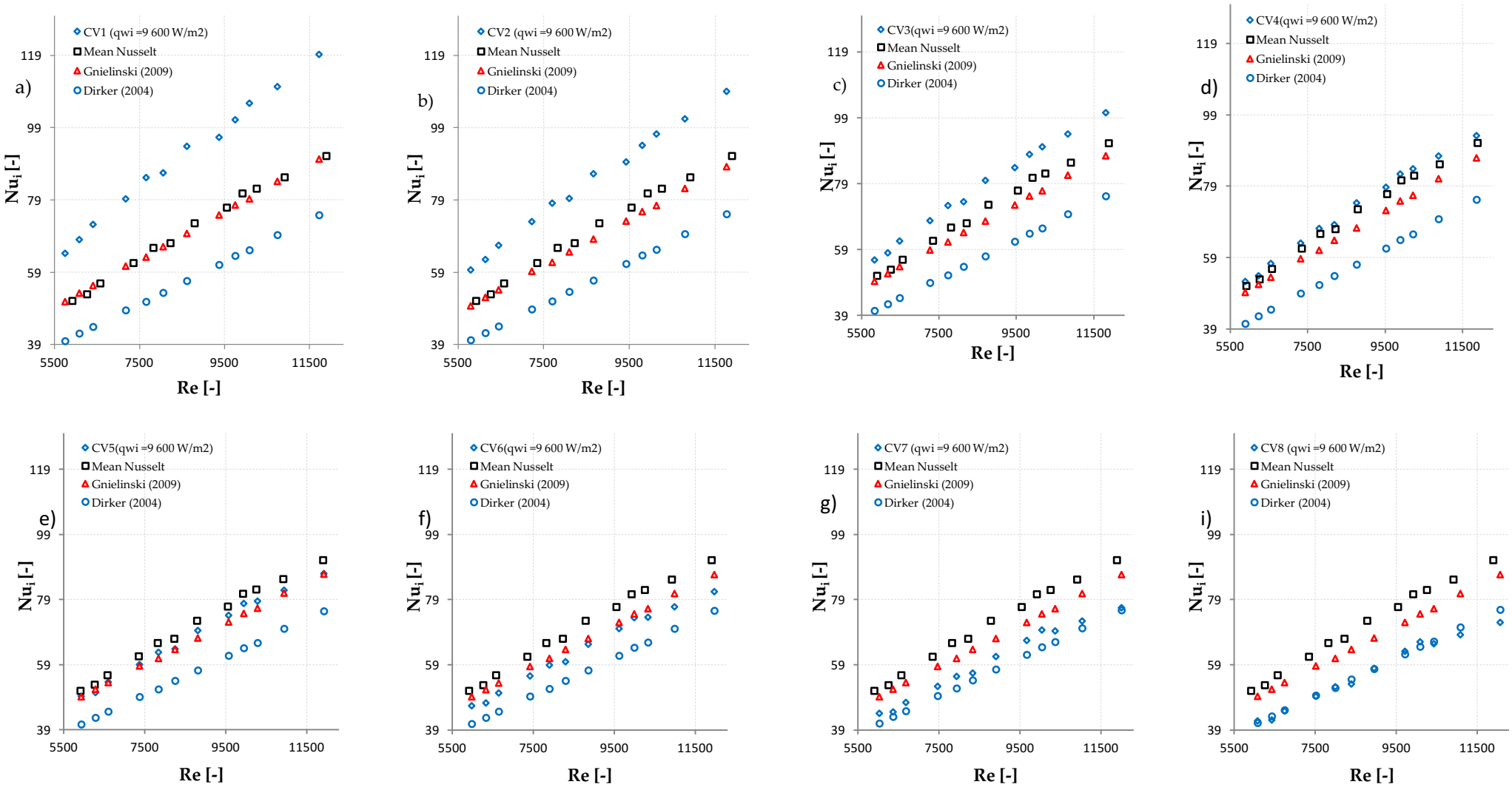

Figure 5-9: Local Nusselt numbers for CV 1 to CV 8 against correlations for heat flux of 9 600 W/m².

In Figure 5-10, the local Nusselt numbers are presented as a function of the axial position along the annulus length for various values of the local Reynolds numbers. Experimental results for each control volume were not taken at precisely the same value of local Reynolds number, since the Reynolds number changes across each section as thermos-physical properties of fluid vary with the bulk temperature getting warmer towards the exit. Therefore, the local Nusselt numbers were obtained via an interpolation process between the neighboring local Nusselt numbers.

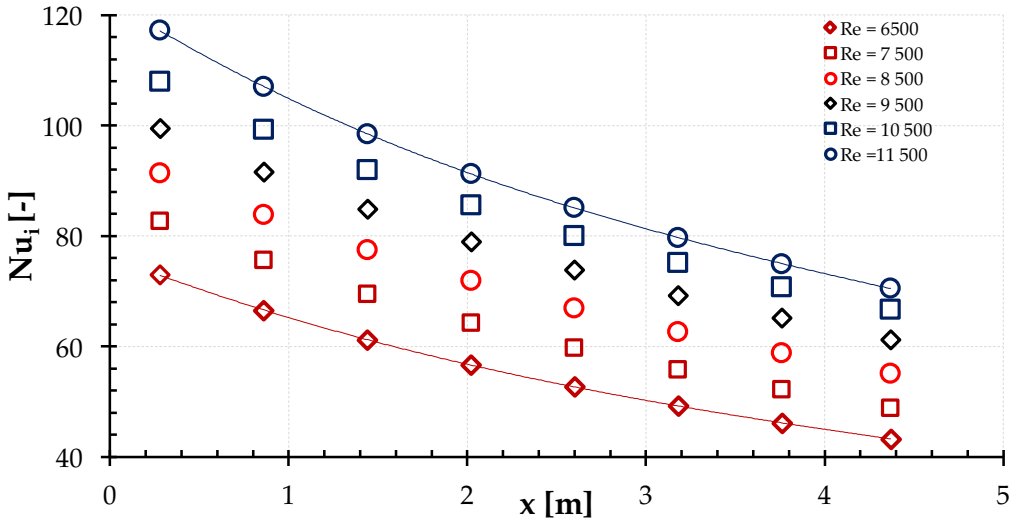

Figure 5-10: Local Nusselt number along the axial length of the annulus for selected constant Reynolds number values.

5.1.4 Friction factors

This section presents friction factors for diabatic cases and will provide the experimental value obtained for *m*, the exponent of the temperature-dependent term. The friction factors were calculated according to the equation 4-19 over the length of the heat exchanger.

Figure 5-11 shows friction factor as a function of the Reynolds numbers for different heat fluxes. It is observed that as the heat flux increases, the friction factor decreases for a particular Reynolds number.

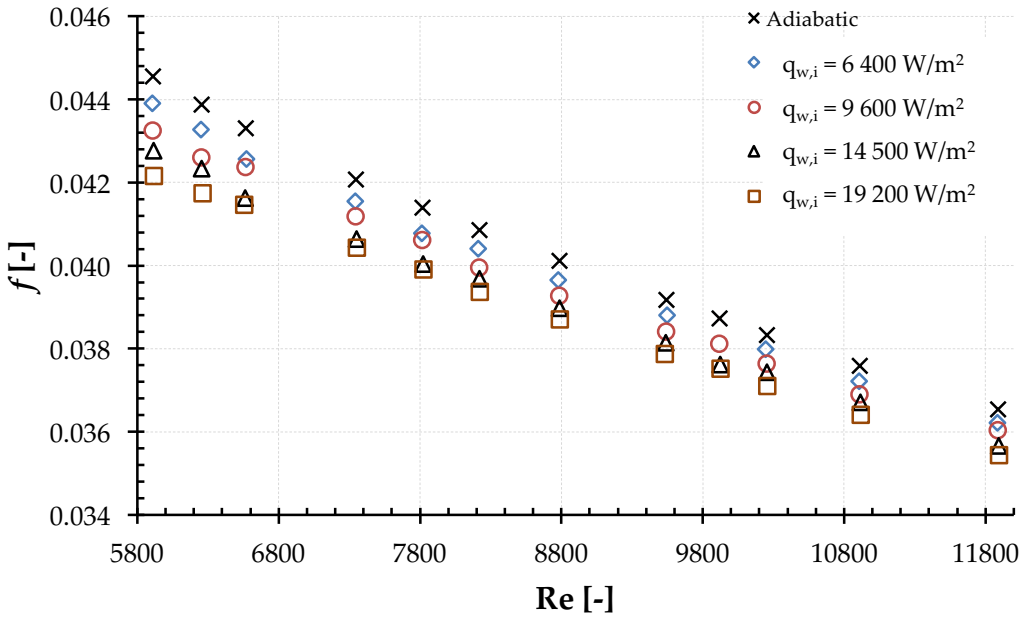

Figure 5-11: Friction factor for the case of heating from the inner wall with four heat fluxes: 6 400 W/m², 9 600 W/m², 14 500 W/m² and 19 200 W/m².

For a Reynolds number close to 6 500, the percentage of decrease compared to the adiabatic case is 1.4 % for heat flux of 6 400 W/m² and peaks to 4. 7% when the heat flux reaches 19 200 W/m². For a particular heat flux, the percentage of decrease seemed to be higher at lower Reynolds numbers as it can be noticed examining Figure 5-12.

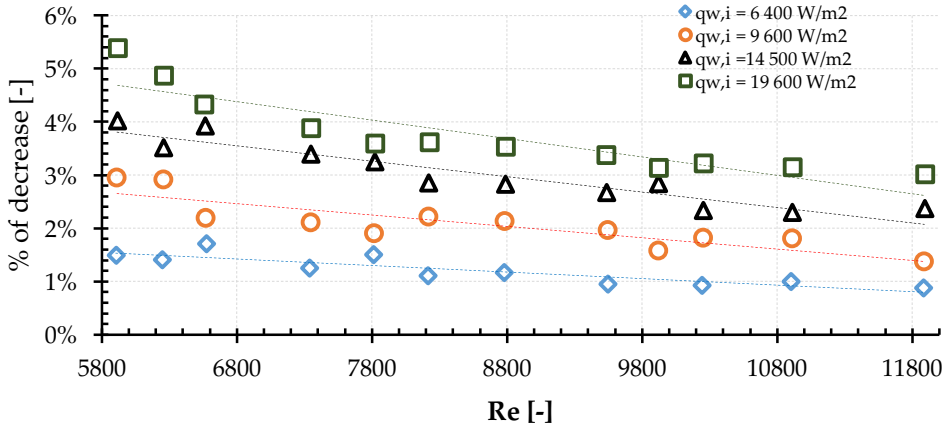

Figure 5-12: Percentage of pressure drop versus the adiabatic case for different heat fluxes.

This behaviour can be justified by the fact that for particularly heat flux at lower Reynolds numbers, the associate lower heat transfer phenomenon induces a higher temperature gradient in the fluid close to the heated wall, which tends to lower the

near-wall viscosity and hence decreases more the wall-shear stress. The near-wall fluid viscosity is determined at the average wall temperature by using the experimental data collected.

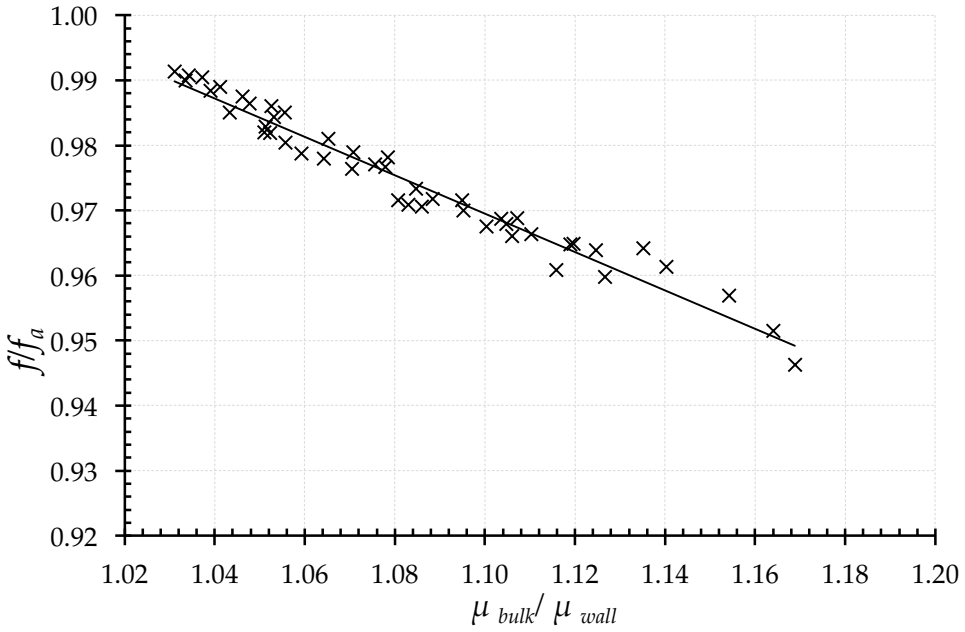

Figure 5-13: Friction factor ratio as a function of viscosity ratio.

Figure 5-13 shows the friction factor ratio as a function of the viscosity ratio for the whole set of data collected for the case of unilateral heating on the inner wall of the annulus. All sets of data are satisfactorily represented by equation 2.8 with a single exponent $m = 0.3271$. This value lies between the values proposed by Leung *et al.* (2005) (m = 0.28) and Dormer and Bergles (1969) (m = 0.35). The friction factor ratio takes the following form :

$$\frac{f}{f_a} = \left(\frac{\mu_{bulk}}{\mu_{wall}}\right)^{-0.3271} \qquad 5\text{-}1$$

5.1.5 *j*-factors

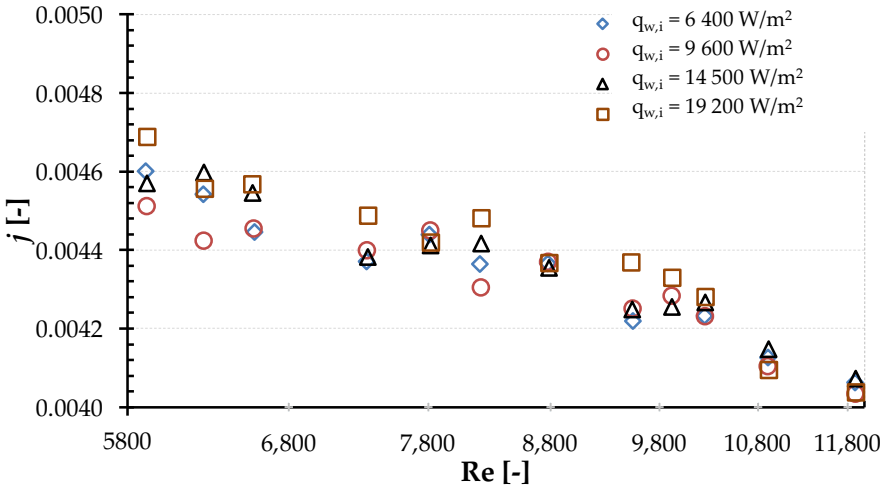

Figure 5-14: *j*- factor as a function of the Reynolds number for all heat fluxes.

It can be seen from Figure 5-14 which plots the Colburn *j*-factor at different wall heat flux levels, that there is a reduction of the *j*-factor as the Reynolds numbers increase. The *j*-factor and the friction factor are both plotted as a function of *Re* in Figure 5-15 for different cases of heat fluxes with the friction factor given at the top and the *j*-factor at the bottom of each figure. The two curves for different cases run almost parallel to one another. The ratio of these quantities is about 0.11 as displayed in Figure 5-16 and seems to increase slightly as Reynolds number increases. This establishes a clear relationship between the friction factor and the Colburn *j*-factor.

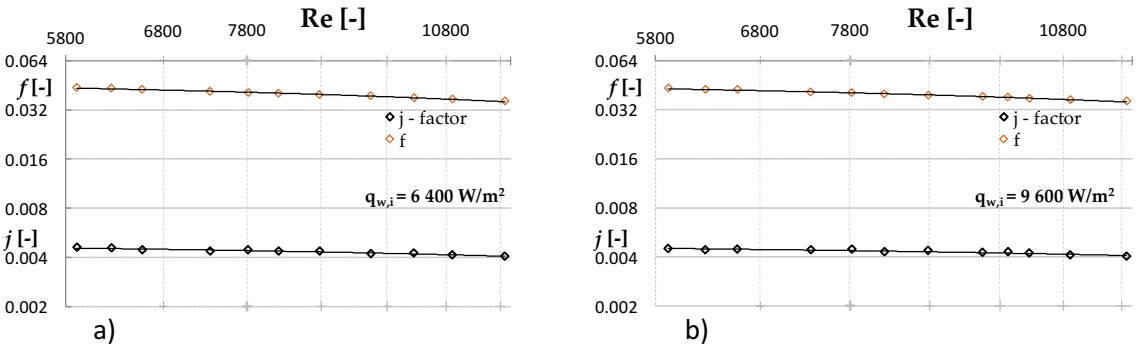

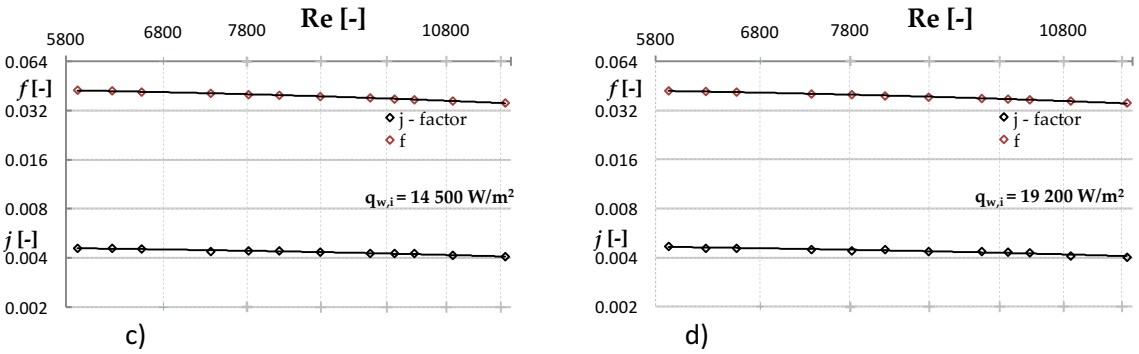

Figure 5-15: f and *j*- factors as a function of the Reynolds number.

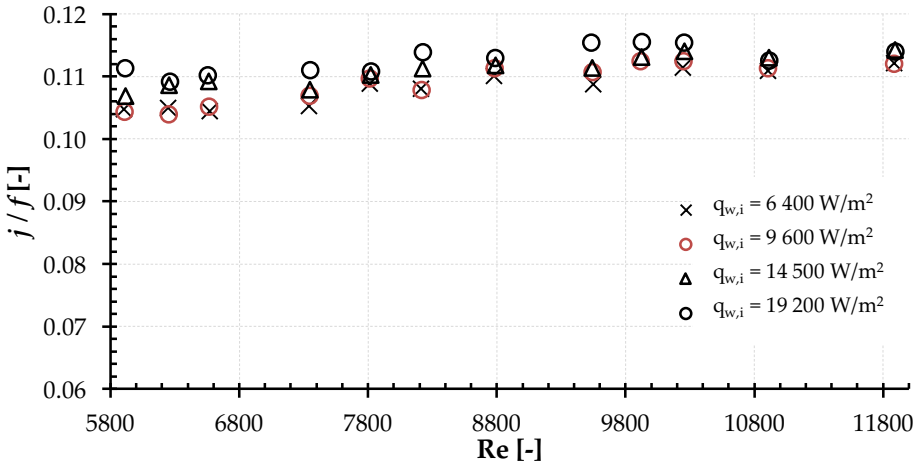

Figure 5-16: Ratio of *j*-factor and *f* as a function of the Reynolds number.

5.2 Heating from the outer wall of the annulus

Results for this boundary condition will be presented in the sequence as they were for the previous case: wall temperature measurement, average Nusselt numbers, local Nusselt numbers, friction factors and *j*-factors. A good indication on the proficiency of the thermal system and experimental accuracy was observed with the highest energy balance being 2.4%. The energy balance decreases with increasing the heat flux.

5.2.1 Wall temperature measurements

As for the thermal boundary of unilateral heating on the inner wall, wall temperature measurement on the heated outer wall could be satisfactorily predicted by linear trends with a "goodness of fit "value of R^2 higher than 97%. Figure 5-17 illustrates wall temperature profiles for Reynolds about 8 040 with four different heat flux densities.

The ratio of the slope of the heated wall and the slope of the bulk temperature is lower compared to the case of heating the inner wall. This may be due by the flow being more thermally developed than for the case of heating from the inner wall.

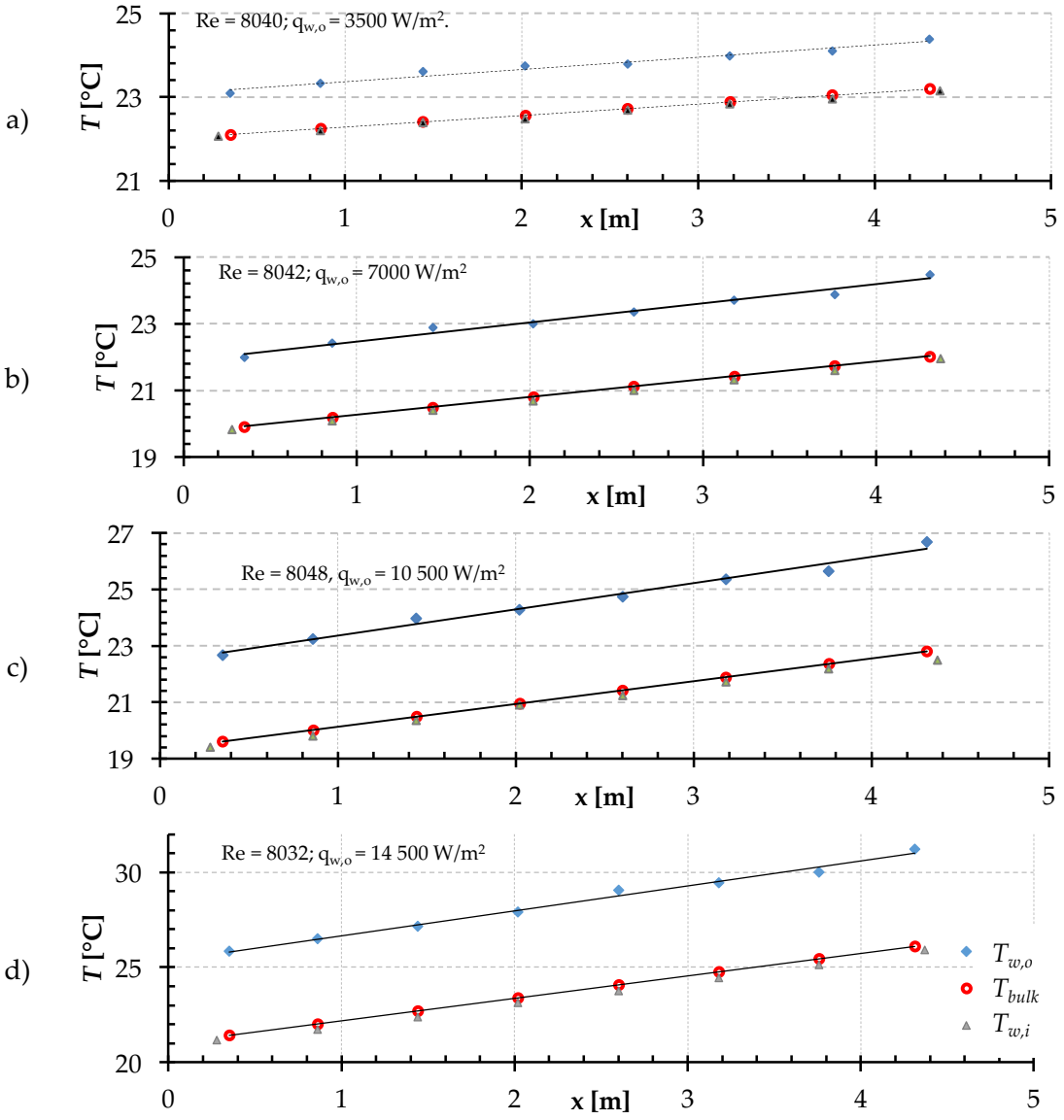

Figure 5-17: Wall temperature measurement for the case of heating from the outer wall with different heat fluxes.

5.2.2 Average LMTD heat transfer coefficients

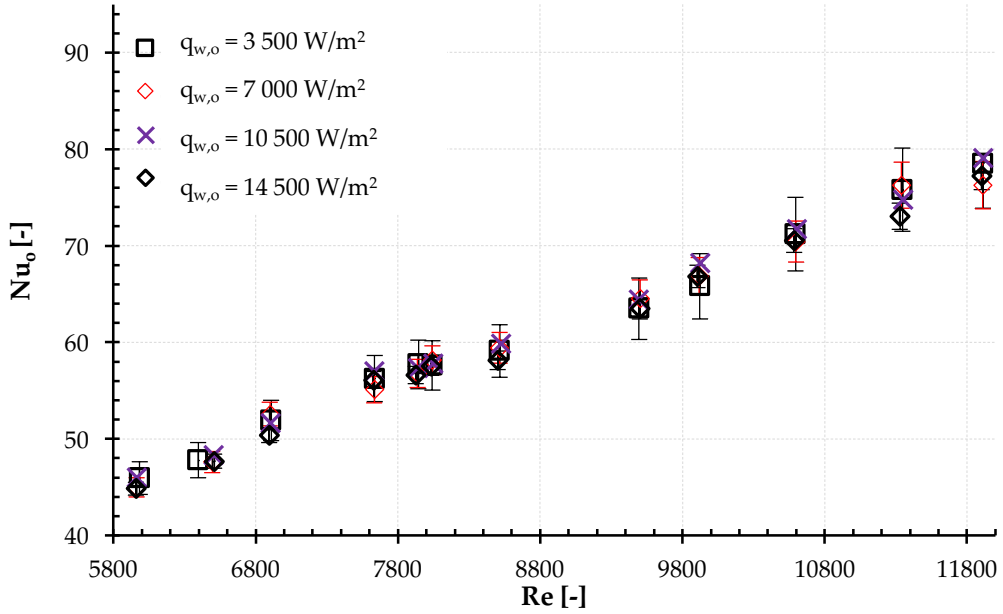

Figure 5-18: The Nusselt number as a function of the Reynolds number for heating from the outer wall of the annulus with different heat fluxes: 3 500 W/m², 7 000 W/m², 10 500 W/m² and 14 500 W/m².

Figure 5-18 presents the Nusselt numbers for the outer wall of the annulus as function of the Reynolds numbers for different heat flux densities. As with the case of heating from the inner wall, Nusselt numbers increase as Reynolds numbers increase but the magnitude of increase in the Nusselt number is lower compared with the case for heating from the inner wall for the same Reynolds number. (For instance at Re = 7800, Nu_o = 55 while Nu_i = 67 as presented earlier in Figure 5-2). While the highest heat flux tested (14 500 W/m²) tends to produce Nusselt numbers which are lower than those for other heat fluxes by up to 2.7 %, the accuracy of the experimental setup in measuring the Nusselt number did not allow to conclude on any dependence of the Nusselt number and the heat flux density.

Uncertainties in computing the Nusselt number for this thermal boundary condition did not exceed 5.8 % for the lowest heat flux density (3 500 W/m²) and that limit decreased towards 2% for the highest heat flux (14 500 W/m²). A detail summary on uncertainty analysis for different flow conditions is given in Appendix A. The experimental data was compared with predictions made from correlations as illustrated in Figure 5-19.

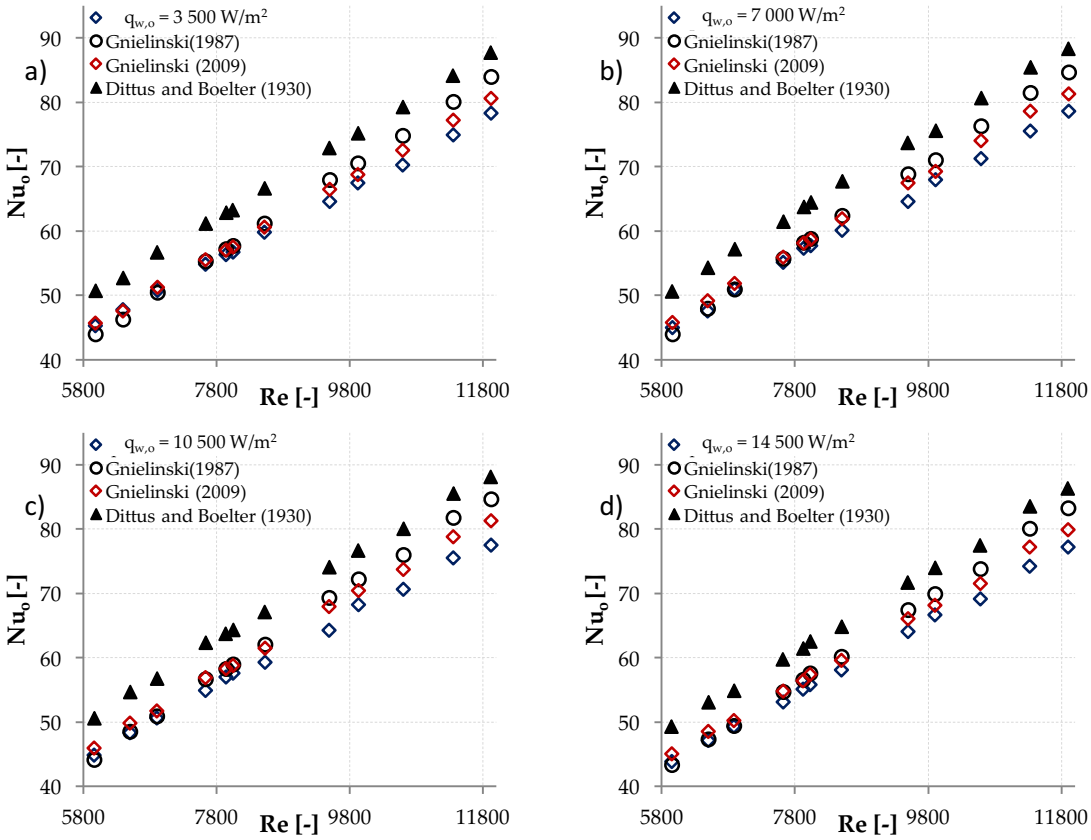

Figure 5-19: Average Nusselt numbers for the heated outer with predictions from correlations.

All correlations over-predict the Nusselt number except for a few cases at lower Reynolds numbers.

Experimental result look to follow closely the correlation of Gnielinski (2009), they are within -2% from that correlation for *Re* less than 9 000 and within -4.2 % for *Re* greater than 9 000. Deviations are much bigger for other correlations, up to 7 % for the correlation of Gnielinski (1987) and 12% for the correlation of Dittus and Boelter (1930).

5.2.3 Local Nusselt numbers

Local Nusselt numbers for all control volumes as a function of Re are presented in Figure 5-20 for the heat flux density of 10 500 W/m² while Figure 5-21 shows local Nusselt numbers for each control volume in comparison with correlation. As for the first boundary condition, the more the control volume is located nearest the annulus inlet, the more its local Nusselt number is higher

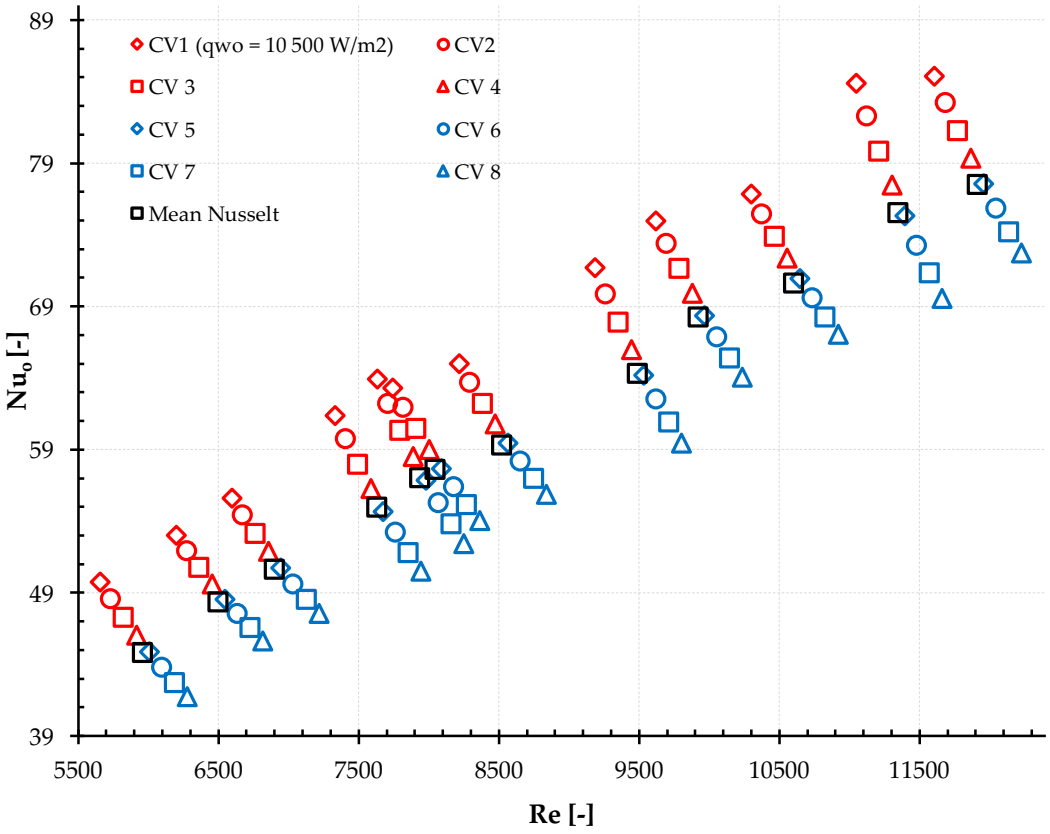

Figure 5-20: Local Nusselt number of CV 1 to CV 8 for heat flux of 10 500 W/m^2.

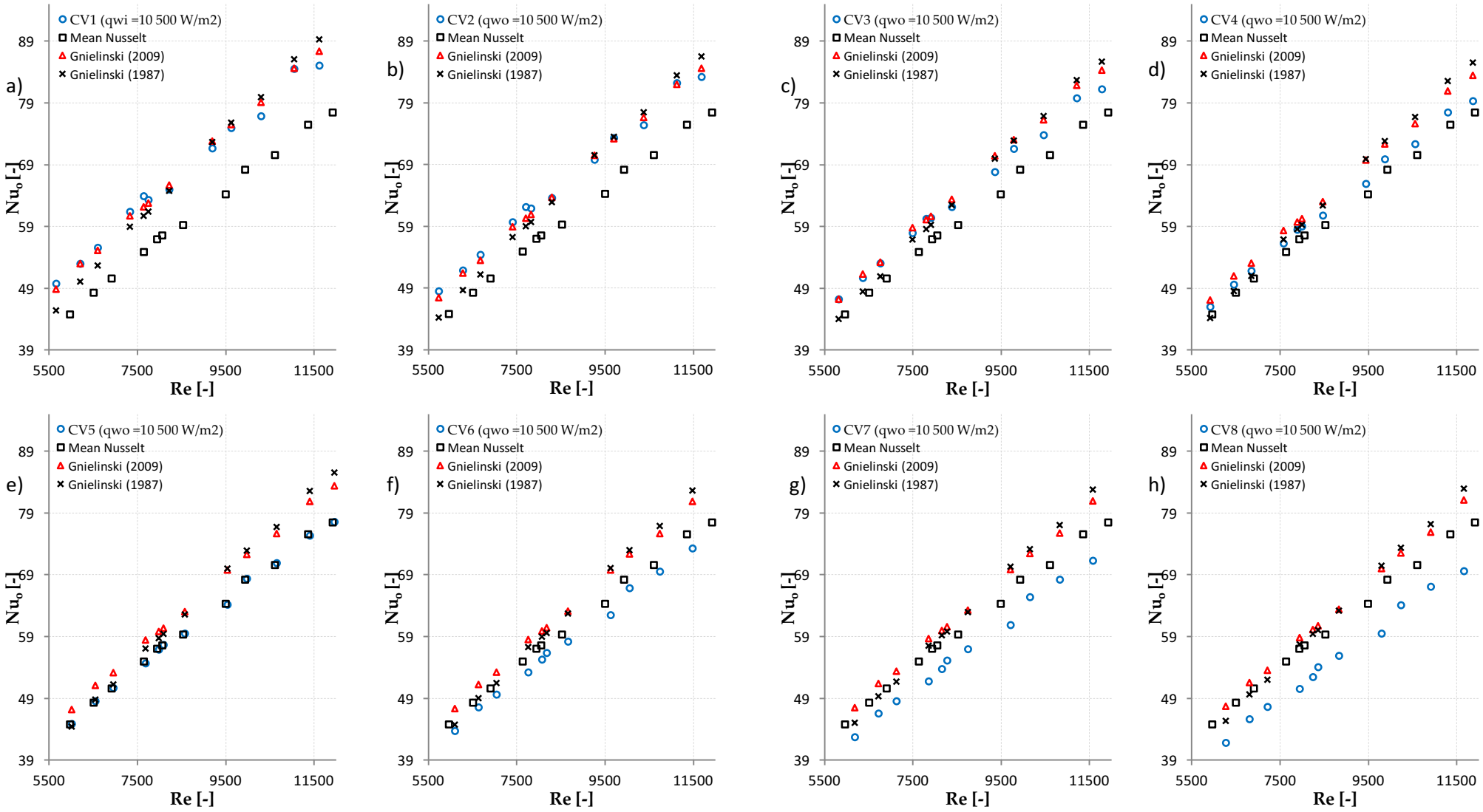

Figure 5-21: Local Nusselt numbers for CV 1 to CV 8 against correlations for heat flux of 10 500 W/m².

No uniform patterns were found between correlations and local Nusselt numbers. Control volume 3 was predicted by the correlation of Gnielinski (2009) within -3 %. Deviations become more significant as the control volumes are more removed from control volume 3. In Figure 5-22, the local Nusselt number is given as a function of the axial length of the annular duct for different Reynolds numbers. A linear decrease of the Nusselt number is seen along the axial length. An average of 15% decrease in the Nusselt Number was observed between the first and last control volume. This value was approximately 40% for the case of heating from the inner wall of the anulus.

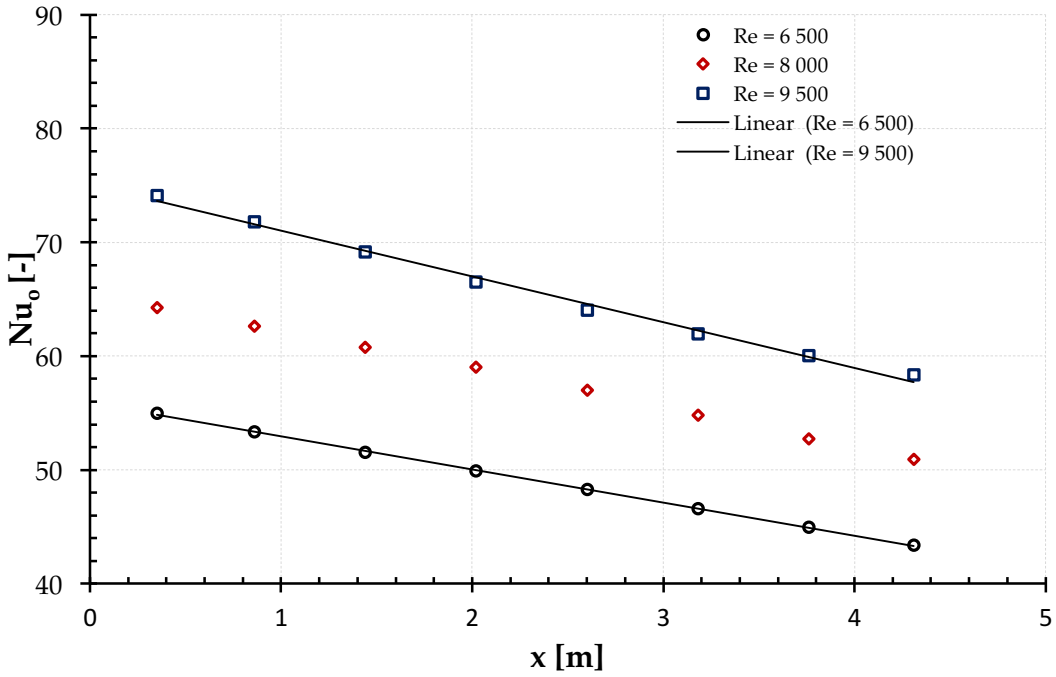

Figure 5-22: Local Nusselt number on the outer wall along the axial length of the annular duct.

5.2.4 Friction factor

Figure 5-23 shows the friction factor as function of *Re* for the thermal boundary of heating the outer wall of the annulus. Similar to the case of heating from the inner wall of the annulus, it is observed that for the turbulent flow regime considered, that the friction factor decreases as the heat flux increases.

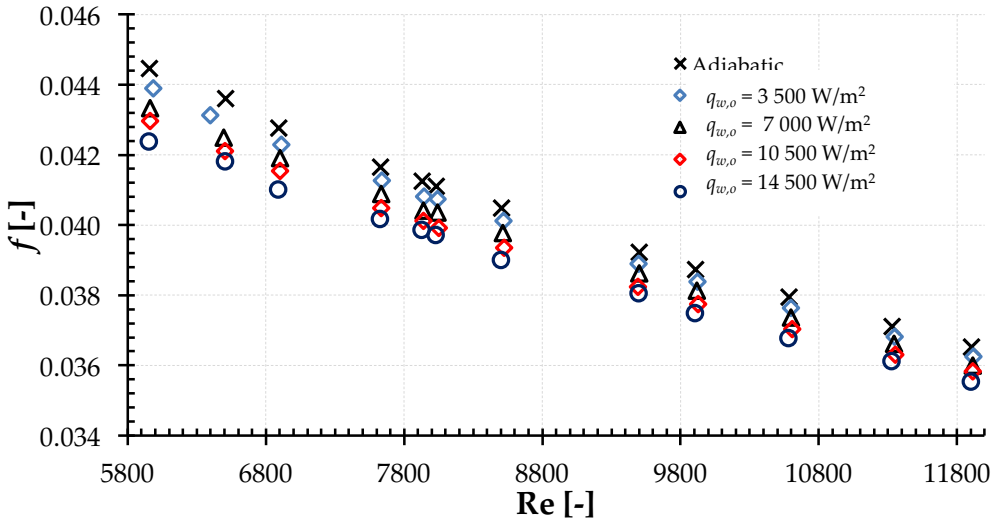

Figure 5-23: friction factor as function of Re for heating the outer wall with different heat fluxes.

Using the representation of the friction factor ratio as a function of the viscosity ratio (see Figure 5-24), it is noticed that dataset for this thermal boundary condition is satisfactorily represented by equation 2-8 with a single exponent $m = 0.3572$ which, in this case, is slightly higher than that found for the inner-heating thermal boundary condition ($m = 0.3271$).

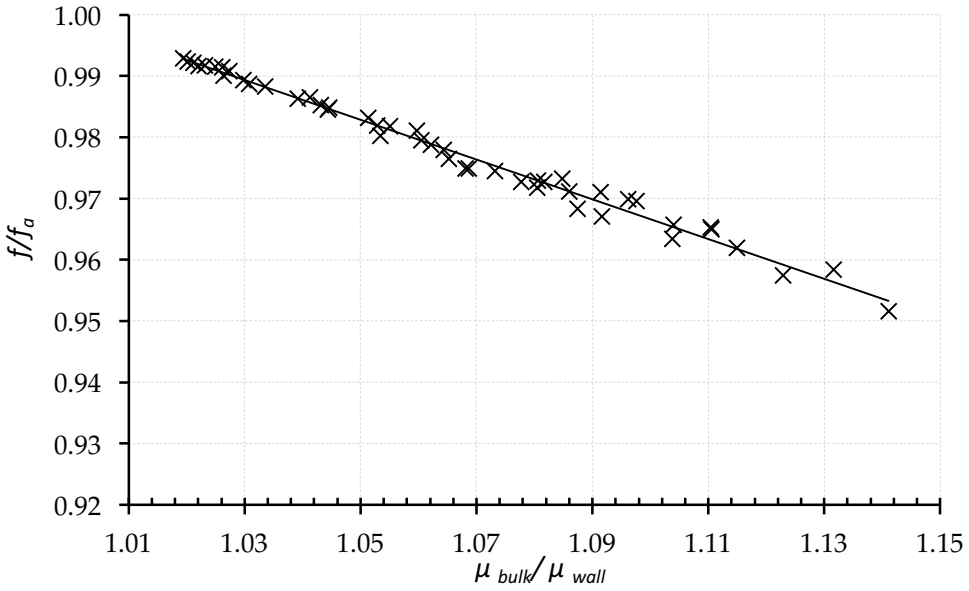

Figure 5-24: Friction factors ratio as a function of viscosity ratio.

5.2.5 *j*-factor

Figure 5-25 to Figure 5-27 are related to the use of the *j*-factor for heating from the outer wall. It is observed that the *j* factor reduces while Re increases and a good parallelism between the *j*-factor and the friction factor exists. The ratio of these two quantities ranges from about 0.091 to 0.095 and tends to slightly increase with increasing the Reynolds number or the heat flux. It is on average lower by 14% compared to the ratio obtained for heating from the inner wall ($j/f = 0.11$). The uncertainty in computing this ratio did not exceed 6%.

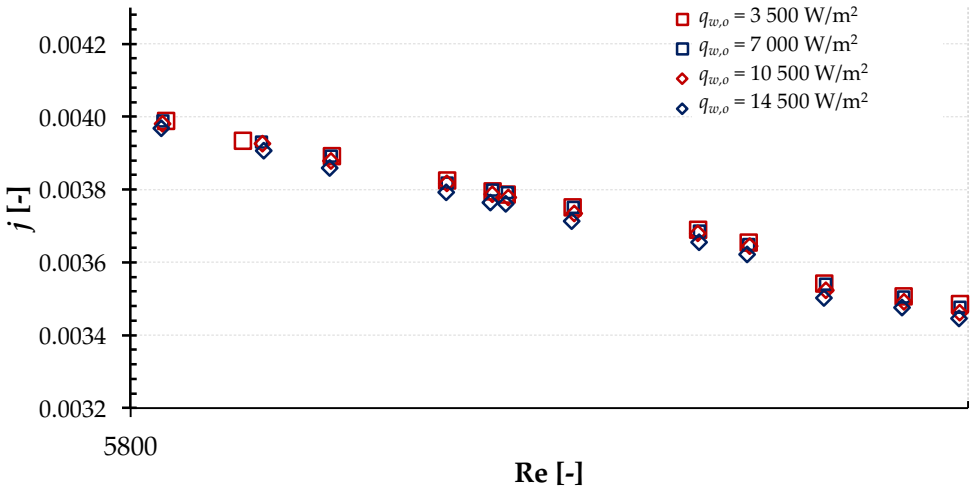

Figure 5-25: *j*-factor as a function of the Reynolds number for the case of heating from the outer wall with different heat fluxes.

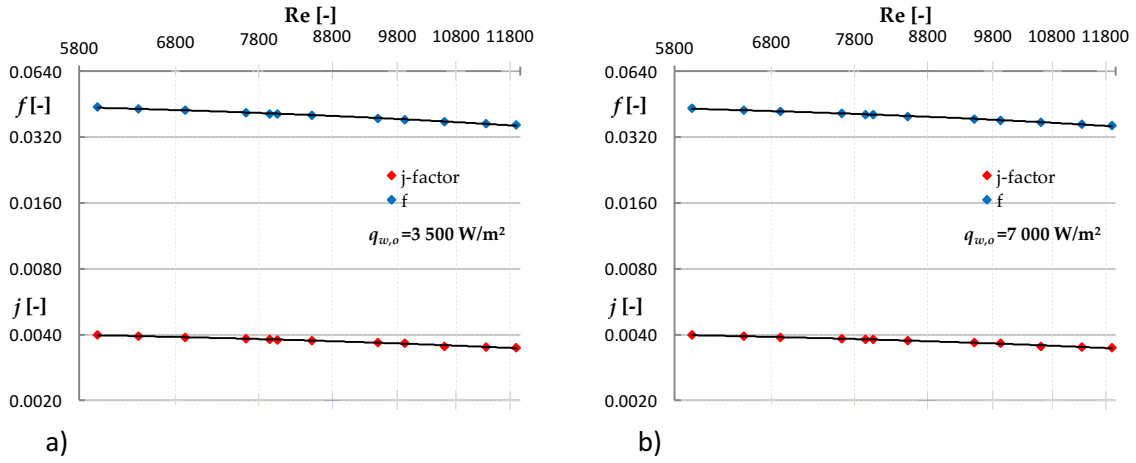

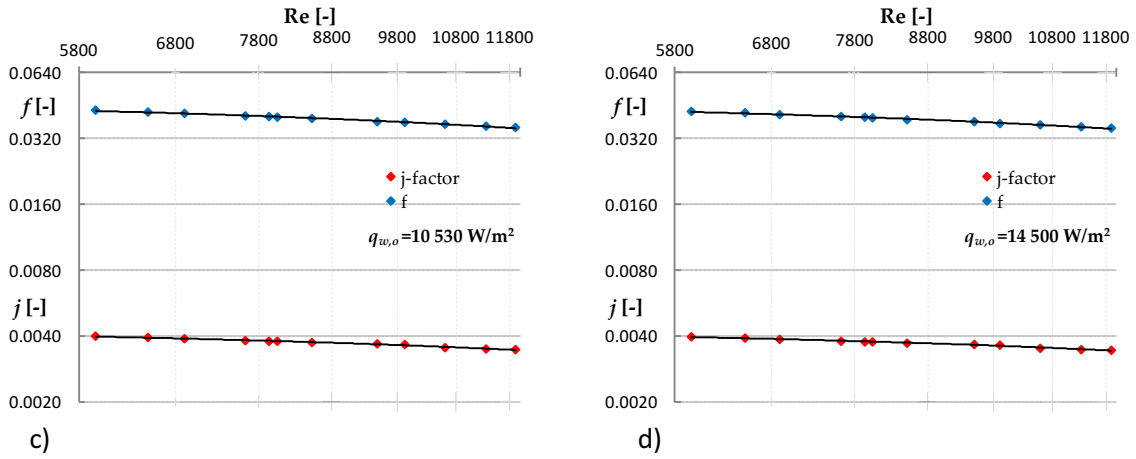

Figure 5-26: *f* and *j*-factor as a function of Re (Outer wall heated).

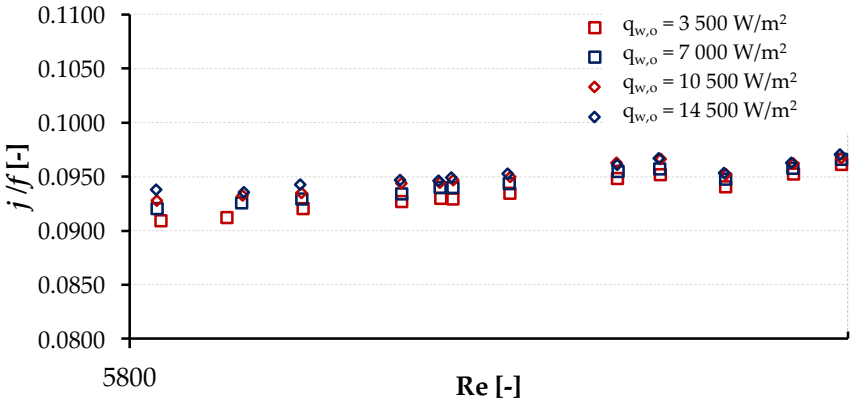

Figure 5-27: ratio of *j*-factor and *f* as a function of Re

5.3 Comparison of average LMTD heat transfer coefficients on inner and outer walls of the annular duct

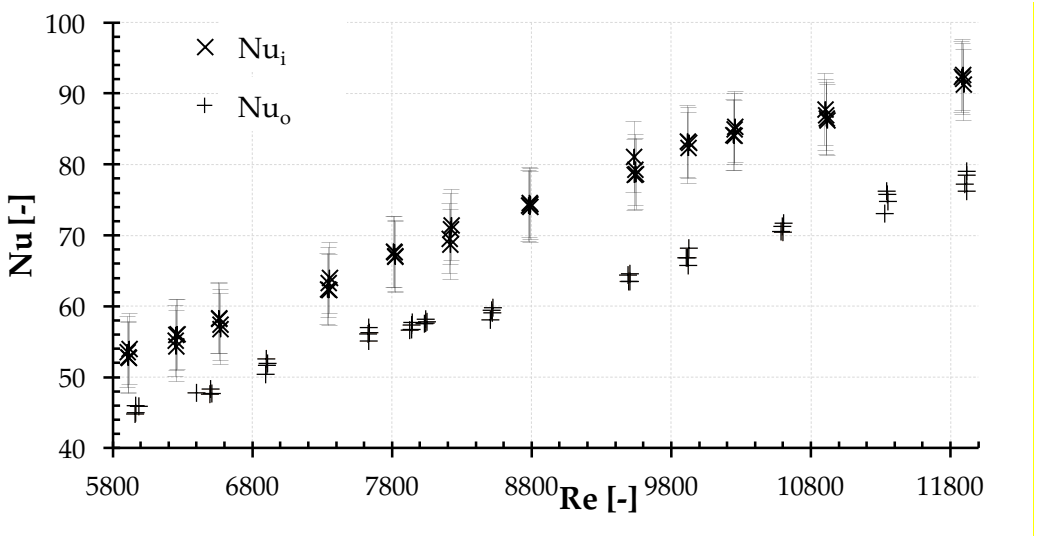

Figure 5-28 : Average Nu_i versus average Nu_o

In Figure 5-28, all average Nusselt numbers for the case of heating only the inner wall of the annular duct are presented on the same plot with all average Nusselt numbers for the case of heating only the outer wall. It can be clearly seen that heat transfer coefficients are higher for the first thermal boundary condition than the latter at a given Reynolds number. Nusselt numbers for the case of heating the inner wall were on average greater than those for the case of heating the outer wall by 16 to 20%.

5.4 Chapter conclusion

In this chapter, computed characteristics for unilateral heating conditions were presented along with comparisons from archival correlations believed to be the most updated. Acceptable agreement was found between results and correlations. Heat transfer coefficients for heating from the inner wall were higher than those for heating from the outer wall. Also for friction factors, a good agreement was found. It can then be concluded that the experimental setup is quite convenient to generate accurate measurements of the heat transfer coefficients and friction factors in the turbulent regime. In the next chapter the bilateral cases will be discussed.

Chapter 6: Results for bilaterally heating conditions

This chapter gives a summary of experimental results for the case of bilateral heating. Results for two Reynolds numbers, 6 500 and 9 500 will be presented. To perform this, four levels of heat fluxes for the outer tube 3 500 W/m², 7 000 W/m², 10 530 W/m² and 14 500 W/m² will be combined with two levels of heat fluxes on the inner tube, 6 400 W/m² and 9 600 W/m². Since heat-flux ratio does not have a universal format, in this investigation, the heat flux ratio was defined as:

$$q^* = \frac{\dot{q}_{w,o}}{\dot{q}_{w,i}} \qquad 6\text{-}1$$

Here $\dot{q}_{w,o}$is the heating flux on the outer tube of the annulus and $\dot{q}_{w,i}$is the heating flux on the inner tube of the annulus. For the heat fluxes mentioned, q^*ranges from 0.36 to 2.27 using different combinations of $\dot{q}_{w,o}$ and $\dot{q}_{w,i}$ as defined in Table 6-1.

Table 6-1: Combination of heat fluxes with corresponding heat flux ratio.

$\dot{q}_{w,i}$ (W/m²)	$\dot{q}_{w,o}$ (W/m²)	q^*
9 600	3 500	0.36
6 400	3 500	0.54
9 600	7 000	0.72
6 400	7 000	1.09
9 600	10 530	1.10
9 600	14 500	1.51
6 400	10 530	1.64
6 400	14 530	2.27

6.1 Average heat transfer coefficients on the inner wall.

Figure 6-1 shows the Nusselt numbers on the inner wall of the annulus obtained for bilateral heating with increasing heat flux ratio from 0.54 to 2.27 and for Reynolds numbers of about 6 500 and 9 500. Also plotted on the same graph are the experimental Nusselt numbers obtained during unilateral heating conditions on the inner wall with heating flux on the inner wall at 9 600 (W/m²).

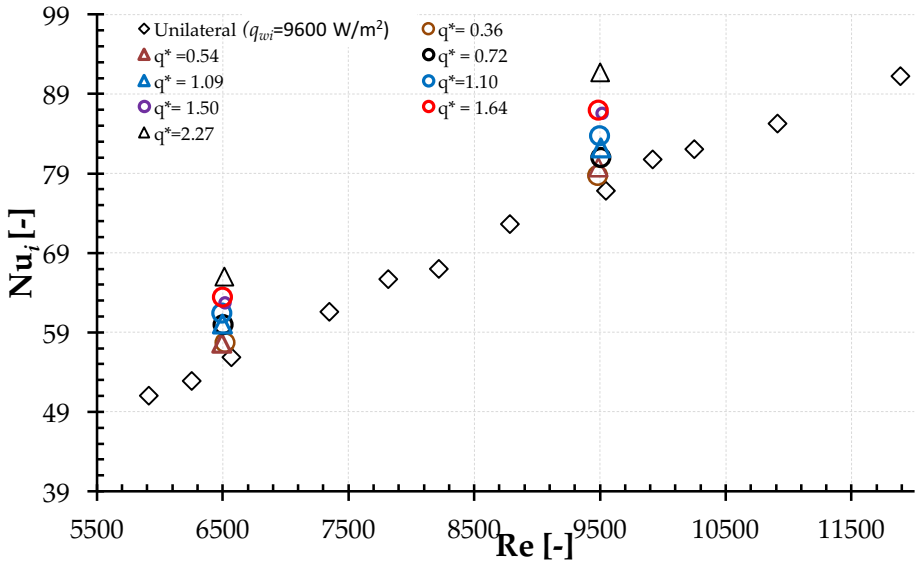

Figure 6-1: Nusselt numbers for the inner wall in the case of bilateral heating with different heat flux ratios.

It can been seen that bilateral heating has an impact on the heat transfer characteristics of an annulus when expressed in terms of a heat transfer coefficient. Compared with the unilaterally heating conditions, the heat transfer at the inner wall of an annulus is enhanced by bilateral heating conditions. The heat transfer improvement is more significant as the heat flux ratio increases (thus, as the heat flux on the outer wall is increased from zero to the maximum that was tested).

From results, it can also be observed that Nusselt numbers look to be more sensitive to the heat flux ratio, rather to the relative magnitudes of the individual heat fluxes on each wall of the annulus. No noticeable difference was found when comparing Nu_i for q^* = 1.09 and q^* = 1.10 or when comparing Nu_i for q^* = 1.50 and q^* = 1.64

Since experiments were conducted at approximately the same values of average Reynolds numbers, 6 504 ± 15, it is possible to present the Nusselt number on the inner wall as a function of the heat flux ratio as is shown in Figure 6-2. Once again it can be seen that for the range of heat flux ratios under investigation, the inner wall Nusselt numbers for bilaterally heated conditions are higher than for unilaterally heating conditions. It is observed that the inner wall Nusselt numbers increase linearly as the

heat flux ratio increases. This increase varies from 0% to 19% as the heat flux ratio changes from 0 to 2.27, irrespective of the Reynolds number.

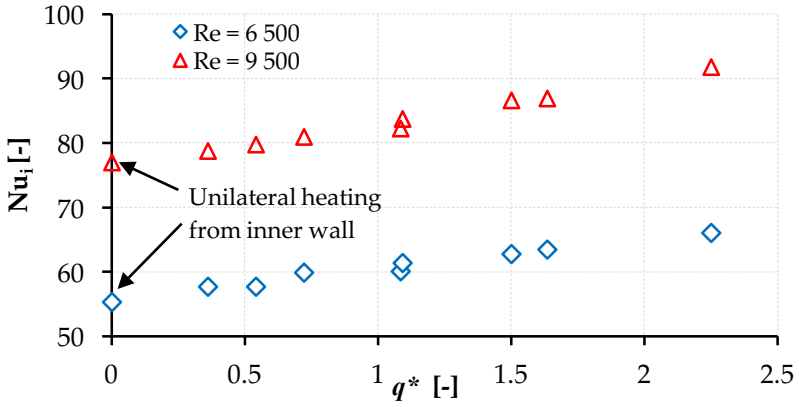

Figure 6-2 : Nusselt numbers on the inner wall of the annulus in terms of the heat flux ratio

Thus, the inner wall Nusselt number at a heat flux ratio of q^*, $Nu_{i,(q^*)}$, can be expressed as follows in terms of the unilateral Nusselt number, $Nu_{i,(q^*=0)}$:

$$Nu_{i,(q^*)} = (1 + 0.084q^*)Nu_{i,(q^*=0)} \qquad 6\text{-}2$$

for L/D_h= 408 , D_h = 10.88 mm, a =0.593

The coefficient of q^* was obtained from a linear line fit to the data.

6.2 Local heat transfer coefficients on the inner wall.

Figure 6-3 shows on a same graph the superposition of the local Nusselt numbers for the case of unilateral heating (9 600 W/m².) and bilateral heating conditions. For each control volume, an increase is observed in the local Nusselt number compared to the case of unilateral heating. Although results showed some scatter among data for the local Nusselt number, it was observed that at low Reynolds numbers, control volumes located near the inlet of the annular duct showed more heat transfer enhancement than control volumes which are located nearest to the exit.

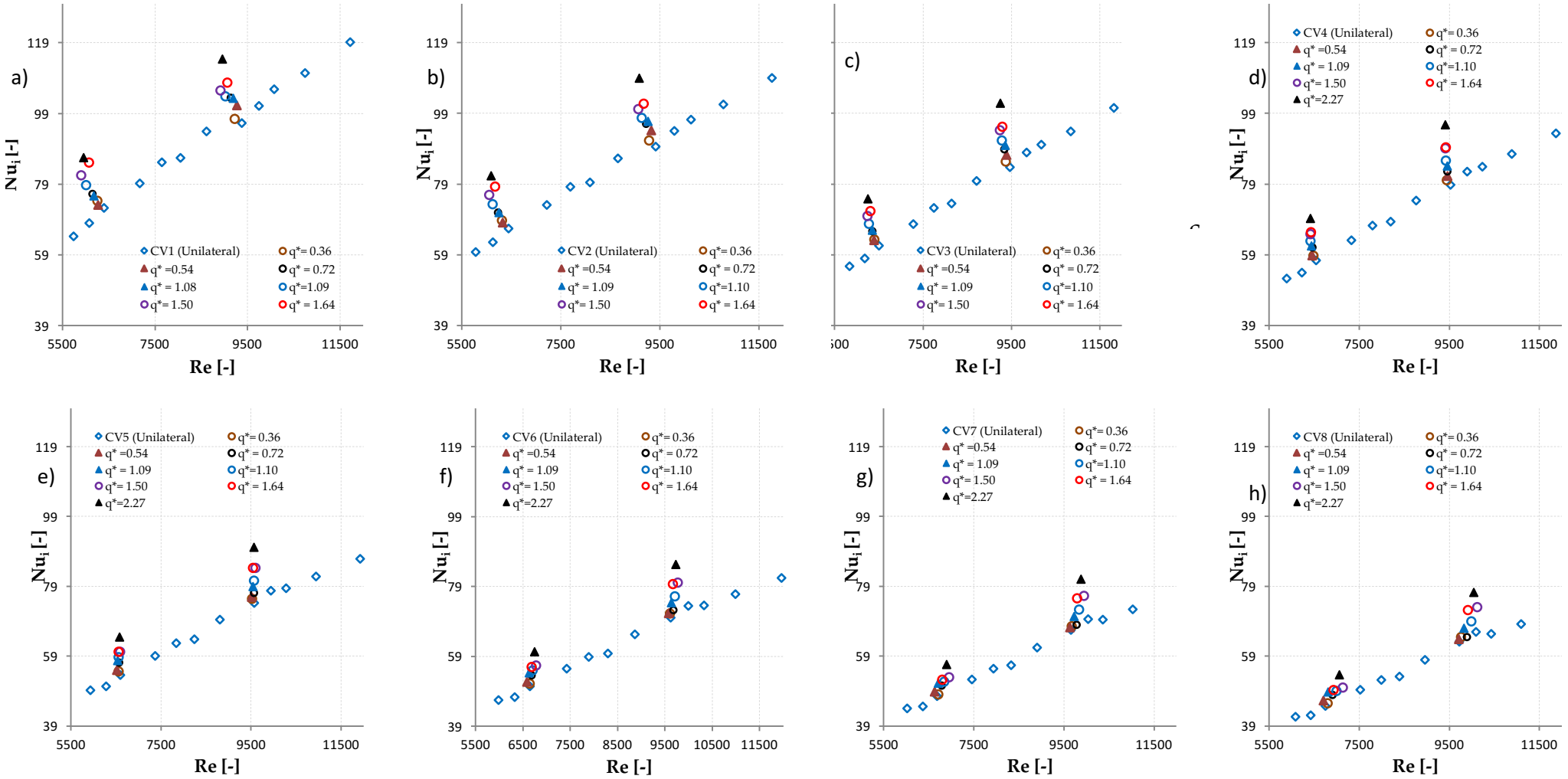

Figure 6-3: Local Nusselt numbers for CV 1 to CV 8 against correlations for heat flux of 9 600 W/m².

As Nusselt numbers were not collected at exactly the same Reynolds number, on Figure 6-4 the local Nusselt number is plotted along the axial length of the annular duct for different heat flux ratios. This was done through interpolation. From this figure, the behaviour described earlier is more obvious: namely that the heat transfer is more enhanced at the inlet of the annular duct than at the outlet.

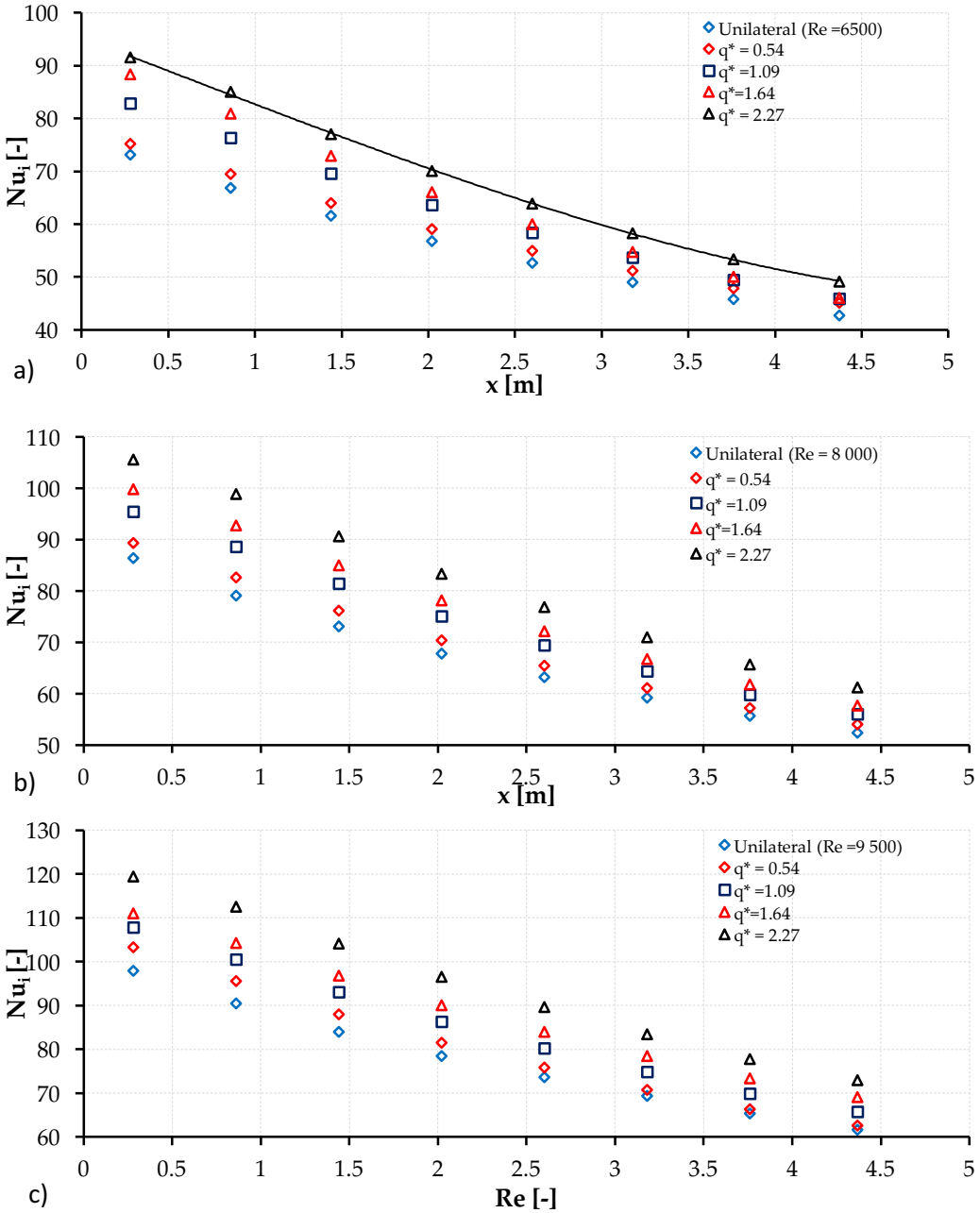

Figure 6-4: Local Nusselt on the inner wall along the axial length of the annulus for the case of bilateral heating for different *Re*.

6.3 Friction factors

In Figure 6-5 the friction factors are presented for bilaterally heating conditions. Since data were collected at approximately the same Reynolds numbers, the friction factors are represented in terms of the heat flux on the outer wall of the annulus. For Reynolds numbers tested in the turbulent regime and for a given value of heating flux on the inner tube of the annulus, it is observed that friction factor decreases as the heat flux on the outer tube of the annulus is brought higher. For similar values of heat flux densities, a reduction in friction factor is higher at low Reynolds number.

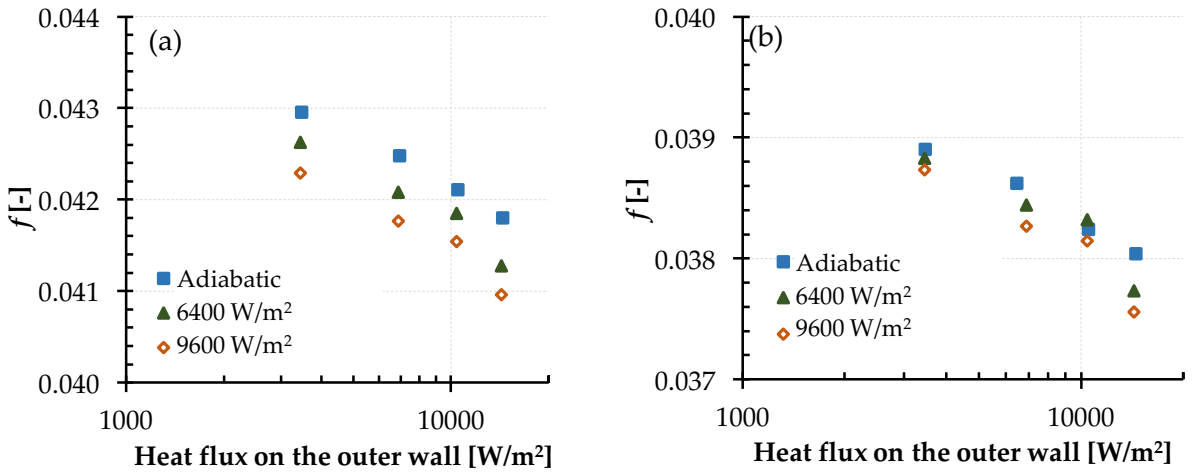

Figure 6-5: Frictions factors in terms of the heat flux on the outer and outer walls for Reynolds numbers of (a) 6500 and (b) 9500

As far as we are aware, there is no a particular correlation to express the friction factor for the case of bilaterally heating conditions. For this reason we follow the approach used in unilaterally heating conditions of expressing the ratio of friction factor as a function of the ratio of viscosities. Therefore, in Figure 6-6 the diabatic-to-adiabatic friction factor ratio is expressed as a quadratic function of ratio of the viscosity ratio. The product of viscosity ratio on the outer wall with the viscosity ratio on the inner wall of the annulus can mathematically be expressed as follows:

$$\frac{f}{f_a} = \left(\frac{\mu_{bulk}}{\mu_{wo}} \cdot \frac{\mu_{bulk}}{\mu_{wi}}\right)^{-m} \qquad 6\text{-}3$$

Using equation 6-3, a fitting curve through data collected for bilateral heating conditions case suggest that collected data could be satisfactorily represented with a single value of $m = 0.3045$ (See Figure 6-6**).** Singular computed values of m showed a minimum value of 0.188 while the maximum value was 0.336.

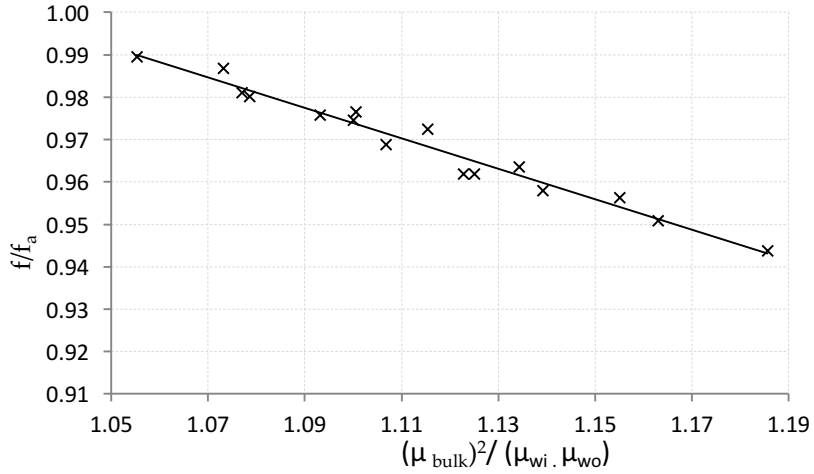

Figure 6-6: Friction factor ratio as a function of product of viscosity ratio for the case of bilateral heating.

Using the above value of $m = 0.3045$, predicted friction factors are plotted against experimental friction factors on Figure 6-7**.** All data collected for bilateral heating conditions case could be predicted within a 1% error band.

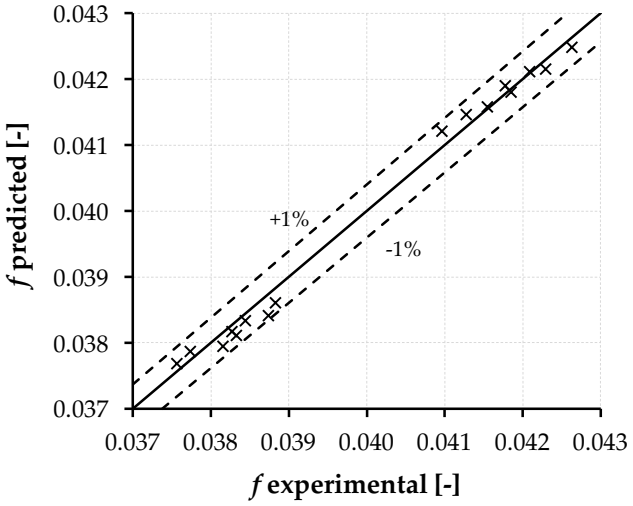

Figure 6-7 : Experimental friction factor versus predicted friction factor

6.4 *j*-factors based on the inner wall

Figure 6-8 to Figure 6-10 describes the behaviour of *j*-factor while increasing the heat flux ratio. It is observed an increase of *j*-factor as the heat flux ratio increases. This increase varies from 4 % at lower heat flux ratio and may reach 21 % for higher heat flux ratio. The same trend of increasing is noted for the ratio *j/f* with the heat flux ratio.

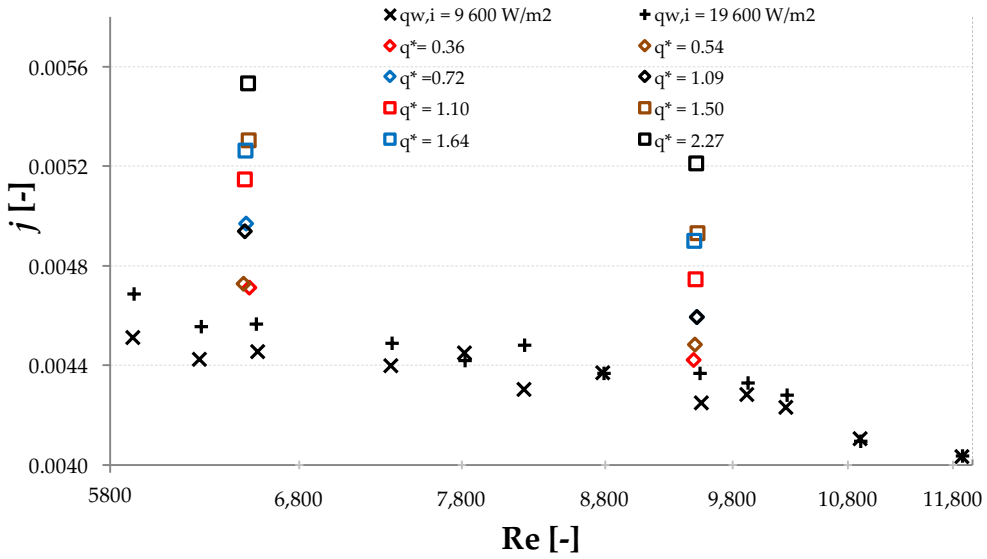

Figure 6-8 : *j*-factor as a function of the Reynolds number for bilateral and unilateral heating conditions.

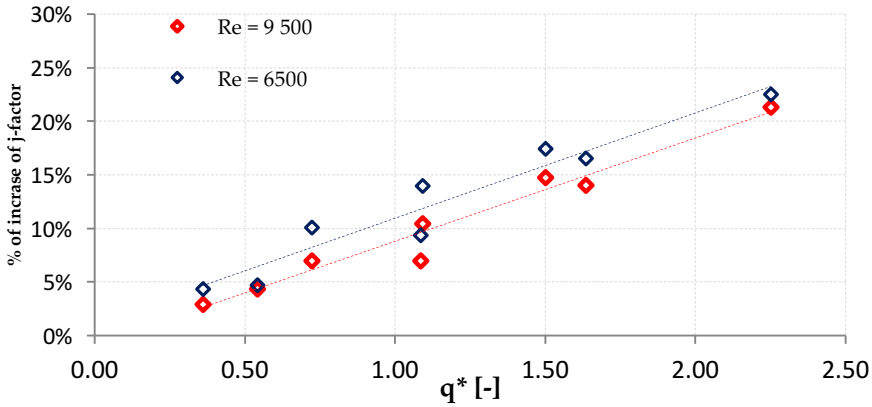

Figure 6-9: Percentage of increase of *j*-factor as function of q*.

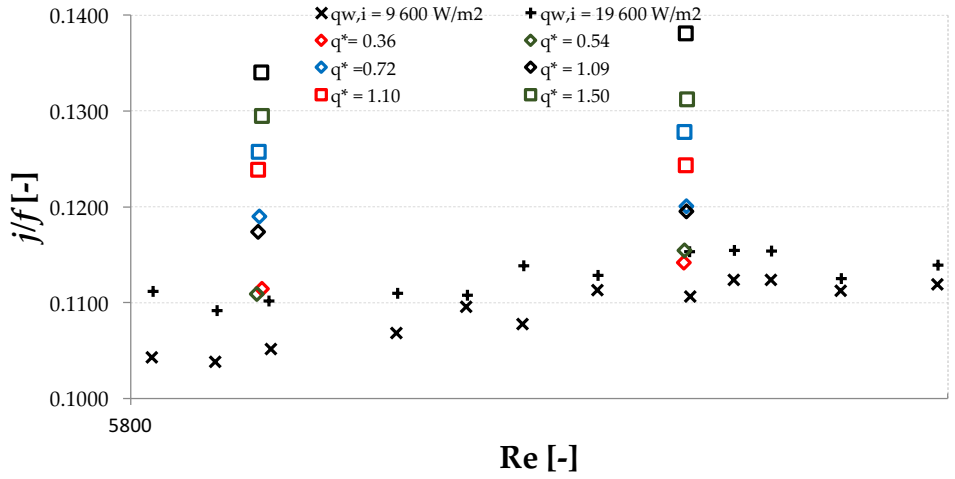

Figure 6-10 : Ratio *j/f* as a function of Re.

6.5 Average heat transfer coefficients on the outer wall

Outer wall Nusselt numbers for bilateral heating are presented in Figure 6-11 and Figure 6-12. In Figure 6-11, the outer wall Nusselt numbers for unilaterally heating from the outer wall ($q^* = \infty$) for $\dot{q}_{w,o}$ = 10 500 W/m² are also given. It is noticed that as the heat flux on the inner wall is increased (represented by a decrease in q^*), the outer wall Nusselt number is enhanced. At q^* = 0.36, the heat transfer coefficient is enhanced by approximately 20%. This trend is clearly showed on Figure 6-12 where the Nusselt numbers on the outer wall are plotted against the inverse of the heat flux ratio.

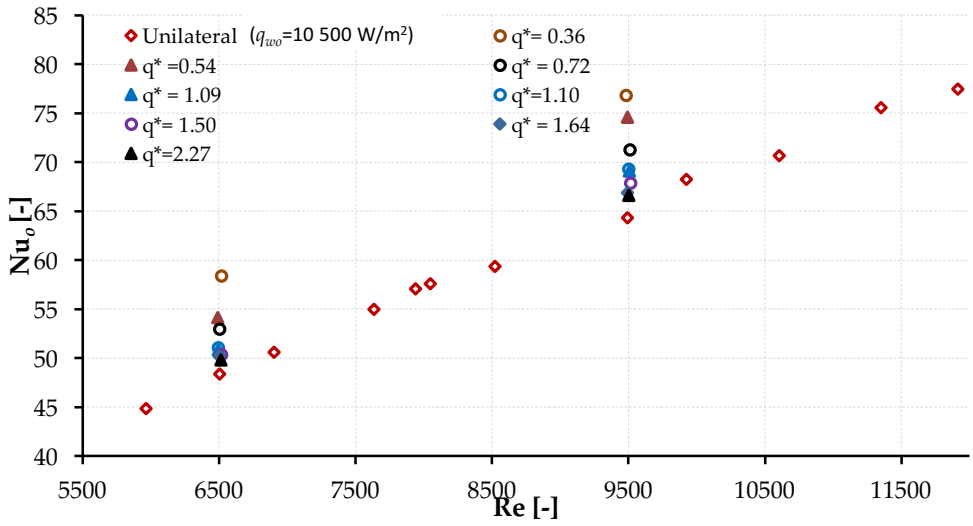

Figure 6-11: Nusselt numbers on the outer wall for the case of bilateral heating with different heat flux ratios.

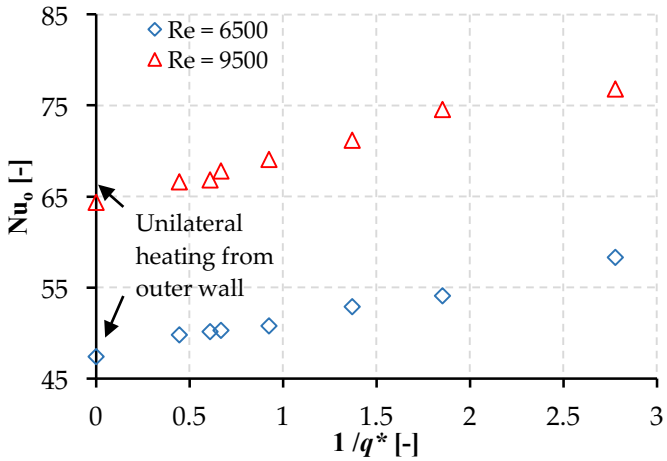

Figure 6-12: Nusselt numbers of the outer wall of the annulus as a function of the heat flux ratio.

By comparing the behaviour of the outer wall Nusselt Numbers against the inverse of the heat flux ratio with that of the inner wall Nusselt numbers against the heat flux ratio (Figure 6-12), it can be seen that there is once again a linear dependence as before. This increase in outer wall Nusselt number varies from 0% to approximately 20% as the inverse of the heat flux ratio changes from 0 ($q^* = \infty$) to 2.78 ($q^* = 0.36$), irrespective of the Reynolds number. Therefore, the outer wall Nusselt number at a heat flux ratio of q^*, $Nu_{o,(q^*)}$, can be expressed as follows in terms of the unilateral Nusselt number, $Nu_{o,(q^*=\infty)}$:

$$Nu_{o,(q^*)} = (1 + 0.079/q^*)Nu_{o,(q^*=0)} \qquad 6\text{-}4$$

for L/D_h= 408, D_h = 10.88 mm, a =0.593

As before, the coefficient of $1/q^*$ was obtained from a linear line fit to the data.

Starting with high values of q*, when heat flux ratio decreases to a value, say about 0.36, the trend shows that the Nusselt number at the outer wall will asymptotically become higher than the Nusselt number at the inner wall; which means that the heat transfer between the outer wall of the annulus and the fluid will surpass the heat transfer between the inner wall of the annulus and the fluid. Since we did not test in this study value of q* less than 0.36, other studies have suggested that the Nusselt number on the outer wall will go increasing while the Nusselt number in the inner

wall will go descending. The trend we observed from this experiment is qualitatively in agreement with the results obtained by Kays and Leung (1963) for bilateral heating conditions. They have also observed an enhancement of heat transfer on the inner wall and a deterioration of heat transfer on the outer wall when the heat flux ratio increases.

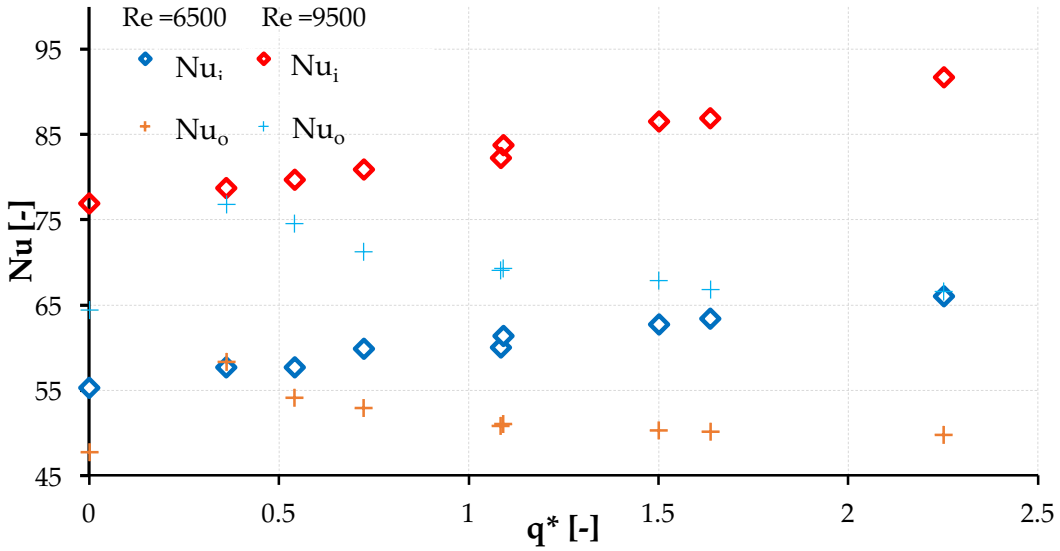

Figure 6-13: Superimposition of Nusselt Numbers on the inner and outer wall of the annulus as a function of heat flux ratio.

6.6 Local heat transfer coefficients on the outer wall

Figure 6-14 presents local Nusselt numbers over the control volumes along the axial length of the annulus. It is observed that, except in a few cases, heat transfer is enhanced on all control volumes as the heat flux ratio decreases and this enhancement is more significant as the heat flux ratio get lesser and lesser. This behaviour is comparable to what was reported in previous sections on average Nusselt numbers. Similar to what was done for the local inner Nusselt number, Figure 6-16 presents the local Nusselt number on the outer wall along the axial length obtained by interpolation of the neighbouring for Reynolds numbers 6 500, 8 000, and 9 500. The lowest heat flux ratio tested $q^* = 0.36$ provides the best heat transfer improvement and control volumes located near the inlet provide great increase. This means that in the presence of bilaterally heating conditions, heat transfer coefficients are also higher in the thermal entry as for the case of unilateral heating conditions.

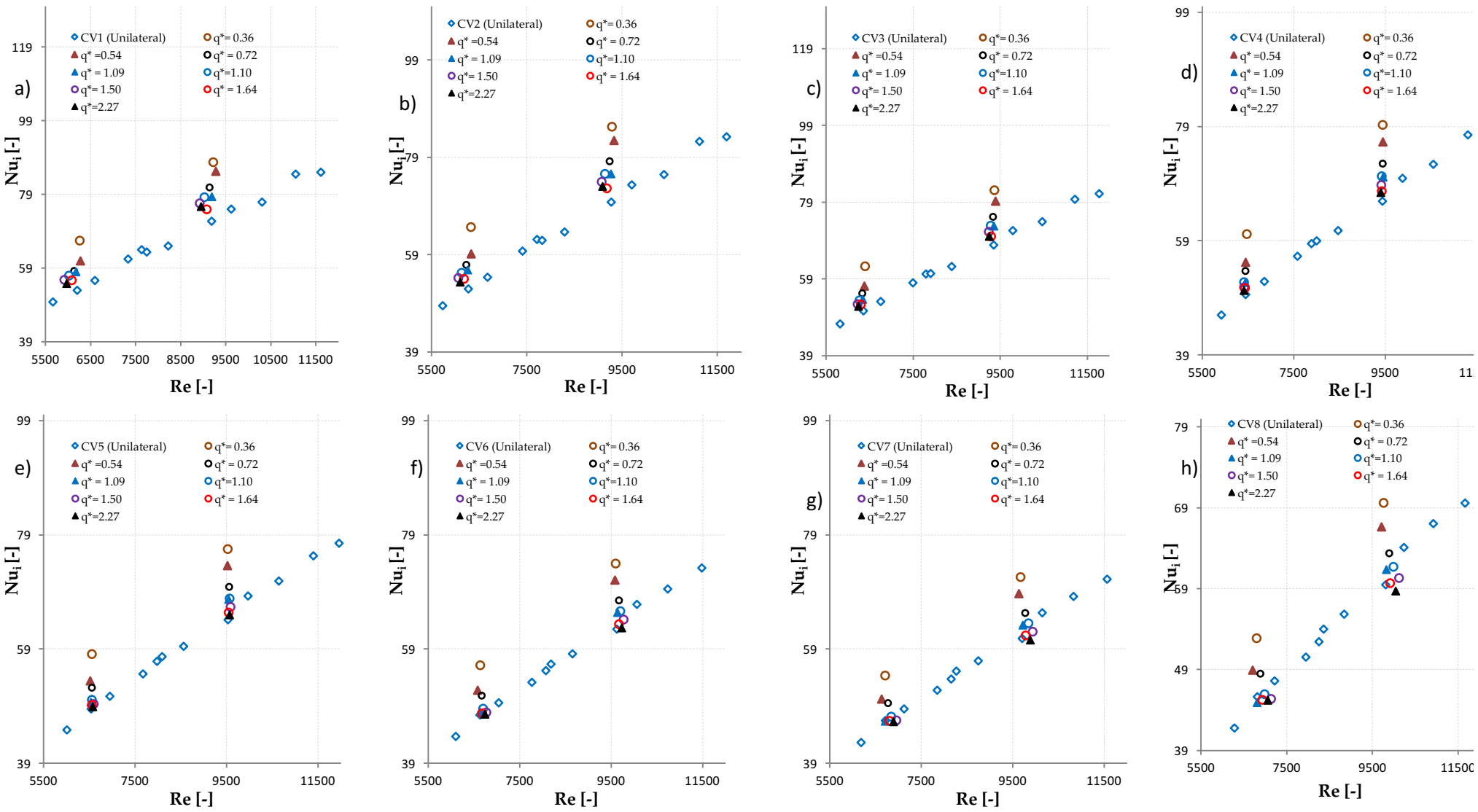

Figure 6-14: Local Nusselt numbers for CV 1 to CV 8 against correlations for heat flux of 10 530 W/m².

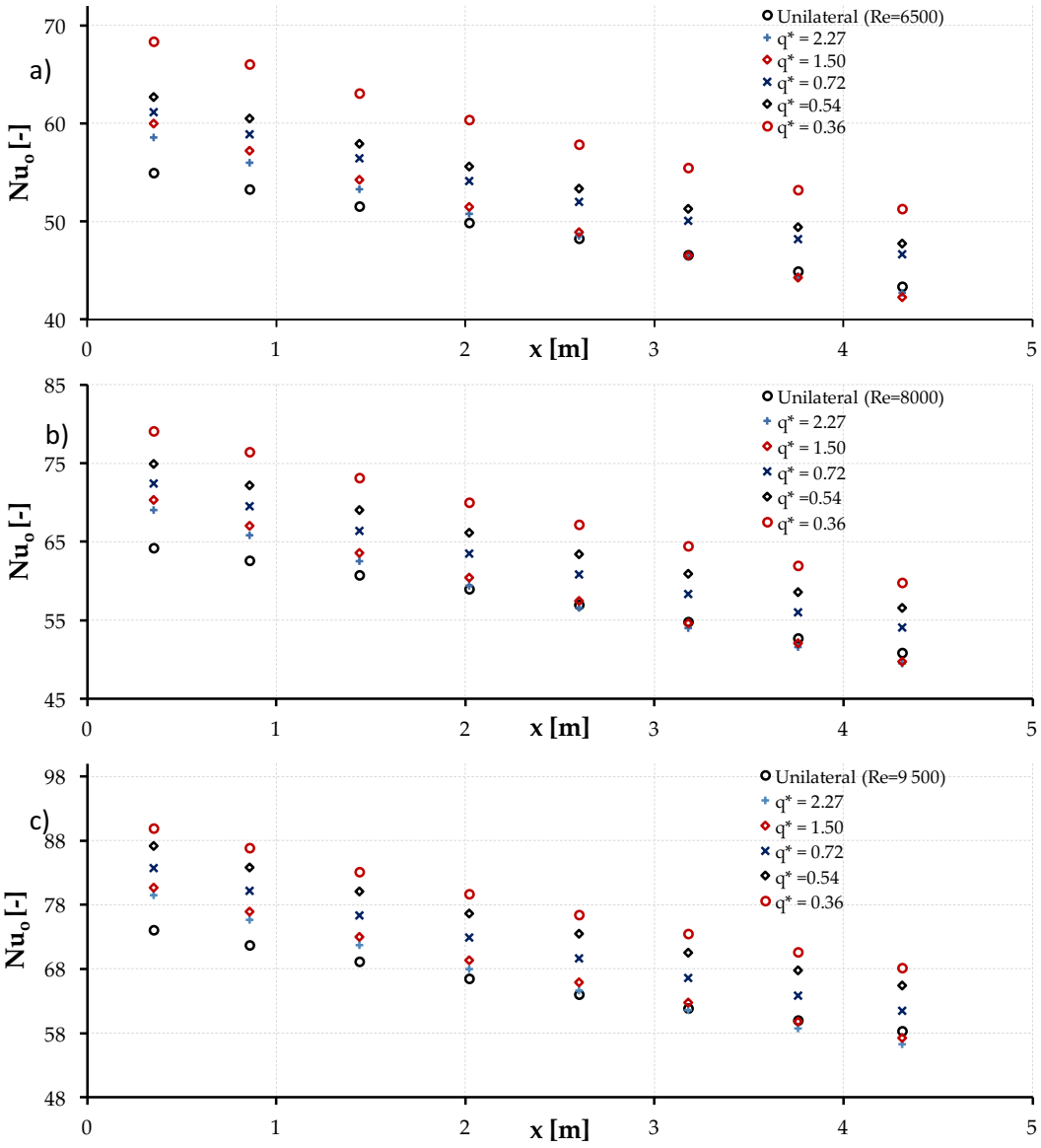

Figure 6-15: Local Nusselt numbers on the outer wall along the axial length of the annulus for the case of bilateral heating with different Re.

6.7 *j*-factor based on the outer wall

j-factor in terms of the Reynolds number for the Nusselt number on the outer wall is examined when changing the heat flux ratio in Figure 6-16. *j*-factor increases as the heat flux ratio decreases. For Re = 6 500, this increase varies from 6 % for q* = 2.27 to 22 % for q* = 0.36 as noticed in Figure 6-17. These values tend to be lower when increasing the Nusselt number.

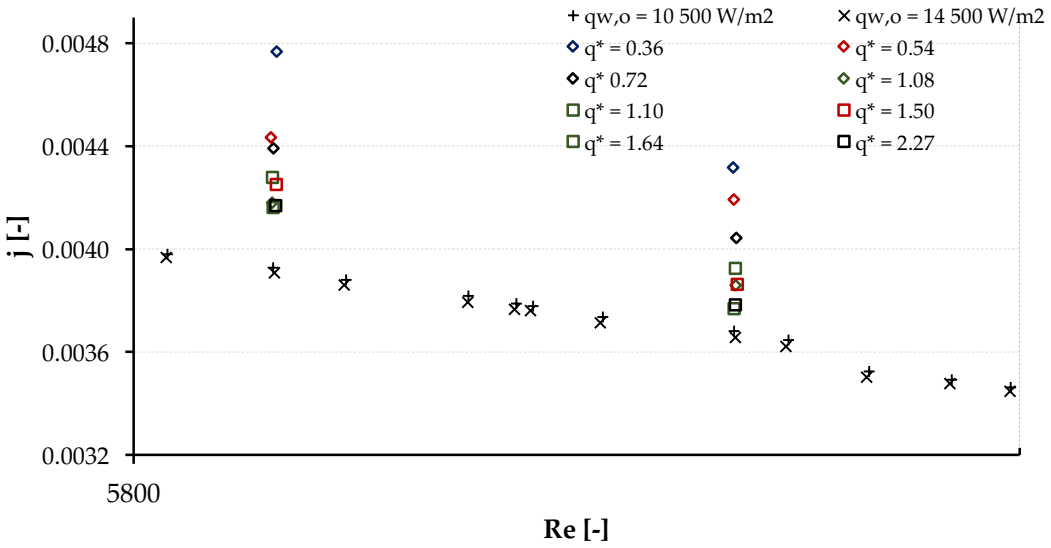

Figure 6-16: *j*-factor as a function of Re (superposition of unilateral and bilateral heating) on the outer wall.

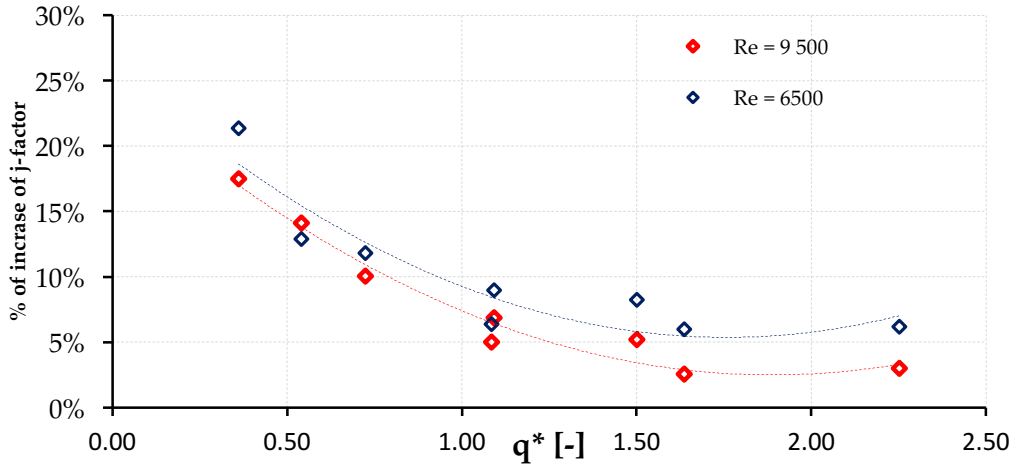

Figure 6-17: Percentage of increase of j-factor as a function of q*. (Outer wall)

Both *Nu* et *j-factor*, two ways used in this study to measure heat transfer, have revealed to significantly change as q* increases. In Figure 6-18, *j/f* is presented for the case of bilaterally heating conditions as a function of *Re*. While *j/f* for the case of bilaterally heating conditions showed to have a quasi-constant value, in the presence of bilaterally heating conditions, *j/f* departs from constant value and seems to be increasing as the heat flux ratio decreases.

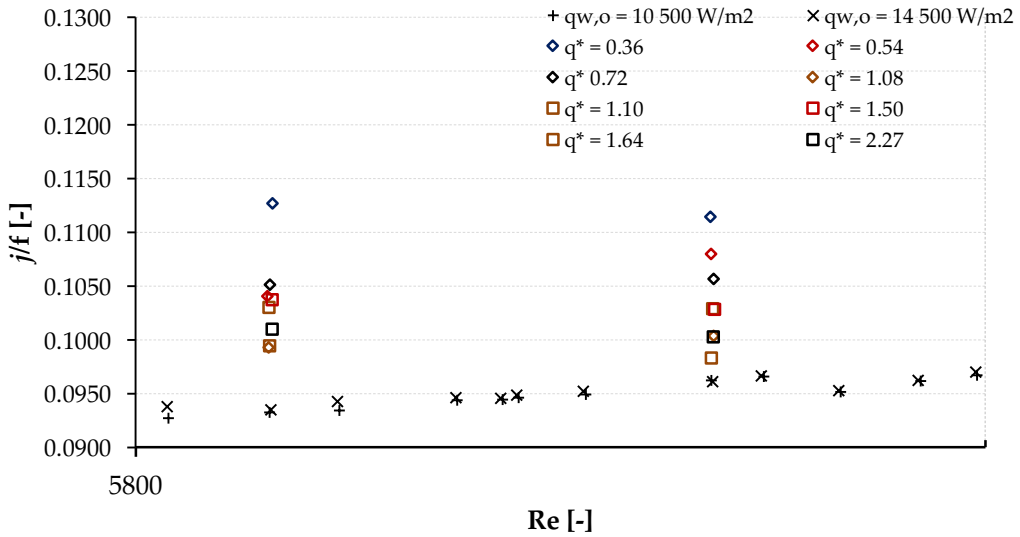

Figure 6-18: *j/f* as a function of Re (superposition of unilateral and bilateral heating).

6.8 Chapter conclusion

In this chapter it was shown that the heat flux ratio has a significant impact on the calculated heat transfer coefficients on both the inner and outer walls. It was found that as the heat flux ratio increases, the Nusselt number on the inner wall increases while the Nusselt number on the outer wall decreases. Inversely when the heat flux ratio decreases, the Nusselt number on the outer tube increases while the Nusselt number on the inner tube decreases. This can also be identified to the effect noted by Kays and Leung (1963) that the Nusselt number on the inner wall which is always greater than the Nusselt number on the outer tube can become, because of the heat flux ratio, lesser than the Nusselt number on the outer wall.

Chapter 7: Conclusion

The purpose of this study was to investigate the behaviour of heat transfer coefficients and friction factors for thermal boundary conditions where both the inner and the outer walls of an annulus are heated in the turbulent flow regime. Experimental and predictive correlations on these quantities for flow in annulus are numerous for the case of unilateral heating, but little investigation have been conducted to determine the impact of heat flux ratio when both walls are heated. It was the objective to collect data for a possible correlation in the future.

Data from the three thermal boundaries were collected: heating from the inner wall, from the outer wall and for both walls. In order to collect these data, an experimental setup was built. The experimental system consisted of an annular duct with heating elements around each wall of the annulus to provide a constant heat flux density along the annular duct. The system allowed for the measurement of the temperature along the test section, the heat flux input and output, the flow rate and the pressure drop. An uncertainty analysis was conducted on the system and accuracy on measurements and computed parameters were within reasonable limits.

Based on results, it was found that heating both walls enhances the individual heat transfer coefficients. With changing the heat flux ratio, when enhancing heat transfer through one wall, the Nusselt number deteriorates on the other. This enhancement was found to be in the same range for the Nusselt number tested.

Based on results in the annular ratio and Reynolds considered, it was found for the case of unilateral heating, no matter of the wall being heated, the Nusselt number is not influenced by the heat flux intensity. Nusselt numbers for the case of heating the inner wall were on average greater than those for the case of heating the outer wall by 16 to 20%.

The friction factor in the turbulent regime is lower for increased heat fluxes which is due to the change on the viscosity near the wall. Friction factors were satisfactorily predicted from results obtained from adiabatic cases with the introduction of a correction term. This correction term is expressed as a power of the viscosity ratio between the fluid and the wall. This exponent was found to be 0.3271 for the case of heating for the inner wall and 0.3572 for heating from the outer wall. Combining the two sets of data, a unique exponent of m = 3393 could be used.

Plots of friction factors and j-factors for cases of unilateral heating showed an approximate parallelism with the case of heating from the outer wall. It was found that j-factor values were on average lower by 14 % compared to those calculating for the case of heating the annulus from its inner wall.

When the annulus is heated from both walls, the calculated Nusselt numbers on each wall are enhanced by increasing the heat flux density on the outer wall while maintaining the heat flux on its own wall at the same level. The variation of the Nusselt number was found to be dependent on the heat flux ratio, rather than on the relative magnitudes of heat applied on each wall. Defining the heat flux ratio as the quotient of the heat flux density on the outer wall by the heat flux density on the inner wall, the Nusselt number on the inner wall was increased by 20 % with q^* = 2.27 while the Nusselt number was improved by 4% with q^* = 0.36 for Re = 9500.

For the case of bilateral heating, a decrease in the friction factor was also observed when more heat was added through walls. Friction factor data was satisfactorily represented with the use of correction factor defined as the product of viscosity ratio of heat wall. It was found that the equation $\frac{f}{f_a} = \left(\frac{T_{bulk}}{T_{wo}} . \frac{T_{bulk}}{T_{wi}}\right)^{-3045}$ predicted best the experimental data.

j-factors for the case of bilateral heating follow similar trends as Nusselt numbers for each wall.

Recommendation

Experimental research, in spite of multiple challenges beyond the design of the experimental setup, it is always a fascinating field to deepen. Different challenges encountered in the realisation of this project did not allow the collection of more data to establish valid correlations to overcome the lack which exists when considering the thermal boundary conditions, object of this study.

After completing this project, there still need for further data to achieve a correlation and an extension to other annular diameter ratios.

Reference List

Abu-Eishah, S. I. 2001. Correlations for the thermal conductivity of metals as a function of temperature. *International Journal of Thermophysics,* 22 (6), 1855-1868.

Afgan, N. H., SchlüNder, International Center for Heat and Mass Transfer. 1974. *Heat exchangers: design and theory sourcebook,* Washington, Scripta Book Co. .

Brighton, J. A. & Jones, J. D. 1964. *Transactions of American Society of Mechanical Engineers. Journal of Basic Engineering 86, 835*.

Carlson, L. W. & Irvine, T. J. 1961. Fully developed pressure drop in triangular shaped ducts. *Journal of Heat Transfer, Transactions of ASME,* 441.

Churchill, S. W. 1999. The conceptual analysis of turbulent flow and convection. *Chemical Engineering and Processing,* 38, 427-439.

Colburn, A. P. 1933. A Method of correlating forced convection heat transfer data and a comparison with fluid friction. *Transactions of American Institute of Chemical Engineers,* 29, 174 - 210.

Davis, E. S. 1943. *Transactions of American Society of Mechanical Engineers* 755.

Dirker, J. & Meyer, J. P. 2004. Convection Heat Transfer in concentric Annuli. *Heat Transfer Engineering,* 26(2), 19-29.

Dittus, P. W. & Boelter, L. M. K. 1930. Heat Transfer in automobile radiators of the tubular type. *University of Columbia Pub. Eng. ,* 2, 443 - 461.

Dormer, T. & Bergles, A. E. 1969. Pressure drop with surface boiling in small-diameter tubes. *International Journal of Heat and Mass Transfer*, 459-470.

Frederickson, A. G. & Bird, R. B. 1958. Friction factors for Axial Non-Newtonian Annular Flow. *Journal of Industrial and Engineering Chemistry,* 50, 1599 - 1600.

Gnielinski, V. 1987. *Single-phase convective heat transfer. Forced convection in Ducts,* Wallingford, UK, Hemisphere Publishing Corporation.

Gnielinski, V. 2009. Heat Transfer Coefficients for Turbulent Flow in Concentric Annular Ducts. *Heat Transfer Engineering,* 30 431 - 436.

Gujarati, D. & Porter, D. 2008. *Basic Econometrics*, Mc Graw-Hill.

Hallquist, M. 2012. *Heat transfer and pressure drop characteristics of smooth tubes at constant heat flux in the transitional regime.* Masters, University of Pretoria.

Jones, O. C. & Leung, J. C. M. 1981. An improvement in the calculation of turbulent friction in smooth concentric annuli. *Journal of Fluids Engineering,* vol 103/ 615.

Jonsson, V. K. & Sparrow, E. M. 1966. Results for laminar flow analysis and turbulent flow experiments for eccentric annuli. *Journal of Fluid Mechanics,* 25, 65.

Kaneda, M., Yu, B., Ozoe, H. & Churchill, S. W. 2003. The characteristics of turbulent flow and convection in concentric annuli. Part I. Flow. *International Journal of Heat and Mass Transfer,* 46 (26), 5045-5057.

Kays, W. M. & Crawford, M. E. 1980. *Convective heat and mass transfer,* New York, McGraw-Hill.

Kays, W. M. & Leung, E. Y. 1963. Heat Transfer in annular passages - Hydrodynamically developed turbulent flow with arbitrarily prescribed heat flux. *International Journal of Heat and Mass Transfer,* 6, 537-557.

Kline, F. J. & McClintok, F. A. 1953. Describing uncertainties in single sample experiments *Mechanical Engineering,* 75**,** 2-8.

Kline, N. & Tavoularis, S. 2016. An Experimental Study of Forced Heat Convection in Concentric and Eccentric Annular Channels. *ASME Journal of Heat Transfer,* 138**,** 012502-1.

Lee, Y. & Barrow, H. 1964. Turbulent Flow and Heat Transfer in Concentric and Eccentric Annuli. Paper 12. *Proc. Inst. Mech. Eng,* 178**,** 1–16.

Leung, L. K. H., Groeneveld, D. C., Teyssedou, A. & Aube, F. 2005. Pressure drops for Steam and Water flow in heated tubes. *Nuclear Engineering and Design,* 235**,** 53-65.

Maudou, L., Choueiri, G. & Tavoularis, S. 2011. An Experimental Study of Mixed Convection in Vertical, Open-Ended, Concentric and Eccentric Annular Channels. . *ASME Journal of Heat Transfer,* 133 (12).

Maurer, G. W. & Letourneau, B. W. 1963. Friction Factors for Fully Developed Turbulent Flow in Ducts With and Without Heat Transfer. *J. Basic Eng 86(3).*

Mills, A. F. 1992. *Heat transfer,* Homewood, IL, Irwin.

Moffat, R. J. 1988. Describing the Uncertainties in Experimental Results. *Experimental Thermal and Fluid Science,* 1**,** 3–17.

Monrad, C. C. & Pelton, J. F. 1942. Heat Transfer by Convection in Annular Spaces. *Transactions of the American Institute of Chemical Engineers,* 38**,** 593-611.

Nikuradse, J. 1933. Laws of flow in rouph pipes. *Translation in Technical Memorandum NACA (1950).*

Olivier, J. A. & Meyer, J. P. 2009. *Single-phase heat transfer and pressure drop of cooling of water inside horizontal circular smooth and enhanced tubes with different inlet geometries in the transition flow regime.* Philosophiae Doctor, University of Pretoria.

Ouild-Rouiss, M., Redjem-Saad, L. & Lauriat, G. 2009. Direct numerical simulation of turbulent heat transfer in annuli: Effect of heat flux ratio. *International Journal of Heat and Fluid Flow,* 30**,** 579-589.

Peng, C. H., Aye, M., Guo, Y., Jia, D. N., Qiu, S. Z., Su, G. H. & Nie, C. H. 2003. Experimental study of flow and heat transfer of narrow annuli with bilaterally heating. *Nuclear Power Engineering,* 24 (Suppl. 6)**,** 92-96.

Pethukov, B. S. & Roizen, L. I. 1963. An Experimental Investigation of Heat Transfer in a Turbulent Flow of gas in Tubes of annular section *Teplofizika VysokihTemperatur,* 1.

Popiel, C. & Wojtkowiak, J. Simple formulas for thermophysical properties of liquid water for heat transfer calculations (from 0 C to 150 C). *Heat Transfer Engineering,* 19 (3)**,** 87 - 101.

Quarmby, A. 1967. An experimental study of turbulent flow through concentric annuli. *International Journal of Mechanical Sciences,* 9**,** 205 - 221.

Quarmby, A. & Anand, R. K. 1969. Fully developed turbulent heat transfer in concentric annuli with uniform wall heat fluxes. *Chemical Engineering science,* 24**,** 171-187.

Rayle, R. E. Influence of orifice geometry on static pressure measurement. *ASME* Paper Number 59 - A - 234.

Rohsenow, W. M. & Clark, J. A. 1951. Heat transfer and pressure drop data for high heat flux densities to water at high subcritical pressures. *Stanford University Press*.

Shah, R. K. & London, A. L. 1978. *Laminar Flow Forced Convection in Ducts,* New York, Academic.

Shigley, J., Mischke, C. & Budynas, R. 2006. *Mechanical Engineering Design*, Mc Graw-Hill

Sieder, E. N. & Tate, G. E. 1936. Heat transfer and pressure drop of liquids in tubes. *Journal of Industrial and Engineering Chemistry* 28 1429–1435.

Stanton, T. E. & Pannel, J. R. 1914. Relation to the Surface Friction of Fluids. *Transactions of the Royal Society,* 214A.

Swamee, P. K., Aggarwall, N. & Aggarwal, P. 2008. Optimum design of double pipe heat exchanger. *International Journal of Heat and Mass Transfer,* 51**,** 2260-2266.

Venkateshan, S. P. 2008. *Mechanical measurements,* New Delhi, India; Boca Raton, FL, Ane Books India ; CRC Press.

W. R. Van ZYL, Dirker, J. & Meyer, J. P. 2012. Single phase convective heat transfer and pressure drop coefficients in smooth concentric annuli. *Proceedings of the ninth International Conference on Heat Transfer, Fluid Mechanics and Thermodynamics* 753-762.

White, F. M. 2009. *Fluid Mechanics*, Mc Graw Hill

Yu, B., Kawaguchi, Y., Ozoe, M. & Churchill, H. 2005a. The computed characteristics of turbulent flow and convection in concentric circular annuli. Part II. Uniform heating on the inner surface. *International Journal of Heat and Mass Transfer,* 48**,** 621-634.

Yu, B., Kawaguchi, Y., Ozoe, M. & Churchill, H. 2005b. The computed characteristics of turbulent flow and convection in concentric circular annuli. Part III. Alternative thermal boundary conditions. *International Journal of Heat and Mass Transfer,* 48**,** 635-646.

Yu, B., Kawaguchi, Y., Ozoe, M. & Churchill, H. 2005c. The computed characteristics of turbulent flow and convection in concentric circular annuli. Part IV. Generalizations. *International Journal of Heat and Mass Transfer,* 48**,** 3057-3072.

Zeng, H. Y., Qiu, S. Z. & Jia, D. N. 2007. Imvestigation on the characteristics of the flow and heat transfer in bilaterally heated narrow annuli. *International Journal of Heat and Mass Transfer,* 50**,** 492-501.

A. Appendix A: Uncertainty analysis

A.1 Introduction

Errors accompany any measurement, however well it has been conducted. The error may originate from the measurement process or it may be induced due to variations in the way the experiment is conducted. These errors may be classified as systematic errors and random errors. In this appendix, a full uncertainty analysis is performed for all parameters which were involved in the calculation of heat transfer coefficients and the friction factors.

A.2 Systematic, random errors and uncertainty theory

A systematic error or bias is due to faulty or improperly calibrated instruments. These may be reduced or eliminated by careful choice and calibration of instruments. Sometimes bias may be linked to a specific cause and estimated by analysis. In such a case a correction may be applied to eliminate or reduce bias. Bias is an indication of the accuracy of the measurement. Smaller the bias, more accurate is the data.

Random errors are due to non-specific causes like natural disturbances that may occur during the measurement process. These cannot be eliminated. The magnitude of the spread of the data due to presence of random errors is a measure of the precision of the data. The smaller the random error, the more precise are the data. Random errors are statistical in nature. These may be characterized by statistical analysis (Venkateshan, 2008).

The magnitudes of the bias and precision errors will correspond to the 95% probability that the actual error will not be more than the estimate. The uncertainty in a single measurement is given by:

$$\delta x_i = \{(B_i)^2 + (P_i)^2\}^{\frac{1}{2}} \qquad \text{A. 1}$$

where x_i is a single observation and δx_i the uncertainty of the measurement observation, B_i is the bias and P_i is the precision.

The result R of an experiment is generally obtained from a set of measurements. Mathematically it can be considered as a set of variables and be written in the following form:

$$R = f(x_1, x_2, \dots, x_p) \qquad \text{A. 2}$$

If we assume that the uncertainties of $x_1, x_2, \dots, p$ are known, the effect of these uncertainties on the result R is:

$$\delta R_{xi} = \frac{\partial R}{\partial x_i}\delta x_i \qquad \text{A. 3}$$

The partial derivative of R is called the sensitivity coefficient of the result R with respect to x_i. The sensitivity coefficient is the effect that the uncertainty of a single measurement for the variable, x_i, with the measurement being in error, has on the overall uncertainty of the result. If R is a function of p independent variables, the uncertainty of R is obtained by means of the root sum squared. Moffat (1988) derived this expression for a function of p independent variables as given below:

$$\delta R = \left\{\left(\frac{\partial R}{\partial x_1}\delta x_1\right)^2 + \left(\frac{\partial R}{\partial x_2}\delta x_2\right)^2 + \cdots + \left(\frac{\partial R}{\partial x_3}\delta x_p\right)^2\right\}^{\frac{1}{2}} \qquad \text{A. 4}$$

The above equation is only true if each measurement is an independent variable, all measurements are repeatable and follow the normal distribution and all uncertainties are initially expressed at the same confidence interval. Moreover, if $\delta {x_i}^2$ are taken to be variances, the validation of the equation is guaranteed without the need for normal distribution.

If R is expressed as:

$$R = x_1^a x_2^b x_3^c \dots x_p^m \quad \text{A. 5}$$

an expression of the relative uncertainty can be derived:

$$\frac{\delta R}{R} = \left\{ \left(a \frac{\delta x_1}{x_1} \right)^2 + \left(b \frac{\delta x_2}{x_2} \right)^2 + \cdots + \left(\left(m \frac{\delta x_p}{x_p} \right)^2 \right) \right\}^{\frac{1}{2}} \quad \text{A. 6}$$

A.3 Uncertainties

A.3.1 Instruments

All instruments used in this work (thermocouples, pressure transducers, Coriolis flow meters, Power supplies) had manufacturer specified accuracy which is considered as the bias. The precision was obtained by capturing 120 data points. The standard deviation was multiplied by two to fall within the 95% confidence interval. Table A 1 shows all the instruments with their ranges, bias, precision and total uncertainty by using equation.

Table A 1: Uncertainties of equipment

Instrument	Range	Bias	Precision	Uncertainty
Thermocouple	200 – 350°C	0.1°C [a]	0.023°C	0.11°C
Flow meter (low flow)	0.015 - 0.603 kg/s	0.1 %	0.08 %	0.14 %
Flow meter (high flow)	0.05 – 1.883 kg/s	0.1 %	0.09 %	0.14 %
Pressure Transducer (low range)	0 – 8.6 kPa	0.25%(FS)	0.9%	
Pressure Transducer (high range)	0 – 22 kPa	0.25%(FS)	1.1%	
Power Supply -Voltage	0 – 360 V	0.72 V	1 V	1.23 V
Power Supply - Current	0 – 30 A	0.06 A	0.01 A	0.061 A

[a] Calibrated with a PT 100 with an uncertainty of 0.1°C.
[b] Percentage of full scale value.
FS: Full scale

A.3.2 Fluid thermophysical properties

All fluid properties and their uncertainties were calculated according to correlations proposed by Popiel and Wojtkowiak (1998). The uncertainties are given in Table A 2.

Table A 2 : Uncertainties on fluid thermos-physical properties.

Fluid Property	Uncertainty
Density	0.004 %
Viscosity	1.0 %
Specific Heat	0.04 %
Prandtl number	2.3 %
Thermal Conductivity	1.0 %

A.3.3 Inlet and outlet temperatures

The inlet and outlet temperatures for the annulus were obtained by averaging readings from four thermocouple measurements. These thermocouples were evenly spaced around the periphery of the inlet and outlet tubes. It reads for the inlet

$$T_{in} = \frac{T_{in,1} + T_{in,2} + T_{in,3} + T_{in,4}}{4} \qquad \text{A. 7}$$

With the uncertainty being calculated as:

$$\delta T_{in} = \left\{ \left(\frac{\delta T_{in,1}}{4}\right)^2 + \left(\frac{\delta T_{in,2}}{4}\right)^2 + \left(\frac{\delta T_{in,3}}{4}\right)^2 + \left(\frac{\delta T_{in,4}}{4}\right)^2 \right\}^{\frac{1}{2}} \qquad \text{A. 8}$$

Since all the thermocouples are the same and have the same uncertainty, the above

$$\delta T_{in} = \sqrt{\frac{1}{4}}\,\delta T = \frac{\delta T}{2} \qquad \text{A. 9}$$

Similarly

$$\delta T_{out} = \sqrt{\frac{1}{4}}\delta T = \frac{\delta T}{2} \qquad \text{A. 10}$$

A.3.4 Inner wall and outer wall average temperatures

The inner tube had eight separate stations along the length of the tube. A reading at a station was obtained from the average of two thermocouples. The inner wall average temperature was given by the average of 16 thermocouple measurements. According to the reasoning made in the previous section, it can be easily derived that the uncertainty of temperature obtained by averaging n similar thermocouples with the same uncertainty is given by:

$$\delta T_x = \sqrt{\frac{1}{n}}\delta T \qquad \text{A. 11}$$

Therefore, the uncertainty of the inner wall average temperature is:

$$\delta T_{wi} = \sqrt{\frac{1}{16}}\delta T = \frac{\delta T}{4} \qquad \text{A. 12}$$

Analogically the uncertainty of the outer wall average temperature (with a total of 24 thermocouples distributed over 8 stations) by:

$$\delta T_{wo} = \sqrt{\frac{1}{24}}\delta T \qquad \text{A. 13}$$

A.3.5 Fluid bulk temperature and temperature difference

The fluid bulk temperature and the temperature difference between the outlet and the inlet are given respectively by the following equations:

$$T_{bulk} = \frac{T_{in} + T_{out}}{2} \quad \text{A. 14}$$

and

$$\Delta T = T_{out} - T_{in} \quad \text{A. 15}$$

By applying the equation A. 4, their respective uncertainties will be:

$$\delta\Delta T_{bulk} = \frac{\sqrt{\delta T_{in}^2 + \delta T_{out}^2}}{2} \quad \text{A. 16}$$

and

$$\delta\Delta T = \sqrt{\delta T_{in}^2 + \delta T_{out}^2} \quad \text{A. 17}$$

A.3.6 Logarithmic mean temperature difference

The logarithmic mean temperature difference with the inner tube being the heat transfer area was defined in equation 4.3 as below:

$$\Delta T_{LMTD} = \frac{(T_{wi,in} - T_{in}) - (T_{wi,out} - T_{out})}{ln[(T_{wi,in} - T_{in})/(T_{wi,out} - T_{out})]}$$

Applying A. 4 with this definition yields to the following expression for the uncertainty on ΔT_{LMTD} :

$$\delta\Delta T_{LMTD} = \left\{\left(\frac{\partial\Delta T_{LMTD}}{\partial T_{in}}\delta T_{in}\right)^2 + \left(\frac{\partial\Delta T_{LMTD}}{\partial T_{out}}\delta T_{out}\right)^2 + \left(\frac{\partial\Delta T_{LMTD}}{\partial T_{wi,in}}\delta T_{wi,in}\right)^2 + \left(\frac{\partial\Delta T_{LMTD}}{\partial T_{wi,out}}\delta T_{wi,out}\right)^2\right\}^{\frac{1}{2}} \quad \text{A. 18}$$

with

$$\frac{\partial\Delta T_{LMTD}}{\partial T_{wi,in}} = \frac{ln\frac{(T_{wi,in} - T_{in})}{(T_{wi,out} - T_{out})} - \frac{(T_{wi,in} - T_{in}) - (T_{wi,out} - T_{out})}{(T_{wi,in} - T_{in})}}{ln^2\frac{(T_{wi,in} - T_{in})}{(T_{wi,out} - T_{out})}} \quad \text{A. 19}$$

$$\frac{\partial \Delta T_{LMTD}}{\partial T_{in}} = \frac{\frac{(T_{wi,in} - T_{in}) - (T_{wi,out} - T_{out})}{(T_{wi,in} - T_{in})} - ln\frac{(T_{wi,in} - T_{in})}{(T_{wi,out} - T_{out})}}{ln^2\frac{(T_{wi,in} - T_{in})}{(T_{wi,out} - T_{out})}} \quad \text{A. 20}$$

$$\frac{\partial \Delta T_{LMTD}}{\partial T_{wi,out}} = \frac{\frac{(T_{wi,in} - T_{in}) - (T_{wi,out} - T_{out})}{(T_{wi,out} - T_{out})} - ln\frac{(T_{wi,in} - T_{in})}{(T_{wi,out} - T_{out})}}{ln^2\frac{(T_{wi,in} - T_{in})}{(T_{wi,out} - T_{out})}} \quad \text{A. 21}$$

$$\frac{\partial \Delta T_{LMTD}}{\partial T_{out}} = \frac{ln\frac{(T_{wi,in} - T_{in})}{(T_{wi,out} - T_{out})} - \frac{(T_{wi,in} - T_{in}) - (T_{wi,out} - T_{out})}{(T_{wi,out} - T_{out})}}{ln^2\frac{(T_{wi,in} - T_{in})}{(T_{wi,out} - T_{out})}} \quad \text{A. 22}$$

A.3.7 Heat transfer rates

The heat transfer rate of the annulus on the inner wall can be computed as:

$$\dot{Q}_{w,i} = R_i I_i^2 - A_{s,i} F \varepsilon \sigma \left(T_{heater}^4 - T_{amb}^4\right) \quad \text{A. 23}$$

And its uncertainty is

$$\delta \dot{Q}_{w,i} = \left\{ \left(\frac{\partial \dot{Q}_{w,i}}{\partial R}\delta R\right)^2 + \left(\frac{\partial \dot{Q}_{w,i}}{\partial I}\delta I\right)^2 + \left(\frac{\partial \dot{Q}_{w,i}}{\partial A_{s,i}}\delta A_{s,i}\right)^2 + \left(\frac{\partial \dot{Q}_{w,i}}{\partial T_{heater}}\delta T_{heater}\right)^2 + \left(\frac{\partial \dot{Q}_{w,i}}{\partial T_{amb}}\delta T_{amb}\right)^2 \right\}^{\frac{1}{2}} \quad \text{A. 24}$$

The resistance R was obtained by $R = \frac{U}{I}$ and according to equation A. 6,

$$\frac{\delta R_i}{R_i} = \sqrt{\left(\frac{\delta U}{U}\right)^2 + \left(\frac{\delta I_i}{I_i}\right)^2} \quad \text{A. 25}$$

And

$$\frac{\partial \dot{Q}_{w,i}}{\partial I_i} = 2R_i.I_i \; ; \; \frac{\partial \dot{Q}_{w,i}}{\partial R_i} = I_i^2 \quad \text{A. 26}$$

$$\frac{\partial \dot{Q}_{w,i}}{\partial T_{heater}} = 4A_{s,i}F\varepsilon\sigma T_{heater}^3; \frac{\partial \dot{Q}_{w,i}}{\partial T_{amb}} = 4A_{s,i}F\varepsilon\sigma T_{amb}^3 \quad \text{A. 27}$$

The heat transfer rate was defined on the outer wall as:

$$\dot{Q}_{w,o} = R_o I_o^2 - \frac{2\pi L_{h,o} k\,(T_{heater} - T_{amb})}{\ln\left(\frac{D_{ins,o}}{D_{ins,i}}\right)} \quad \text{A. 28}$$

The heat transfer rate of the bulk fluid temperature is given:

$$\dot{Q}_{output} = \dot{m}C_p(T_{out} - T_{in}) = \dot{m}C_p\Delta T \quad \text{A. 29}$$

Its uncertainty is:

$$\delta\dot{Q}_{output} = \left\{\left(\frac{\partial \dot{Q}_{output}}{\partial \dot{m}}\delta\dot{m}\right)^2 + \left(\frac{\partial \dot{Q}_{output}}{\partial C_p}\delta C_p\right)^2 + \left(\frac{\partial \dot{Q}_{output}}{\partial \Delta T}\delta\Delta T\right)^2\right\}^{\frac{1}{2}} \quad \text{A. 30}$$

$$= \left\{\left(C_p\Delta T\delta\dot{m}\right)^2 + \left(\dot{m}\Delta T\delta C_p\right)^2 + \left(\dot{m}C_p\delta\Delta T\right)^2\right\}^{\frac{1}{2}}$$

A.3.8 LMTD heat transfer coefficient

The LMTD heat transfer coefficient for inner heating is defined as:

$$h_i = \frac{\dot{Q}_{w,i}}{A_{s,i}\Delta T_{LMTD}} \quad \text{A. 31}$$

with

$$\delta h_i = \left\{\left(\frac{\partial h_i}{\partial \dot{Q}_{w,i}}\delta\dot{Q}_{w,i}\right)^2 + \left(\frac{\partial h_i}{\partial A_{s,i}}\delta A_{s,i}\right)^2 + \left(\frac{\partial h_i}{\partial \Delta T_{LMTD}}\delta\Delta T_{LMTD}\right)^2\right\}^{\frac{1}{2}} \quad \text{A. 32}$$

$$= \left\{ \left(\frac{1}{A_{s,i}\Delta T_{LMTD}} \delta \dot{Q}_{w,i} \right)^2 + \left(-\frac{\dot{Q}}{A_{s,i}^2 \Delta T_{LMTD}} \delta A_{s,i} \right)^2 + \left(-\frac{\dot{Q}}{A_{s,i}\Delta T_{LMTD}^2} \delta \Delta T_{LMTD} \right)^2 \right\}^{\frac{1}{2}}$$

Or alternatively using A. 6,

$$\frac{\delta h_i}{h_i} = \sqrt{\left(\frac{\delta \dot{Q}_{w,i}}{\dot{Q}_{w,i}} \right)^2 + \left(\frac{\delta A_{s,i}}{A_{s,i}} \right)^2 + \left(\frac{\delta \Delta T_{LMTD}}{\Delta T_{LMTD}} \right)^2}$$

Similar expressions can be derived for $h_o$or $\frac{\delta h_o}{h_o}$.

A.3.9 Geometric dimensions

Diameters were measured with a Vernier calliper having an uncertainty of 20 μm while lengths were measured with a measuring tape of uncertainty of 1 mm.

The hydraulic diameter is:

$$D_h = D_o - D_i$$

and

$$\delta D_h = \left\{ \left(\frac{\partial D_h}{\partial D_o} \delta D_o \right)^2 + \left(\frac{\partial D_h}{\partial D_i} \delta D_i \right)^2 \right\}^{\frac{1}{2}} \quad \text{A. 33}$$

$$= \{ (\delta D_o)^2 + (-\delta D_i)^2 \}^{\frac{1}{2}}$$

The inner heat transfer area is defined by:

$$A_{s,i} = \pi D_i L_{h,i}$$

$$\delta A_{s,i} = \left\{ \left(\frac{\partial A_{s,i}}{\partial D_i} \delta D_i \right)^2 + \left(\frac{\partial A_{si}}{\partial L_{h,i}} \delta L_{h,i} \right)^2 \right\}^{\frac{1}{2}} \quad \text{A. 34}$$

$$= \left\{ \left(\pi L_{h,i} \delta D_i \right)^2 + \left(\pi D_i \delta L_{h,i} \right)^2 \right\}^{\frac{1}{2}}$$

Alternately using A. 6

$$\frac{\delta A_{s,i}}{A_{s,i}} = \sqrt{\left(\frac{\delta D_i}{D_i}\right)^2 + \left(\frac{\delta L_{h,i}}{L_{h,i}}\right)^2} \qquad \text{A. 35}$$

The derivation of

$$\delta A_{s,o} = \left\{\left(\pi L_{h,o}\delta D_o\right)^2 + \left(\pi D_o \delta L_{h,o}\right)^2\right\}^{\frac{1}{2}}$$

is straightforward.

The annulus cross sectional area is:

$$A_c = \frac{\pi}{4}(D_o^2 - D_i^2)$$

therefore

$$\delta A_c = \left\{\left(\frac{\partial A_c}{\partial D_o}\delta D_o\right)^2 + \left(\frac{\partial A_c}{\partial D_i}\delta D_i\right)^2\right\}^{\frac{1}{2}}$$

$$= \left\{\left(\frac{\pi}{2} D_o \delta D_o\right)^2 + \left(\frac{\pi}{2} D_i \delta D_i\right)^2\right\}^{\frac{1}{2}} \qquad \text{A. 36}$$

A.3.10 Reynolds number

The Reynolds number is defined as:

$$Re = \frac{\dot{m} D_h}{\mu A_c}$$

With the uncertainty being:

$$\delta Re = \left\{\left(\frac{\partial Re}{\partial \dot{m}}\delta \dot{m}\right)^2 + \left(\frac{\partial Re}{\partial D_h}\delta D_h\right)^2 + \left(\frac{\partial Re}{\partial \mu}\delta \mu\right)^2 + \left(\frac{\partial Re}{\partial A_c}\delta A_c\right)^2\right\}^{\frac{1}{2}} \qquad \text{A. 37}$$

$$= \left\{\left(\frac{D_i}{A_i\mu_i}\delta\dot{m}_i\right)^2 + \left(\frac{\dot{m}_i}{A_i\mu_i}\delta D_i\right)^2 + \left(-\frac{\dot{m}_i D_i}{A_i^2\mu_i}\delta A_i\right)^2 + \left(-\frac{\dot{m}_i D_i}{A_i\mu_i^2}\delta\mu_i\right)^2\right\}^{\frac{1}{2}}$$

Or alternatively using A. 6,

$$\frac{\delta Re}{Re} = \sqrt{\left(\frac{\delta\dot{m}}{\dot{m}}\right)^2 + \left(\frac{\delta D_h}{D_h}\right)^2 + \left(\frac{\delta\mu}{\mu}\right)^2 + \left(\frac{\delta A_c}{A_c}\right)^2} \qquad \text{A. 38}$$

A.3.11 Nusselt number

The LMTD Nusselt number is defined as:

$$Nu_i = \frac{h_i\, D_h}{k}$$

And its uncertainty is:

$$\delta Nu_i = \left\{\left(\frac{\partial Nu}{\partial h_i}\delta h_i\right)^2 + \left(\frac{\partial Nu_i}{\partial D_h}\delta D_h\right)^2 + \left(\frac{\partial Nu_i}{\partial k}\delta k\right)^2\right\}^{\frac{1}{2}}$$

$$= \left\{\left(\frac{D_h}{k}\delta h_i\right)^2 + \left(\frac{h_i}{k}\delta D_h\right)^2 + \left(\frac{-h_i D_h}{k^2}\delta k\right)^2\right\} \qquad \text{A. 39}$$

Or using A. 6,

$$\frac{\delta Nu_i}{Nu_i} = \sqrt{\left(\frac{\delta h_i}{h_i}\right)^2 + \left(\frac{\delta D_h}{D_h}\right)^2 + \left(\frac{\delta k}{k}\right)^2}$$

Similar expressions can be readily derived for Nu_o.

A.3.12 Friction Factor

The friction factor is obtained from the following equation

$$f = \frac{2\rho D_h A_c^2 \Delta P}{\dot{m} L_{pd}}$$

Its uncertainty is given as:

$$\delta f = \left\{ \left(\frac{\partial f}{\partial \rho}\delta\rho\right)^2 + \left(\frac{\partial f}{\partial D_h}\delta D_h\right)^2 + \left(\frac{\partial f}{\partial A_c}\delta A_c\right)^2 + \left(\frac{\partial f}{\partial \Delta P}\delta\Delta P\right)^2 + \left(\frac{\partial f}{\partial L_{pd}}\delta L_{pd}\right)^2 + \left(\frac{\partial f}{\partial \dot{m}}\delta\dot{m}\right)^2 \right\}^{\frac{1}{2}} \quad \text{A. 40}$$

With

$$\frac{\partial f}{\partial \rho} = \frac{2A_c^2 D_h \Delta P}{\dot{m}^2 L_{pd}} \quad \text{A. 41}$$

$$\frac{\partial f}{\partial D_h} = \frac{2\rho A_c^2 \Delta P}{\dot{m}^2 L_{pd}} \quad \text{A. 42}$$

$$\frac{\partial f}{\partial \Delta P} = \frac{2\rho A_c^2 D_h}{\dot{m}^2 L_{pd}} \quad \text{A. 43}$$

$$\frac{\partial f}{\partial L_{pd}} = \frac{-2\rho A_c^2 D_h \Delta P}{\dot{m}^2 L_{pd}} \quad \text{A. 44}$$

$$\frac{\partial f}{\partial \dot{m}} = \frac{-4\rho A_c^2 D_h \Delta P}{\dot{m}^3 L_{pd}} \quad \text{A. 45}$$

A.3.13 j Factor

The *j*-factor was defined in the following ratio form:

$$j = \frac{Nu}{\mathrm{Pr}^{1/3}\, Re}$$

Using A. 6,

$$\frac{\delta j}{j} = \sqrt{\left(\frac{\delta Nu}{Nu}\right)^2 + \left(1/3\,\frac{\delta Pr}{Pr}\right)^2 + \left(\frac{\delta Re}{Re}\right)^2} \qquad \text{A. 46}$$

A.4 Summary of uncertainties

Table A 3 : Summary of uncertainties of geometric and calculated parameters. Part 1.

Properties	Values
T_{in}, T_{out}	0.055°C
T_{wi}	0.029°C
T_{wo}	0.033°C
T_{bulk}	0.039°C
ΔT	0.078°C
$L_{h,i}$, $L_{h,o}$, $L_{p,d}$	0.001 m
D_i , D_o	0.00002 m
D_h	0.26 %
$A_{s,i}$	0.13 %
$A_{s,o}$	0.08 %
A_c	0.268 %

Table A 4 : Summary of uncertainties of geometrical and calculated parameters. Part 2

	Heating from the inner wall								Heating from the outer wall							
	$\dot{q}_{w,i}$ = 6400 W/m²		$\dot{q}_{w,i}$ = 9600 W/m²		$\dot{q}_{w,i}$=14 400 W/m²		$\dot{q}_{w,i}$ = 19200 W/m²		$\dot{q}_{w,o}$ =3500 W/m²		$\dot{q}_{w,o}$ =7000 W/m²		$\dot{q}_{w,o}$=10530 W/m²		$\dot{q}_{w,o}$=14500 W/m²	
	Re ≈ 5 900	Re ≈12 000	Re ≈ 5 900	Re ≈12 000	Re ≈ 5 900	Re ≈12 000	Re ≈ 5 900	Re ≈12 000	Re ≈ 5 900	Re ≈12 000	Re ≈ 5 900	Re ≈12 000	Re ≈ 5 900	Re ≈12 000	Re ≈ 5 900	Re ≈12 000
ΔT_{LMTD}	2.2 %	3.62 %	1.33 %	2.40 %	0.87 %	1.60 %	0.67 %	1.15 %	3.07%	5.40%	1.52%	2.67%	1.00%	1.73%	0.71%	1.27%
R	1.19 %	1.19 %	0.97 %	0.97 %	0.79 %	0.79 %	0.68 %	0.68 %	0.83%	0.83%	0.59%	0.59%	0.48%	0.48%	0.41%	0.41%
I	1.17 %	1.17 %	0.95 %	0.95 %	0.77 %	0.77 %	0.67 %	0.67 %	0.66%	0.66%	0.46%	0.46%	0.38%	0.38%	0.32%	0.32%
Q_w	2.62 %	2.62 %	2.14 %	2.14 %	1.74 %	1.74 %	1.50 %	1.50 %	1.76%	1.76%	1.17%	1.17%	0.93%	0.93%	0.78%	0.78%
h	3.32 %	4.47 %	2.52 %	3.21 %	1.95 %	2.36 %	1.64%	1.89 %	3.54%	5.68%	1.92%	2.92%	1.37%	1.97%	1.06%	1.49%
Nu	3.47 %	4.59 %	2.72 %	3.37 %	2.21 %	2.58 %	1.94 %	2.15 %	3.70%	5.80%	2.28%	3.09%	1.80%	2.22%	1.48%	1.81%
f	1.44 %	1.26 %	1.43 %	1.24 %	1.49 %	1.25%	1.49 %	1.25 %	1.28%	1.05%	1.29%	1.04%	1.29%	1.05%	1.37%	1.06%
j	3.72 %	4.78 %	3.03 %	3.62 %	2.57 %	2.90 %	2.35 %	2.53 %	3.92%	5.93%	2.55%	3.37%	2.17%	2.59%	1.99%	2.24%
$A_{s,I\text{-}CV}$	0.216 %	0.216 %	0.216 %	0.216 %	0.216 %	0.216 %	0.216 %	0.216 %								
$A_{s,o\text{-}CV}$									0.19%	0.19%	0.19%	0.19%	0.19%	0.19%	0.19%	0.19%
Nu_{CV}	7.86 %	25 %	4.17 %	11 %	2.58 %	5.5 %	2.11 %	3.31 %	12.08%	28.00%	2.96%	9.00%	2.11%	3.80%	1.56%	2.48%